

3416

NATIONAL LIBRARY

OTTAWA



BIBLIOTHÈQUE NATIONALE

OTTAWA

NAME OF AUTHOR... Dwain Hervey Sykes.....
TITLE OF THESIS... A study of ^{27}Mg via the $^{26}\text{Mg}(\text{d},\text{p}\gamma)^{27}\text{Mg}$ reaction
.....
.....
UNIVERSITY..... University of Alberta.....
DEGREE..... Ph. D..... YEAR GRANTED.... 1968.....

Permission is hereby granted to THE NATIONAL
LIBRARY OF CANADA to microfilm this thesis and to
lend or sell copies of the film.

The author reserves other publication rights,
and neither the thesis nor extensive extracts from
it may be printed or otherwise reproduced without
the author's written permission.

(Signed)..... *Dwain Sykes*.....

PERMANENT ADDRESS:

..... 3836 Cameron St.
..... Regina Sask.
..... Canada

DATED.... January 2 19 69

THE UNIVERSITY OF ALBERTA

A STUDY OF ^{27}Mg VIA THE $^{26}\text{Mg}(\text{d},\text{p}\gamma)^{27}\text{Mg}$ REACTION

by



Dwain Hervey Sykes

A THESIS

SUBMITTED TO THE FACULTY OF GRADUATE STUDIES
IN PARTIAL FULFILLMENT OF THE REQUIREMENTS FOR THE DEGREE
OF DOCTOR OF PHILOSOPHY

DEPARTMENT OF PHYSICS

EDMONTON, ALBERTA

September, 1968

UNIVERSITY OF ALBERTA
FACULTY OF GRADUATE STUDIES

The undersigned certify that they have read, and recommend to the Faculty of Graduate Studies for acceptance, a thesis entitled A STUDY OF ^{27}Mg VIA THE $^{26}\text{Mg}(\text{d},\text{p}\gamma)^{27}\text{Mg}$ REACTION, submitted by Dwain Hervey Sykes in partial fulfillment of the requirements for the degree of Doctor of Philosophy.

J. J. Doyle for W. C. Allen
(Supervisor)

Gerald Ray

G. B. Walker

E. C. ...

Birthe Paul Singh

External Examiner

Date Oct 11, 1968

TABLE OF CONTENTS

	Page
CHAPTER I INTRODUCTION	1
CHAPTER II EXPERIMENTAL METHOD	5
2.1 Theory	5
2.2 Method of Analysis	9
2.3 Experimental Apparatus	11
2.4 Electronics	13
2.5 Spectrum Analysis	16
CHAPTER III EXPERIMENTAL RESULTS	21
3.1 Yield Curve and Choice of Bombarding Energies	21
3.2 The 0.984 MeV Level	30
3.3 The 1.692 MeV Level	30
3.4 The 1.936 MeV Level	31
3.5 The 3.109 MeV Level	33
3.6 The 3.470 - 3.484 MeV Doublet	34
3.7 The 3.564 MeV Level	34
3.8 The 3.757 - 3.782 MeV Doublet	35
3.8.1 Decay Modes	35
3.8.2 The 3.757 MeV Level	36
3.8.3 The 3.782 MeV Level	37
3.9 The 3.880 MeV Level	38
3.10 The 4.146 MeV Level	39
3.11 The 4.394 MeV Level	39
3.12 The 4.549 MeV Level	40
3.13 The 4.763 - 4.816 MeV Doublet	41
3.14 The 4.982 - 5.017 MeV Doublet	42
3.15 The 5.365 - 5.405 MeV Doublet	43

CHAPTER IV	NUCLEAR MODEL CALCULATIONS	44
4.1	The Nilsson Model	44
4.1.1	Theory	44
4.1.2	Application to ^{27}Mg	51
4.2	The Shell Model	58
CHAPTER V	CONCLUSIONS	63
REFERENCES		65
APPENDIX A	GAMMA-RAY PEAK FITTING PROGRAM	68

LIST OF TABLES

		Page
Table 3.1	A summary of spin assignments and mixing ratio solutions	22
Table 3.2	A summary of the branching ratio measurements	26
Table 3.3	A summary of a_2 and a_4 coefficients from Legendre polynomial fits to the angular distributions	28
Table 4.1	The Nilsson model parameters which fit the energies of four assumed band heads (refer to fig. 4.3)	55
Table 4.2	Single-particle energy spacings from (a) Wildenthal <u>et al.</u> (Wi 68) and (b) Kuo (Ku 67)	60
Table 4.3	The distribution of particles amongst the $d_{5/2}$, $s_{1/2}$ and $d_{3/2}$ single-particle orbits allowed for the shell model calculation using the matrix elements and single-particle energies of Kuo (Ku 67)	61

LIST OF FIGURES

Fig. 1.1	A summary of previously available information on the low-lying energy levels and branching ratios of ^{27}Mg	3 [†]
Fig. 2.1	The target chamber	11
Fig. 2.2	The electronics	13
Fig. 3.1	A summary of spin and parity assignments for ^{27}Mg from (a) previous work and a summary of the decay modes and spin assignments from (b) the present work. Unlikely spin assignments are enclosed in parenthesis. The x indicates the existence of a decay whose relative strength is unknown	21
Fig. 3.2	The charged-particle spectrum measured at 180° to the beam in coincidence with a gamma-ray detector at 55° for a deuteron bombarding energy of 5.5 MeV. The proton peaks are identified by the excitation energies of the states in ^{27}Mg to which they correspond. The open circles are points on the simultaneous randoms spectrum. The window settings used for sorting are marked below the spectrum	21
Fig. 3.3	The angular distribution and χ^2 versus $\arctan x$ for the least-squares fit to the 1.692 ± 0 MeV transition from the 1.692 MeV level in ^{27}Mg	30
Fig. 3.4	The gamma-rays measured in coincidence with protons populating the 1.936 MeV level of ^{27}Mg . The open circles are points on the simultaneous randoms spectrum	31
Fig. 3.5	The gamma-rays in coincidence with protons populating the 3.109 MeV level of ^{27}Mg . The open circles are points on the simultaneous randoms spectrum	33

[†]Page numbers refer to the page immediately preceding the figure and its caption.

Fig. 3.6	The angular distribution and χ^2 versus $\arctan x$ for the least-squares fit to the $3.109 \rightarrow 1.936$ MeV transition from the 3.109 MeV level in ^{27}Mg	33
Fig. 3.7	The gamma-rays in coincidence with protons populating the 3.470 - 3.484 MeV doublet of ^{27}Mg . The open circles are points on the simultaneous randoms spectrum	34
Fig. 3.8	The gamma-rays in coincidence with protons populating the 3.564 MeV level of ^{27}Mg . The open circles are points on the simultaneous randoms spectrum	34
Fig. 3.9	The gamma-rays in coincidence with protons populating the 3.757 - 3.782 MeV doublet of ^{27}Mg . The spectrum obtained (a) by gating on the 3.757 MeV side of the charged-particle peak and (b) by gating on the 3.782 MeV side of the peak. The open circles are points on the simultaneous randoms spectrum	35
Fig. 3.10	The angular distribution and χ^2 versus $\arctan x$ for the simultaneous fit to the $3.757 \rightarrow 1.692 \rightarrow 0$ MeV transitions for the 3.757 MeV level of ^{27}Mg . The dotted curves in the χ^2 plot are for $P(\pm 2.5) = 0.05$ $P(\pm 0.5)$	36
Fig. 3.11	The gamma-rays in coincidence with protons populating the 3.880 MeV level of ^{27}Mg . The open circles are points on the simultaneous randoms spectrum	38
Fig. 3.12	The gamma-rays in coincidence with protons populating the 4.146 MeV level of ^{27}Mg . The open circles are points on the simultaneous randoms spectrum	39
Fig. 3.13	The gamma-rays in coincidence with protons populating the 4.394 MeV level of ^{27}Mg . The open circles are points on the simultaneous randoms spectrum	39
Fig. 3.14	The gamma-rays in coincidence with protons populating the 4.549 MeV level of ^{27}Mg . The open circles are points on the simultaneous randoms spectrum	40

- Fig. 3.15 The gamma-rays in coincidence with the protons populating the 4.763 - 4.816 MeV doublet of ^{27}Mg measured at a bombarding energy of 5.5 MeV. The open circles are points on the simultaneous randoms spectrum 41
- Fig. 3.16 The gamma-rays in coincidence with protons populating the 4.763 - 4.816 MeV doublet of ^{27}Mg measured at a bombarding energy of 6.0 MeV with the gamma detector at 55° . The spectrum obtained with the gate set on the 3.763 MeV peak is shown in the upper part of the figure and the spectrum obtained with the gate set on the 4.816 MeV peak is shown in the bottom part of the figure. The locations of these windows are shown in the insets. The open circles are points on the simultaneous randoms spectrum 41
- Fig. 3.17 The gamma-rays in coincidence with protons populating the 4.982 - 5.017 MeV doublet of ^{27}Mg . The open circles are points on the simultaneous randoms spectrum 42
- Fig. 3.18 The gamma-rays in coincidence with protons populating the 5.365 - 5.405 MeV doublet of ^{27}Mg . The open circles are points on the simultaneous randoms spectrum 43
- Fig. 4.1 Nilsson model orbits as a function of the deformation parameter, η , for $\mu = 0.1$ and $\kappa = 0.1$. The value of K and the parity for each orbit are marked on the right side of the figure. The orbit numbers are those given by Nilsson (Ni 55). The energy scale was obtained with $\hbar\omega_0 = 41$
 $-\frac{1}{3}$
 (27) 47
- Fig. 4.2 The energy level spectra of four nuclei with the 15th particle as the odd particle from Gove (Go 60). The solid lines denote levels built on Nilsson orbit 9 and the dotted lines denote levels built on orbit 8 52

Fig. 4.3	The Nilsson model prediction of the positive parity levels of ^{27}Mg . The parameters used to fit each band are shown directly below the band. For assumption 1, the 3.782 MeV level is a $K = 3/2^+$ band head built on orbit 8 and for assumption 2, it is a $K = 3/2^+$ band head built on orbit 7	54
Fig. 4.4	The branching of the 1.936 MeV level as a function of the Nilsson parameters μ and η . The experimental branching ratio is from this work (refer to table 3.2)	56
Fig. 4.5	The ratio of the spectroscopic factor of the 0.984 MeV level to that for the ground state as a function of the Nilsson parameters μ and η . The experimental ratios are from (a) Cu 64, (b) Gl 65 and (c) Si 64	56
Fig. 4.6	The decoupling parameter of the $K = 1/2^+$ orbit 11 and $K = 1/2^+$ orbit 9 bands as a function of the Nilsson parameters μ and η . The experimental values are from this work (refer to fig. 4.3)	56
Fig. 4.7	The level spectrum for the $T = 3/2$ positive parity states of ^{27}Mg as predicted by the shell model. The spectrum (a) was obtained using two active orbits and (b) was obtained using three active orbits. The experimental spectrum is from this work (refer to fig. 3.1)	60

ABSTRACT

The spins, branching ratios and multipole mixing ratios for excited states of ^{27}Mg have been investigated via the $^{26}\text{Mg}(d,py)^{27}\text{Mg}$ reaction. Spin assignments are consistent with those of other investigations. The present results combined with previous work leads to a unique assignment of $J = 3/2^+$ for the 3.782 MeV level. The spins of the previously unstudied 3.109 and 4.394 MeV levels have been limited to $J = 3/2$ or $J = 7/2$ and $J = 3/2$, $J = 5/2$ or $J = 9/2$, respectively.

Branching ratios have been obtained for 15 levels including the previously unobserved decay of the 3.757, 3.782, 3.880, 4.146, 4.394, 4.549, 4.763, 4.816, (4.982-5.017), and (5.365-5.405) MeV levels. Mixing ratios have also been obtained for a number of transitions.

The experimental results have been compared with the predictions of the Nilsson model and the shell model with an effective interaction.

ACKNOWLEDGEMENTS

I would like to thank my supervisor Dr. W.C. Olsen for his support and encouragement during the course of this work.

I wish to express a special thanks to my colleagues, Cliff Vermette and Dave Hutcheon, for their assistance, close cooperation and many helpful discussions. Additional thanks should be given to Dave Hutcheon for his assistance in writing both the gamma-ray peak fitting program and the program used to do the Nilsson model calculations.

Thanks are also due to Jan Bogaards for his assistance during the early phases of this work.

I appreciate the efforts of Dr. W.K. Dawson and Jim Easton in providing computer programs for the SDS 920 computer.

I am grateful to Dr. S.S.M. Wong for providing the shell model program and for his assistance in using the program.

I would like to express my gratitude to J.B. Elliott, L. Holm, C. Green and the other members of the technical staff of the Nuclear Research Center for their cooperation and assistance.

I would also like to thank Miss Elsie Hawirko for her very careful and efficient typing of this thesis.

I would like to express my thanks to my wife for her understanding and patience over the last three years.

Finally, the financial assistance of the National Research Council in the form of a studentship for the past three years is gratefully acknowledged.

CHAPTER I

INTRODUCTION

In recent years there has been considerable interest in the s-d shell nuclei. Part of this stems from the discovery that the Nilsson model (Nil 55) is capable of explaining the low-lying spectrum of ^{25}Al and ^{25}Mg (Lil 58). This success has prompted investigation of neighboring nuclei since the information which is presently available for a number of these nuclei is insufficient to provide a proper test of the model.

The nucleus of ^{27}Mg is particularly interesting since it is found that in the region of $A = 27$ the nuclear deformation changes sign (Go 60). The deformation changes abruptly from a positive (prolate) deformation for $A \leq 25$ to a negative (oblate) deformation for $A \geq 29$. It is not clear what either the magnitude or the sign of the deformation should be for ^{27}Mg and, therefore, it is desirable to obtain information about this nucleus which will assist in establishing the deformation and provide a proper test of the model.

A variety of information may be used to test a nuclear model. The first test is to determine if the model can predict the experimental spectra of levels of known spin and parity. In order to make this comparison, the spins and parities of the states must be determined. However, this information is not sufficient if one is to provide a sensitive test of the nuclear wave functions.

The properties of the electromagnetic decay of excited states provide a much more sensitive test of the nuclear wave functions. The matrix elements for the decay of a level by the emission of a gamma ray of a given multipolarity can be calculated using the model and the results can be compared to experimental data. These electromagnetic matrix elements provide a direct and accurate test of the nuclear wave functions since it is not necessary to refer to relatively unknown factors related to nuclear forces or reaction mechanisms.

Some of the properties of ^{27}Mg have been measured previously. The first major investigation of these properties was that of Hinds, Marchant and Middleton (Hi 61). The energies of 42 levels of ^{27}Mg were measured to ± 10 keV via the reactions $^{26}\text{Mg}(d,p)^{27}\text{Mg}$ and $^{25}\text{Mg}(t,p)^{27}\text{Mg}$ using a magnetic spectrograph.

Following this, a series of measurements of (d,p), (t,d), (t,p) and (α , τ) stripping were made which yielded information on spectroscopic factors and the angular momentum transferred in the reaction. Only two of these measurements will be mentioned here and the reader is referred to the compilation of Endt and van der Leun (En 67) for additional information. The first measurement was by Čujec (Cu 64) who used the $^{26}\text{Mg}(d,p)^{27}\text{Mg}$ reaction to obtain the following ℓ -values:

0.984(2), 1.692(2), 3.470(0), 3.484(2), 3.564(1), 3.757-3.782(2,3), 4.549(2), and 4.816(1).

The second measurement was by Glover (Gl 64, Gl 65) using the $^{26}\text{Mg}(t,d)$, $^{26}\text{Mg}(d,p)$ and $^{25}\text{Mg}(t,p)$ reactions. The following spin assignments were made:

0.984(3/2+), 1.692(5/2+), 1.936(5/2+), 3.470(1/2+, 3/2+), 3.484(3/2+) and 3.782(3/2+, 5/2+).

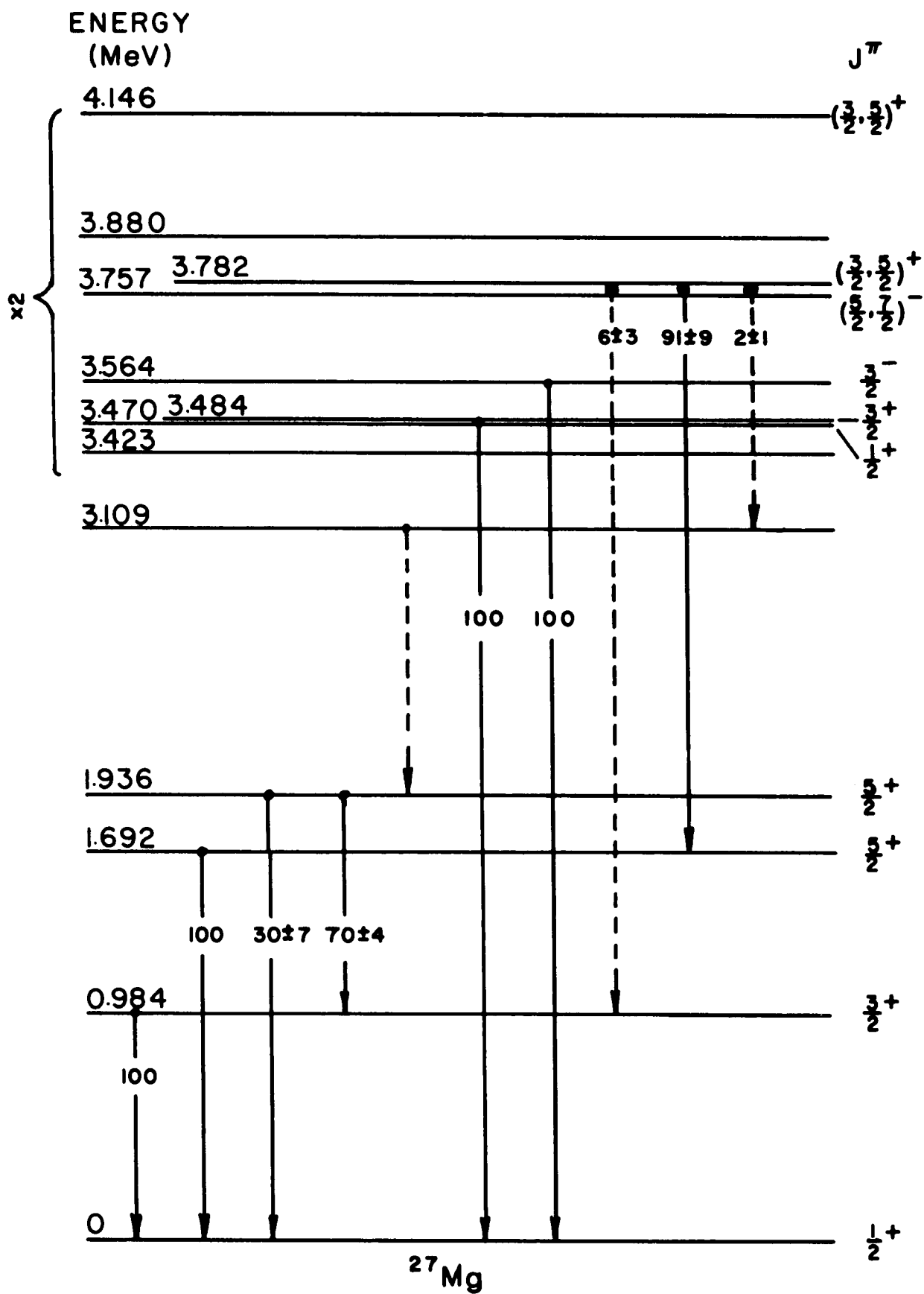
The gamma-ray decay of ^{27}Mg was first observed by Becker, Mitchell and Donovan (Be 64) who measured branching ratios for the 0.984, 1.692, 1.936, 3.109, (3.470, 3.484), 3.564, and (3.757, 3.782) MeV levels. A second measurement of these branching ratios was made by Lacambra, Tilley and Roberson (La 67) who also placed limitations on the spins of the 0.984, 1.692, 1.936, 3.564 and 3.757-3.782 MeV levels. The multipole mixing ratios for transitions from these levels were measured in a non-axial geometry and analyzed using plane wave stripping theory. Consequently, the mixing ratios obtained are not rigorous. Measurements using an axially symmetric system have been made (Es 67, Es 68) and limitations were placed on the spins of the first two excited states of ^{27}Mg ; however, limitations were not placed on the possible mixing ratios.

A summary of the previously known information on the spins, parities and branching ratios of levels of ^{27}Mg is shown in fig. 1.1.

There have been relatively few nuclear model calculations for ^{27}Mg and most of these dealt with ^{27}Mg as part of a general survey of nuclei in the shell. These calculations have been limited to two models, the intermediate coupling model (Bo 65, Bo 67) and the Nilsson model (Ni 55).

The intermediate coupling model calculations were part of a general survey of s-d shell nuclei (Bo 65, Bo 67). The level ordering

Fig. 1.1 A summary of previously available information on the
low-lying energy levels and branching ratios of ^{27}Mg .



of nuclei with $18 < A < 38$ was calculated as a function of the relative strength of the spin-orbit and central forces. The predicted spin sequence for ^{27}Mg of $1/2$, $5/2$, $3/2$ and $9/2$ was in disagreement with the observed sequence of $1/2$, $3/2$, $5/2$ and $5/2$.

One of the first of a series of Nilsson model calculations for ^{27}Mg was that of Bishop (31 59) who assumed that the deformation of ^{27}Mg was the same as ^{27}Al which was found to have a positive deformation characterized by a deformation parameter of $\eta = +3.2$. Using this, Bishop determined the other parameters of the Nilsson model necessary to fit low-lying levels of ^{27}Mg .

Another Nilsson model calculation was that of Glover (G1 65) in which it was concluded that the deformation of ^{27}Mg was negative. It was found that the observed spectroscopic factors could be explained for $\eta = -2$ assuming completely different configurations for the first few excited states from those used in Bishop's calculations.

Recently, Lacambra et al. (La 67) found that the mixing-ratio of the $0.984 \rightarrow 0$ MeV transition could be explained on the basis of the Nilsson model if a positive deformation of about $\eta = 2$ was assumed.

Thus, the distortion of ^{27}Mg has definitely not been well established, primarily due to a lack of information on excited states of this nucleus. More detailed information on the excited states and their decay properties is necessary if the distortion of ^{27}Mg is to be firmly established and a proper test of the model is to be made.

CHAPTER II

EXPERIMENTAL METHOD

2.1 Theory

The basic theory involved in particle-gamma-ray correlation work has been developed in detail by Litherland and Ferguson (Li 61) and Rose and Brink (Ro 67). Therefore, no attempt will be made in this thesis to derive the detailed expressions involved in the theory. Instead the principles and ideas involved in particle-gamma-ray correlation measurements will be stressed including the limitations which are encountered. The notation used follows that of Rose and Brink (Ro 67).

The nuclear reaction considered is of the form $A(a,b)B^*$, where A is the target nucleus, a and b are the incoming and outgoing particles respectively and B^* is the residual nucleus left in an excited state. The particles, b , leading to a state of spin J_1 in the residual nucleus are detected in a counter located on the beam axis. The angular distribution of the gamma rays from the de-excitation of the state $|J_1\rangle$ measured in coincidence with these particles provides information relating to the state $|J_1\rangle$.

In these measurements the beam and target nucleus are both unpolarized and the excited states of B are assumed to have definite parity. Under these conditions and the condition of cylindrical

symmetry about the beam axis the state $|J_1\rangle$ will not be polarized but, rather, it will be aligned. An aligned state is one in which the probability of population of the magnetic substate with projection M_1 on the beam axis is the same as that for $-M_1$. This alignment condition greatly simplifies the form which the angular distribution of gamma rays from the state $|J_1\rangle$ can take. The angular distribution can be expressed as a Legendre polynomial expansion in even order terms only since for odd order the terms in M_1 cancel those in $-M_1$.

The equation describing the angular distribution of gamma rays from the decay of $|J_1\rangle$ to $|J_2\rangle$ is given by (Ro 67)

$$\begin{aligned} W(\theta) &= \sum_{k(\text{even})} a_k P_k(\cos\theta) \\ &= \sum_{k(\text{even})} B_k(J_1) R_k(J_1 J_2) P_k(\cos\theta), \end{aligned} \quad (2.1)$$

where $W(\theta)$ is the intensity of gamma rays at an angle θ to the beam, $P_k(\cos\theta)$ is a Legendre polynomial of order k and a_k , $B_k(J_1)$ and $R_k(J_1 J_2)$ are coefficients describing the angular distribution. The coefficient $B_k(J_1)$ is a function of the nuclear alignment and is independent of the decay of the state. The coefficient $R_k(J_1 J_2)$ describes the gamma-ray decay of $|J_1\rangle$ but is independent of the nuclear alignment. Detailed expressions for these coefficients have been derived by Rose and Brink (Ro 67).

The $R_k(J_1 J_2)$ coefficients are functions of three factors, the spin of the initial state, J_1 , the spin of the final state, J_2 , reached through the emission of a gamma ray, and the relative

strengths of the multipoles involved in the transition. The multipole order may have all values between $|J_1 + J_2|$ and $|J_1 - J_2|$; however, in the most common case in practice, only two multipoles are significant, the lowest possible multipole and the next highest. In this case, the parameter involved is the multipole mixing ratio, x , the square of which is the ratio of transition rates of the $(\bar{L} + 1)$ th multipole to the \bar{L} th multipole, where \bar{L} is the lowest order multipole possible. For example x^2 may be the ratio of E2 transition strength to M1 transition strength. The sign of x is related to the sign of the reduced matrix elements of the multipole operator (Ro 67) and this sign as well as the magnitude of x can be compared to the predictions of nuclear models.

The $B_k(J_1)$ coefficients are a function of two factors, the spin of the state $|J_1\rangle$ and the relative populations of the magnetic substates, $w(M_1)$. In general, all magnetic substates with $|M_1| \leq J_1$ can be populated by the reaction and the $w(M_1)$ depend critically on the reaction mechanism and cannot be reliably predicted. Therefore, these population parameters must be treated as unknowns. The number of these parameters is limited, however, when the particles are detected on axis at 180° (or 0°). This is because the orbital angular momentum has zero projection along the direction of motion of the particle and only those magnetic substates with M_1 less than $M_1(\text{MAX})$ will have non zero population parameters, where $M_1(\text{MAX})$ is given by

$$M_1(\text{MAX}) = |S_A| + |S_a| + |S_b|, \quad (2.2)$$

where S_A , S_a and S_b are the spins of the target nucleus, incoming and outgoing particle, respectively. In very favorable cases such as (α, p) reactions on a spin zero nucleus only the $\pm 1/2$ substates may be populated and the $w(\pm 1/2)$ just corresponds to a normalization factor. In the case of $^{26}\text{Mg}(d, p)^{27}\text{Mg}$ $M_1(\text{MAX})$ is $3/2$ so both the $\pm 1/2$ and $\pm 3/2$ magnetic substates may be populated. This introduces an extra unknown into the correlation equation.

The limitations placed on the populations of the magnetic substates are applicable only where the particles, b , are detected exactly on axis and it is necessary to consider what effect a finite sized particle detector will have. When particles are detected at some small angle, ξ , with respect to the beam axis the substates with M_1 greater than $M_1(\text{MAX})$ will be populated to a small extent due to orbital angular momentum. Litherland and Ferguson (Li 61) have considered this problem and showed that the contribution of this finite-size effect to the population of $M_1(\text{MAX}) + 1$ is proportional to ξ^2 . The exact amount of this contribution can be calculated only if the details of the reaction mechanism are known. In the absence of such detailed information, one can only estimate a maximum value for this effect.

A finite sized gamma-ray counter also has an effect on the correlation, however, this effect can be taken into account in a straightforward manner (Fe 65). A finite sized gamma-ray detector simply reduces the variation of counting rate with angle (i.e. the effective a_k are smaller) which can be accounted for by inserting an attenuation coefficient, Q_k

in equation 2.1. The Q_k coefficients are tabulated by Rutledge (Ru 59).

One is not restricted to observing the angular distribution of the primary gamma ray from the state $|J_1\rangle$. The primary member may be unobserved and the gamma ray from the transition $|J_2\rangle$ to $|J_3\rangle$ may be observed instead. In this case, the correlation equation becomes

$$W(\theta) = \sum_{k(\text{even})} Q_k B_k(J_1) U_k(J_1 J_2) R_k(J_2 J_3) P_k(\cos\theta), \quad (2.3)$$

where the additional coefficient $U_k(J_1 J_2)$ describes the unobserved decay from $|J_1\rangle$ to $|J_2\rangle$. These coefficients are functions of J_1 , J_2 and the mixing ratio for the transition $J_1 \rightarrow J_2$. These coefficients are given by Rose and Brink (Ro 67). The same unknowns are involved in this expression as in equation 2.1 in addition to the spin J_3 and the mixing ratio for the secondary transition.

The correlation equation can be easily generalized to the case of a cascade of n unobserved transitions with the $(n + 1)$ th transition observed by inserting n U_k coefficients into the equation.

2.2 Method of Analysis

The angular distribution of gamma rays is fitted using equation 2.1 for each possible spin combination. Two unknown factors, other than the spins, enter into the expression, the $w(M_1)$ and the mixing ratio. If the $w(M_1)$ and x are taken as continuous variables, then the angular distribution can be fitted using a non-linear least-

squares analysis. It is more convenient in practice to allow only the $w(M_1)$ to vary continuously and to step through discrete values in x . For each x the values of $w(M_1)$ are found which yield the lowest χ^2 , where

$$\chi^2 = \frac{1}{n} \sum_1 \frac{[Y(\theta_1) - W(\theta_1)]^2}{[E(\theta_1)]^2}, \quad (2.4)$$

in which $E(\theta_1)$ is the uncertainty assigned to the gamma-ray yield $Y(\theta_1)$, at angle θ_1 , and n is the number of degrees of freedom. For a given J_1 , J_2 and x , the value of n is the number of angles at which data have been taken minus the number of substates which can be populated.

The angular distribution is fitted for a given J_1 , J_2 and x using a χ^2 least-squares computer program and the I.B.M. 360/67 computer. The computer program was written by E.K. Warburton (refer to Po 65) and modified to allow a simultaneous fit to both members of an unresolved doublet.

The χ^2 is calculated for a given J_1 , J_2 and discrete values of $\arctan x$ taken over the range $-\infty$ to ∞ . To facilitate the presentation of the results of this calculation, χ^2 is plotted against $\arctan x$. The probability that a set of J_1 , J_2 and x are correct solutions can be found by referring to χ^2 probability tables (Wa 59). In this work, the 0.1% confidence limit is the χ^2 value above which a solution may be rejected. For the correct solution, the expectation value of χ^2 is unity and the probability that χ^2 exceeds that 0.1% limit is 0.1%.

In this thesis χ^2 as a function of x is calculated first assuming

no finite size effect for the particle counter, and a second time assuming that the population of the $M_1 = \pm 5/2$ magnetic substates is $0.05 w(\pm 1/2)$ or $0.05 w(\pm 3/2)$. A comparison of the results indicates how important the finite size effect is. If the effect proves to be large, one would be forced to reduce the solid angle subtended by the detector.

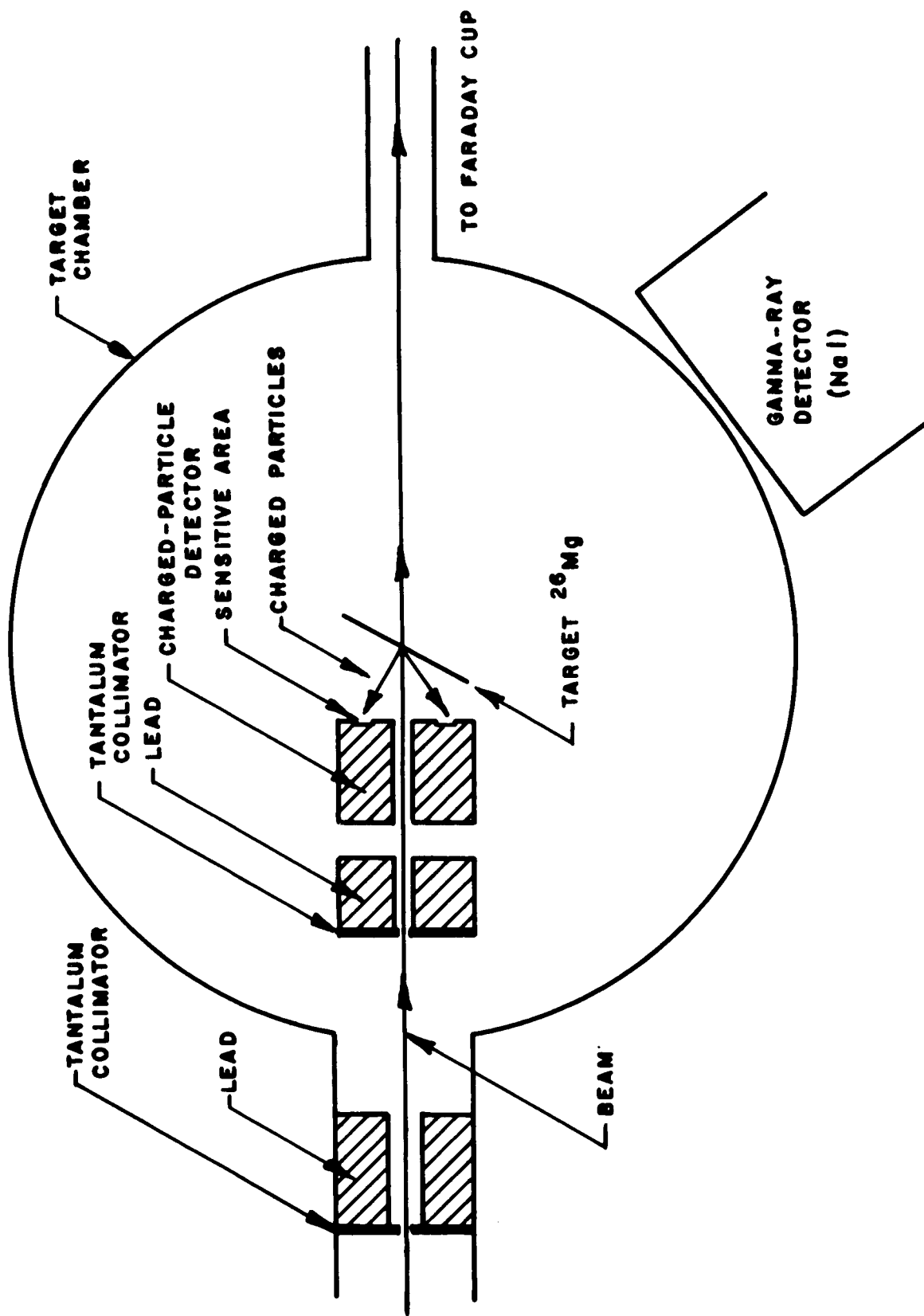
2.3 Experimental Apparatus

The states of ^{27}Mg were excited by means of the $^{26}\text{Mg}(d,p)^{27}\text{Mg}$ reaction using 5.5 and 6.0 MeV deuterons from the University of Alberta Van de Graaff[†]. The experimental arrangement illustrated in fig. 2.1 shows the deuteron beam as it passes through collimators, a hole in the charged particle detector, and the target. It is then stopped and measured by a Faraday cup located approximately one meter from the target. The charged particles from the reaction are detected at angles close to 180° with respect to the beam direction by the charged particle detector. The gamma rays are detected in a NaI(Tl) counter which can be moved in an arc about the center of the target in the plane of the paper (refer to fig. 2.1).

The collimators consisted of a two-foot long system of lead-backed tantalum apertures which were $3/8$, $1/4$, $1/8$, $1/16$ and $3/32$ in. diameter in that order. A liquid nitrogen carbon trap was located between the

[†]Model CN, High Voltage Engineering, Burlington, Massachusetts, U.S.A.

Fig. 2.1 The target chamber.



first and second collimator to reduce carbon buildup on the target. The first four collimators were backed by lead cylinders 1-1/2 in. long with a 1/4 in. hole in the center. The final collimator which was located inside the target chamber (refer to fig. 2.1) was backed by 1 in. of lead with an 1/8 in. hole. It served to prevent the beam from striking the back of the charged-particle detector and to reduce the intensity of low energy gamma rays from the collimator which would adversely affect the resolution of the particle detector. Typically, the beam current on target with this system was about 30 nanoamperes. The beam continued on through the target and was stopped in a Faraday cup at the end of the one meter long beam catching tube. The 180° scattering from the beam stop into the charged-particle detector was negligible.

The charged particles were detected in an annular silicon surface barrier detector[†] located 180° to the beam approximately 2 cm. from the target. The central hole in the detector was 3 mm. diameter with an inner and outer diameter of the sensitive surface of 5.5 mm and 7.5 mm respectively. The sensitive area was covered by two 0.05 mm mylar foils to degrade the α -particles produced in the $^{26}\text{Mg}(d,\alpha)^{24}\text{Na}$ reaction.

The gamma rays were detected in a 7.6 cm. x 7.6 cm. NaI(Tl) crystal^{††} with its front face 10 cm. from the target. A 1/8 in.

[†]Nuclear Diodes, 10,000 Ω -cm., 750 microns depletion depth at 200 volts bias.

^{††}Harshaw "Integral Line" Assembly type 12S12/3.

thick lead sheet was placed in front of the detector to reduce the intensity of low energy gamma rays. The gamma-ray detector support assembly, or goniometer, was modeled after a design obtained from Brookhaven National Laboratory. The detector was positioned at angles between 31° and 90° to the beam direction. It was not possible to place the detector at angles smaller than 31° due to interference of the beam catching tube.

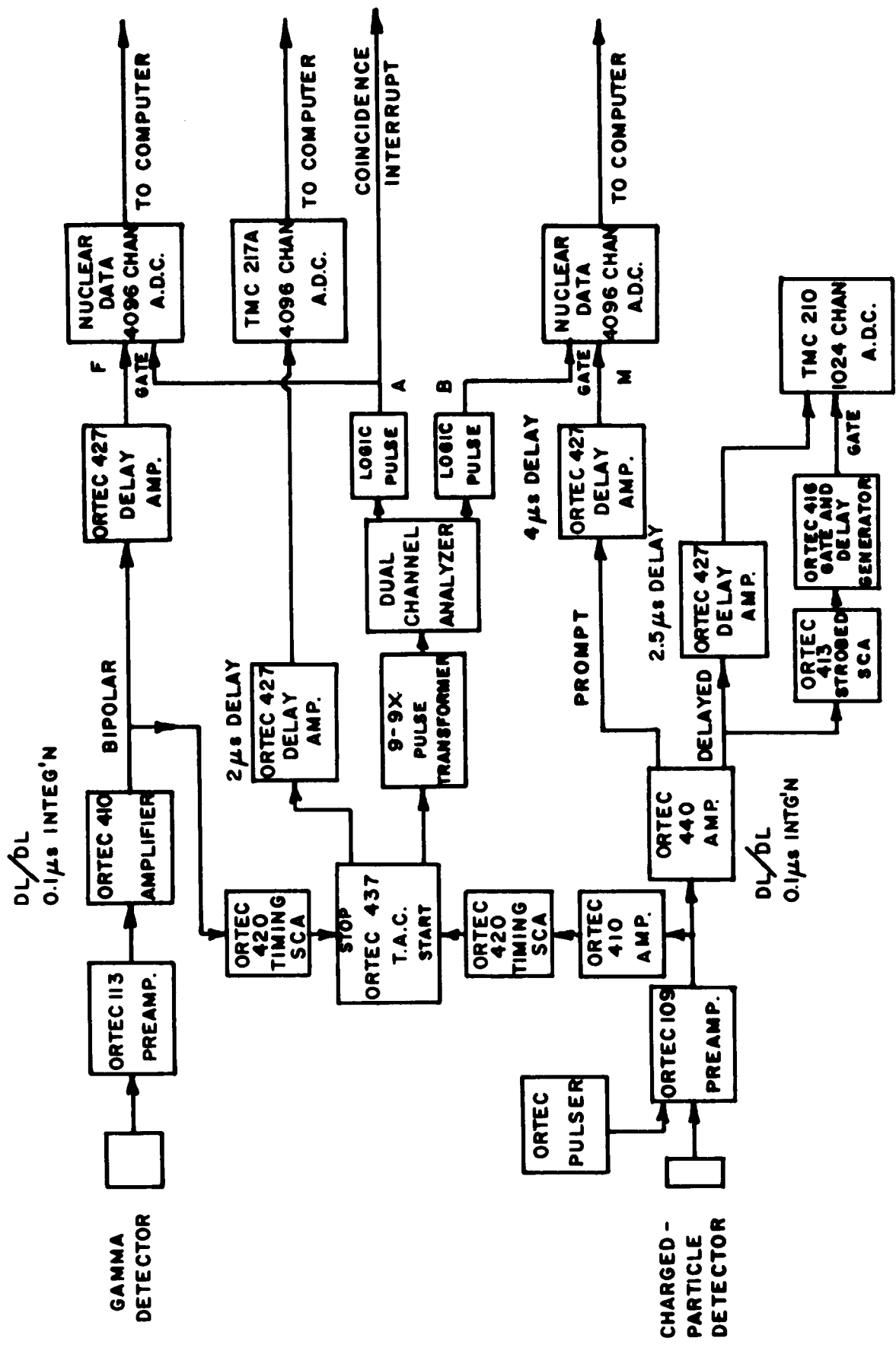
The target, target chamber, gamma-ray detector and goniometer were aligned mechanically so that the center of the target was on the axis of rotation of the gamma-ray counter to within $\pm 1/2$ mm. This alignment was checked experimentally using the $^{12}\text{C}(^3\text{He},p)^{14}\text{N}$ reaction to excite the $J^\pi = 0^+$, 2.31 MeV level of ^{14}N which has an isotropic gamma-ray angular distribution. The gamma-ray intensity was measured at four angles with respect to the beam and found to be isotropic to within the statistical uncertainty of 2% ($a_2/a_0 = 0.011 \pm 0.025$, $a_4/a_0 = -0.006 \pm 0.047$).

The target was an isotopically pure self-supporting foil of 99.4% ^{26}Mg rolled to a thickness of $210 \mu\text{g}/\text{cm}^2$ by Oak Ridge National Laboratory.

2.4 Electronics

A block diagram of the electronics is shown in fig. 2.2. This arrangement is a standard fast-slow coincidence between the gamma-ray counter and the charged-particle counter. The coincidence pulses were

Fig. 2.2 The electronics.



used to gate two analog-to-digital converters (ADC's) which were interfaced on-line with a SDS 920 computer.

The pulses from the charged-particle detector were preamplified[†] and fanned out into two amplifiers. One signal went through an Ortec 410 amplifier^{††} and into a timing single channel analyzer (SCA) which provided a timing signal to start the time-to-amplitude converter (TAC). The other signal was fed through an amplifier and delay into the M side of a 4096 channel ND-161F Dual Analog to Digital Converter^{†††} (ADC).

The pulses from the gamma-ray detector were preamplified^{††††} fed into an Ortec 410 amplifier and fanned out. One signal was fed into an Ortec 420 timing SCA which provided a timing signal for the stop input of the TAC. The other signal went through a delay and into the F side of the Nuclear Data ADC.

The output of the TAC was fed through a 9 - 9X transformer into a dual channel analyzer^{†††††} with which two adjacent 40 nanosecond windows were set on the time spectrum. The lower window was set around the time-coincidence peak and corresponded to true-plus-random events. The upper window was set on the flat portion of the time

[†]Ortec Model 109 Transistor Preamplifier.

^{††}Unless stated otherwise the electronic components are from the Ortec Model 400 series.

^{†††}Nuclear Data Inc., Palatine, Illinois

^{††††}Ortec Model 113 Scintillation Preamplifier.

^{†††††}F.S. Goulding and R.A. McNaught, Nucl. Instr. and Methods 9 (1960) 282.

spectrum and corresponded to random events only. The output corresponding to the lower window (marked A in fig. 2.2) was used to gate the F side of the Nuclear Data ADC and the output corresponding to the upper window (marked B in fig. 2.2) was used to gate the M side of the ADC. Both the F and M sides of the ADC were modified so that both gates would be open when there was a signal from either A or B.

The Nuclear Data ADC's were interfaced with an SDS 920 on-line computer. The computer had eight levels of priority interrupt and a memory capacity of 16,834 words of 24 bits each.

The computer was used primarily for sorting the gamma-ray counts into different regions of memory according to charged-particle pulse height. Up to 18 windows could be set on the charged-particle spectrum at one time. In addition, the spectra could be further subdivided into true-plus-randoms spectra and randoms only spectra by making use of the computer interrupt signal (refer to fig. 2.2). Thus, up to 32 gamma-ray spectra of 256 channels each could be stored in memory along with 1024 channels of the total true-plus-randoms charged particles and the corresponding 1024 channels of the total randoms charged particles.

The computer was also used to monitor the true-plus-randoms window set on the TAC. By making use of the coincidence interrupt signal, the computer was able to store those events falling within the true-plus-randoms window in one 128 channel region of memory and the total TAC spectrum in another region.

It was possible to display any of the spectra on a display unit while counting was in progress. This enabled continuous monitoring

of these spectra to check for any gain shifts.

In addition, a portion of the ungated charged-particle spectrum was monitored on a separate ADC[†]. This was done by using the second output from the Ortec 440 amplifier which was fanned out to an Ortec 427 delay amplifier and a strobed SCA. The delayed output was fed to the ADC while the output from the SCA was shaped by a gate and delay generator and used to gate the ADC. Selected peaks in this spectrum were used to normalize the points on the gamma-ray angular distributions.

The data stored in the computer during each run was transferred to magnetic tape for further processing off-line on the University of Alberta IBM 360/67 computer. The programs used in this analysis are described in the next section.

2.5 Spectrum Analysis

A gamma ray loses energy in a detector by one or more of three processes, photoelectric absorption, Compton scattering and positron-electron pair production. Photoelectric absorption and multiple processes, such as Compton scattering followed by photoelectric absorption of the scattered gamma ray, produce pulses corresponding to the gamma ray losing all its energy in the crystal. These processes give rise to a full energy peak in the spectrum. Compton scattering produces

[†]Technical Measurements Corp. Model 210 1024 Channel Pulse Height Analyzer.

a continuous distribution of pulse heights from the detector with a maximum pulse height less than that produced by the full energy peak. Pair production results in a peak at the full energy, E_γ , minus 0.511 MeV corresponding to the escape of one 0.511 MeV gamma ray from the annihilation of the positron-electron pair and a peak at the full energy minus 1.022 MeV corresponding to the escape of both 0.511 MeV gamma rays. The cross-sections for these three processes vary strongly with gamma-ray energy. Therefore, the total line shape produced by a monoenergetic gamma ray will be a strong function of the gamma-ray energy.

Since it is not feasible to obtain monoenergetic gamma-ray sources for every gamma-ray energy of interest some form of interpolation is necessary to construct standard shapes. The method used to generate the standard shapes for this thesis is based on a method used by Sowerby (So 67). This method is described in detail in an internal report[†] and will only be outlined here (refer to Appendix A).

Peaks of unit height and zero width are placed at the full energy of the gamma ray, at $E_\gamma - 0.511$ MeV and $E_\gamma - 1.022$ MeV. A modified Gaussian distribution of the form used by Heath et al. (He 65) was folded into each of these peaks to account for the finite resolution of the gamma-ray detector. Experimental data for the variation of the relative heights of these three peaks was used to adjust the

[†]D.H. Sykes and D.A. Hutcheon, University of Alberta Internal Report, 1968.

escape peak heights relative to the height of the full energy peak.

The Compton distribution was calculated from theory and modified to account for the finite resolution of the detector and multiple Compton scattering effects. An accurate correction for multiple Compton scattering would be exceedingly difficult; however, the following approximate corrections proved to be adequate. The absorption curve for gamma rays in a NaI crystal (Ev 55) was used to remove the Compton scattered gamma rays which interact with the crystal again after being Compton scattered. Those gamma rays undergoing more than one Compton scattering were approximately accounted for by folding into the distribution a modified Gaussian distribution (He 65) the width of which is adjusted to give the best fit to the standard spectra. These standard spectra were obtained from previous data (Ve 68) and gamma-ray sources.

This Compton distribution was added to the peaks using experimental data from the standard spectra to adjust the height of the Compton distribution relative to the full energy peak.

The intensities of the individual gamma rays in the gamma-ray spectra from ^{27}Mg were obtained using a least-squares spectrum stripping program. The line shapes used in the fitting procedure were constructed as described above. These line shapes were felt to be adequate because when they were used to fit the present data, the χ^2 values which resulted were typically close to the 50% confidence limit. Error in the line shapes was taken into consideration by multiplying the error bars produced in the fitting by $\sqrt{\chi^2}$ for χ^2 greater than 1.0.

The spectrum stripping program could be used either to "strip off" the individual gamma-ray line shapes starting at the highest energy gamma-ray in the spectrum or to fit a group of as many as 20 peaks at one time. The program could also vary the positions (energy) of any number of gamma-ray peaks to search for the positions yielding the lowest χ^2 . In the present work, the peaks were normally fixed in position according to their energy and the calibration curve. The errors in the intensity were adjusted to allow for any error in the calibration curve. Only in cases where the peaks had very good statistics were the peak positions allowed to vary freely.

It was found necessary to correct the peak intensities produced in this manner in some cases to account for the overlapping of the tails of the charged-particle peaks since "clean" windows could not be set on some of the peaks of interest. The numbers used in this correction were obtained by fitting the spectrum using a peak fitting program written by Tepel (Te 66). This program was modified so that it was possible to obtain the fraction of every peak falling within a given window. These numbers were used to unfold the contributions to the gamma-ray spectra from each level. This procedure also corrected for any error introduced due to gain shifts in the charged-particle spectrum.

Branching ratios were obtained from the angular distributions by fitting each distribution with a Legendre polynomial expansion using a least-squares analysis. The a_0 coefficient obtained in the fit is proportional to the intensity of gamma-ray emission into

a solid angle of 4π steradians. The a_0 coefficients for all transitions for a given level were used to calculate the branching ratios. The errors in the branching ratios were determined from the error in the a_0 coefficients determined in the least-squares fitting procedure.

CHAPTER III

EXPERIMENTAL RESULTS

The following is a detailed discussion of the experimental results which are summarized in tables 3.1, 3.2 and 3.3. In addition, a summary of the previously known information concerning the spins and parities of levels of ^{27}Mg is shown in fig. 3.1 together with data concerning the spins and branching ratios measured in the present work.

In the following discussion, the gamma-ray spectrum for each of the observed levels has been included. Each spectrum is the sum of 7 spectra measured at 5 angles with respect to the beam unless stated otherwise.

3.1 Yield Curve and Choice of Bombarding Energies

A charged-particle yield curve was measured over an energy range from 2.5 to 6.1 MeV in steps of 0.1 MeV. The levels of interest appeared to have a maximum or near maximum yield at 5.5 and 6.0 MeV bombarding energy, therefore, these energies were selected for coincidence measurements. A typical charged-particle spectrum measured at a bombarding energy of 5.5 MeV in coincidence with a gamma-ray detector at 55° to the beam direction is shown in fig. 3.2. The window settings used for sorting the gamma rays into different

Fig. 3.1 A summary of spin and parity assignments for ^{27}Mg from
(a) previous work and a summary of the decay modes and
spin assignments from (b) the present work. Unlikely
spin assignments are enclosed in parentheses. The x
indicates the existence of a decay whose relative
strength is unknown.

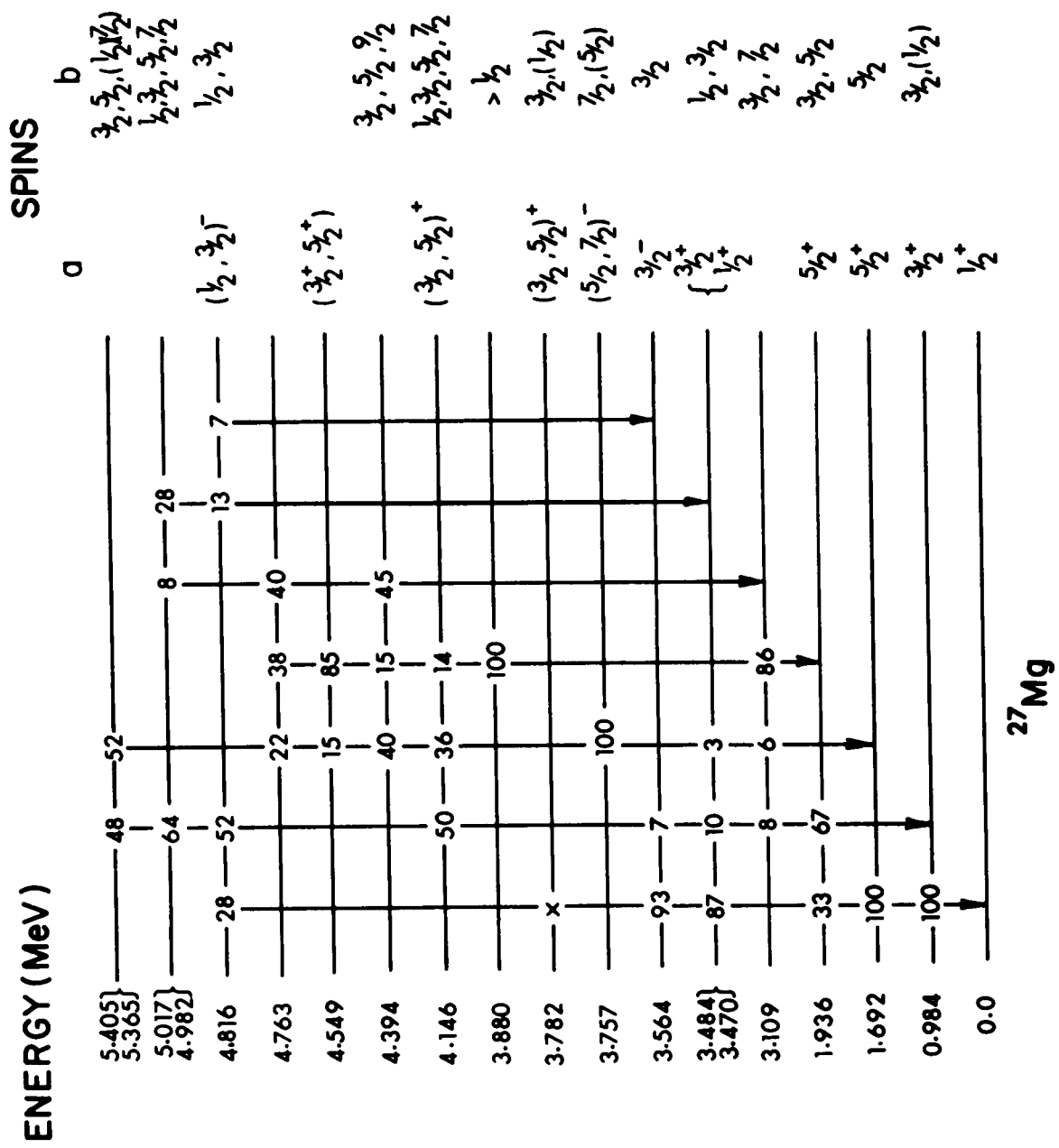


Fig. 3.2 The charged-particle spectrum measured at 180° to the beam in coincidence with a gamma-ray detector at 55° for a deuteron bombarding energy of 5.5 MeV. The proton peaks are identified by the excitation energies of the states in ^{27}Mg to which they correspond. The open circles are points on the simultaneous randoms spectrum. The window settings used for sorting are marked below the spectrum.

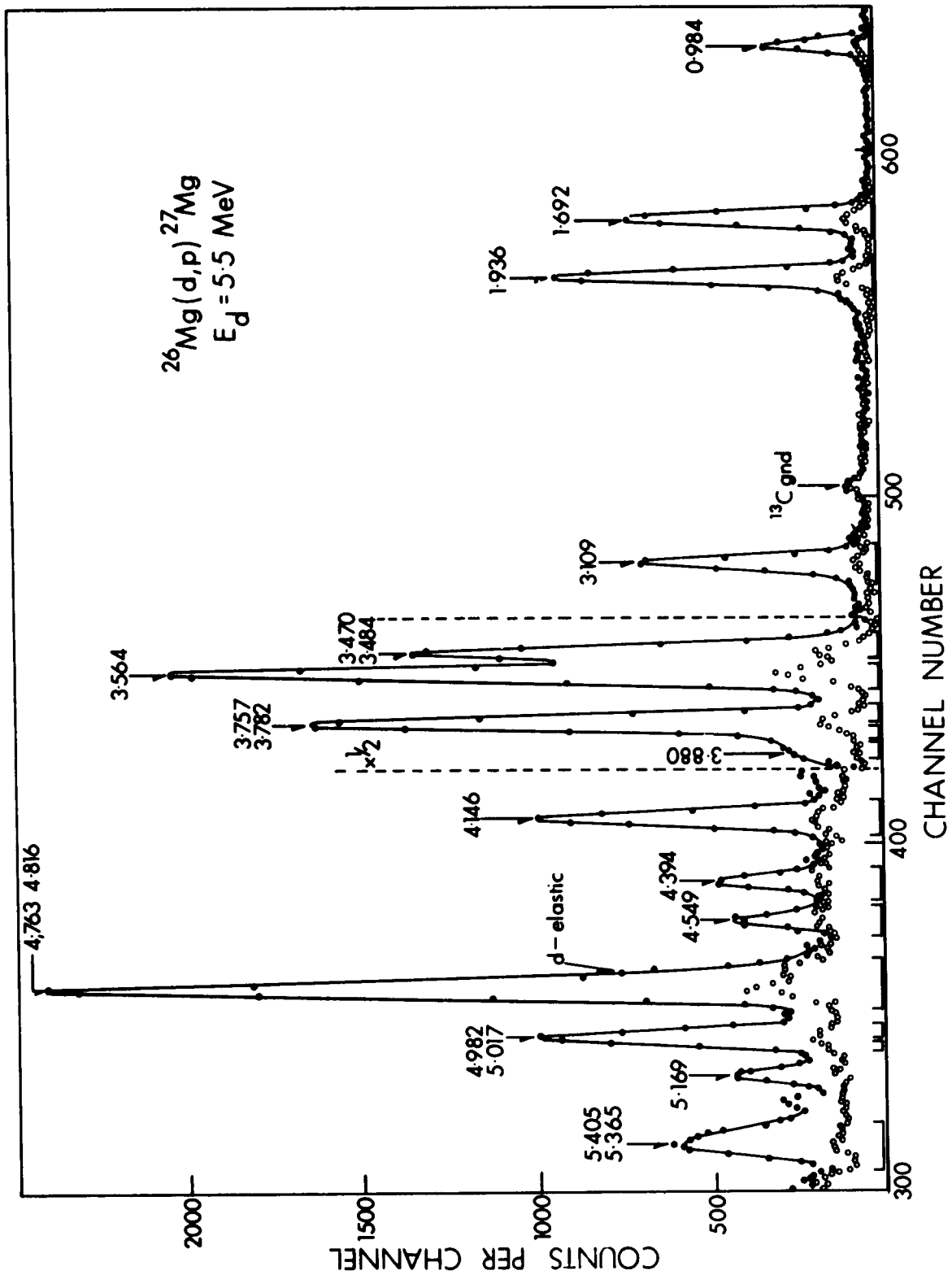


TABLE 3.1

A Summary of Spin Assignments and Mixing Ratio Solutions

Energy Level (MeV)	Decay Transition	Assumed Spin Sequence	χ^2_{\min}	Solutions of Mixing Ratio x
0.984	0.984 \rightarrow 0	$\frac{1}{2} \rightarrow \frac{1}{2}$ $\frac{3}{2} \rightarrow \frac{1}{2}$	1.9 0.32	UNDEFINED
1.692	1.692 \rightarrow 0	$\frac{5}{2} \rightarrow \frac{1}{2}$	1.2	$(-5.7^{+3.6}_{-5.7})$, $(-0.6^{+0.10}_{-0.40})$, $(0.14^{+0.22}_{-0.16})$ or $(2.0^{+1.3}_{-0.7})$
1.936	1.936 \rightarrow 0 (1) 1.936 \rightarrow 0.984 (2) 0.984 \rightarrow 0	$\frac{3}{2} \rightarrow \frac{1}{2}$ $\frac{5}{2} \rightarrow \frac{1}{2}$ $\frac{3}{2} \rightarrow \frac{3}{2} \rightarrow \frac{1}{2}$ $\frac{5}{2} \rightarrow \frac{3}{2} \rightarrow \frac{1}{2}$	0.84 0.84 0.47 0.7	UNDEFINED $-0.47 \leq x \leq \infty$ $(-\infty \leq x_1 \leq 0.3)$ or $(+0.6 \leq x_1 \leq \infty)$, x_2 UNDEFINED $0.5 \leq x_1 \leq 4.0$, x_2 UNDEFINED
3.109	3.109 \rightarrow 1.936	$\frac{3}{2} \rightarrow \frac{5}{2}$ $\frac{7}{2} \rightarrow \frac{5}{2}$	0.62 0.58	$-7.0 \leq x \leq -0.38$ $0.09 \leq x \leq 2.6$
$\left. \begin{matrix} 3.470 \\ 3.484 \end{matrix} \right\}$	$\left. \begin{matrix} 3.470 \\ 3.484 \end{matrix} \right\} \rightarrow 0$	$\frac{1}{2} \rightarrow \frac{1}{2}$ $\frac{3}{2} \rightarrow \frac{1}{2}$	2.1 2.6	UNDEFINED
3.564	3.564 \rightarrow 0	$\frac{3}{2} \rightarrow \frac{1}{2}$	1.9	$(-\infty \leq x \leq -0.55)$, $(-0.02 \leq x \leq 1.8)$ or $(57 \leq x \leq \infty)$

Table 3.1 (continued)

Energy Level (MeV)	Decay Transition	Assumed Spin Sequence	χ^2_{\min}	Solutions of Mixing Ratio x
3.757	(1) 3.757→1.692	$\frac{5}{2} \rightarrow \frac{5}{2} \rightarrow \frac{1}{2}$	2.0	$x_1 = 0.93 \pm 0.15$ for $x_2 = -5.7$ or -0.6
	(2) 1.692→0	$\frac{7}{2} \rightarrow \frac{5}{2} \rightarrow \frac{1}{2}$	0.95	$x_1 = 0.02 \pm 0.07$ for $x_2 = 0.14$ or 2.0
3.782	3.782→0	$\frac{1}{2} \rightarrow \frac{1}{2}$	3.6	UNDEFINED
		$\frac{3}{2} \rightarrow \frac{1}{2}$	0.97	
3.880	3.880→1.936	$\frac{1}{2} \rightarrow \frac{5}{2}$		
4.146	(1) 4.146→0.984	$\frac{1}{2} \rightarrow \frac{3}{2}$	1.4	
	(2) 4.146→1.692	$\frac{1}{2} \rightarrow \frac{5}{2}$		
	4.146→0.984	$\frac{3}{2} \rightarrow \frac{3}{2}$	0.2	UNDEFINED
		$\frac{5}{2} \rightarrow \frac{3}{2}$	0.2	$-0.36 \leq x \leq \infty$
		$\frac{7}{2} \rightarrow \frac{3}{2}$	0.9	$0.17 \leq x \leq 3.8$
	4.146→1.692	$\frac{3}{2} \rightarrow \frac{5}{2}$	0.7	UNDEFINED
		$\frac{5}{2} \rightarrow \frac{5}{2}$	0.5	$-\infty \leq x \leq 1.3$
		$\frac{7}{2} \rightarrow \frac{5}{2}$	0.6	$(-\infty < x < -0.1)$ or $(x > 5.7)$
	4.146→1.936	$\frac{3}{2} \rightarrow \frac{5}{2}$	1.1	UNDEFINED
		$\frac{5}{2} \rightarrow \frac{5}{2}$	1.2	UNDEFINED
		$\frac{7}{2} \rightarrow \frac{5}{2}$	1.2	$(-\infty < x < 0.35)$ or $(1.4 < x < \infty)$

Table 3.1 (continued)

Energy Level (MeV)	Decay Transition	Assumed Spin Sequence	χ^2_{\min}	Solutions of Mixing Ratio x
4.394	(1) 4.394 \rightarrow 3.109 (2) 4.394 \rightarrow 1.692	$\frac{3}{2} \rightarrow \frac{3}{2}$ }	0.62	$-3.7 \leq x_1 \leq 0$ $(-\infty \leq x_2 \leq 0.18)$ or $x_2 \geq 2.1$
		$\frac{3}{2} \rightarrow \frac{5}{2}$ }		
		$\frac{5}{2} \rightarrow \frac{3}{2}$ }	0.61	$0 \leq x_1 \leq 3.7$ $-3.7 \leq x_2 \leq 0.36$
		$\frac{5}{2} \rightarrow \frac{5}{2}$ }		
		$\frac{3}{2} \rightarrow \frac{7}{2}$ }	1.4	$-2.7 \leq x_1 \leq -0.6$ $0.27 \leq x_2 \leq 2.7$
		$\frac{3}{2} \rightarrow \frac{5}{2}$ }		
		$\frac{5}{2} \rightarrow \frac{7}{2}$ }	0.54	$-11.4 \leq x_1 \leq -0.18$ $-11.4 \leq x_2 \leq +0.27$
		$\frac{5}{2} \rightarrow \frac{5}{2}$ }		
	4.394 \rightarrow 3.109	$\frac{9}{2} \rightarrow \frac{7}{2}$	0.9	$0.09 \leq x \leq 3.7$
	4.394 \rightarrow 1.692	$\frac{9}{2} \rightarrow \frac{5}{2}$	0.8	UNDEFINED
4.816	4.816 \rightarrow 0	$\frac{1}{2} \rightarrow \frac{1}{2}$	2.2	UNDEFINED
		$\frac{3}{2} \rightarrow \frac{1}{2}$	1.9	
	4.816 \rightarrow 0.984	$\frac{1}{2} \rightarrow \frac{3}{2}$	1.1	UNDEFINED
		$\frac{3}{2} \rightarrow \frac{3}{2}$	1.6	

Table 3.1 (continued)

Energy Level (MeV)	Decay Transition	Assumed Spin Sequence	χ^2_{\min}	Solutions of Mixing Ratio x
4.982 } 5.017 }	4.982 } 5.017 } $\rightarrow 0.984$	$\frac{1}{2} \rightarrow \frac{3}{2}$	1.4	$(-\infty \leq x \leq -4.0)$ or $(-1.3 \leq x \leq \infty)$ $-0.1 \leq x \leq \infty$
		$\frac{3}{2} \rightarrow \frac{3}{2}$	1.8	
		$\frac{5}{2} \rightarrow \frac{3}{2}$	1.6	
		$\frac{7}{2} \rightarrow \frac{3}{2}$	1.7	
5.365 } 5.405 }	5.365 } 5.405 } $\rightarrow 0.984$	$\frac{1}{2} \rightarrow \frac{3}{2}$	3.4	$-0.25 \leq x \leq 30$ $0.45 \leq x \leq 1.8$
		$\frac{3}{2} \rightarrow \frac{3}{2}$	0.32	
		$\frac{5}{2} \rightarrow \frac{3}{2}$	0.32	
		$\frac{7}{2} \rightarrow \frac{3}{2}$	3.4	

TABLE 3.2

A Summary of the Branching Ratio Measurements

Initial State	Final State	E_γ (MeV)	Branching Ratio	
			Present	Previous
1.692	0	1.692	100	100
	0.984	0.708	< 5	
1.936	0	1.936	33 ± 2	30 ± 7
	0.984	0.952	67 ± 2	70 ± 4
	1.692	0.244	< 5	
3.109	0	3.109	< 3	
	0.984	2.125	8 ± 2	
	1.692	1.417	6 ± 2	
	1.936	1.173	86 ± 4	(100)
3.470 } 3.484 }	0		87 ± 2	100
	0.984		10 ± 2	
	1.692		3 ± 2	
3.564	0	3.564	93 ± 2	100
	0.984	2.580	7 ± 2	
3.757	0.984	2.773	< 5	6 ± 3
	1.692	2.065	100	91 ± 9
	1.936	1.821	< 5	
	3.109	0.648	< 3	2 ± 1
3.782	0	3.782	NOT DEFINED	

Table 3.2 (continued)

Initial State	Final State	E_γ (MeV)	Branching Ratio	
			Present	Previous
3.880	1.936	1.944	100	
4.146	0.984	3.162	50 ± 3	
	1.692	2.454	36 ± 3	
	1.936	2.210	14 ± 3	
4.394	0	4.394	< 3	
	1.692	2.702	40 ± 6	
	1.936	2.458	15 ± 5	
	3.109	1.285	45 ± 6	
4.549	0.984	3.565	< 15	
	1.692	2.857	15 ± 7	
	1.936	2.613	85 ± 13	
4.763	1.692	3.071	22 ± 4	
	1.936	2.827	38 ± 7	
	3.109	1.654	40 ± 15	
4.816	0	4.816	28 ± 5	
	0.984	3.832	52 ± 8	
	3.470, 3.484	1.33, 1.34	13 ± 10	
	3.564	1.252	7 ± 5	
	3.880	0.936	< 15	
4.982 } 5.017 }	0.984		64 ± 10	
	1.692		< 5	
	3.109		8 ± 5	
	3.423		≤ 15	
	3.470, 3.484		28 ± 15	
	3.564		≤ 30	
	3.880		≤ 5	
5.365 } 5.405 }	0.984		48 ± 8	
	1.692		52 ± 8	

TABLE 3.3

A Summary of a_2 and a_4 Coefficients from Legendre Polynomial Fits
to the Angular Distribution

Energy Level (MeV)	Decay Transition	a_2/a_0	a_4/a_0	χ^2
0.984	0.984 \rightarrow 0	-0.113 ± 0.041	-0.0066 ± 0.077	0.15
1.692	1.692 \rightarrow 0	0.398 ± 0.277	-0.469 ± 0.048	0.5
1.936	1.936 \rightarrow 0	0.202 ± 0.059	0.009 ± 0.103	0.35
3.109	3.109 \rightarrow 1.936	-0.717 ± 0.05	-0.054 ± 0.98	0.25
	3.109 \rightarrow 0.984	0.276 ± 0.27	0.355 ± 0.48	0.47
3.470-3.484	3.470-3.484 \rightarrow 0	-0.0133 ± 0.04	0.079 ± 0.069	1.7
3.564	3.564 \rightarrow 0	-0.498 ± 0.028	0.113 ± 0.051	0.2
3.757	3.757 \rightarrow 1.692	-0.348 ± 0.024	-0.017 ± 0.044	0.25
	1.692 \rightarrow 0	0.371 ± 0.032	-0.250 ± 0.051	0.5
3.782	3.782 \rightarrow 0	-0.360 ± 0.111	0.049 ± 0.206	0.4
4.146	4.146 \rightarrow 0.984	-0.142 ± 0.076	0.108 ± 0.144	0.03
	4.146 \rightarrow 1.692	0.319 ± 0.113	0.221 ± 0.20	0.17
	4.146 \rightarrow 1.936	0.173 ± 0.274	-0.750 ± 0.50	0.3
4.394	4.394 \rightarrow 3.109	-1.05 ± 0.163	-0.29 ± 0.29	0.2
	4.394 \rightarrow 1.692	0.559 ± 0.19	-0.386 ± 0.35	0.3
	4.394 \rightarrow 1.936	-0.288 ± 0.52	1.29 ± 0.98	0.3
	3.109 \rightarrow 1.936	-0.619 ± 0.200	0.116 ± 0.393	0.2
4.549	4.549 \rightarrow 1.936	0.29 ± 0.15	0.47 ± 0.29	3.1
4.816	4.816 \rightarrow 0	-0.049 ± 0.045	0.028 ± 0.083	1.7
	4.816 \rightarrow 0.984	-0.023 ± 0.063	0.147 ± 0.115	0.65
4.982-5.017	4.982-5.017 \rightarrow 0.984	-0.061 ± 0.119	-0.172 ± 0.221	1.2
5.365-5.405	5.365-5.405 \rightarrow 0.984	-0.228 ± 0.073	0.109 ± 0.142	0.1
	5.365-5.405 \rightarrow 1.692	0.08 ± 0.134	0.017 ± 0.239	3.2

regions of computer memory are indicated below the spectrum.

Two separate gamma-ray angular distributions were measured at 5.5 MeV. One set of measurements was taken at four angles with respect to the beam, 31° , 45° , 60° and 90° with repeat measurements at two of these angles to check reproducibility. Another set of measurements was taken at 5 angles, 31° , 43° , 55° , 66° and 90° with repeat measurements at three of these angles where these angles were chosen to give approximately equal steps in $\cos^2\theta$. The angular distributions obtained from these two measurements showed very good agreement.

It is desirable to take into consideration both sets of data to determine spins and multipole mixing ratios. Therefore, both gamma-ray angular distributions were normalized to their a_0 coefficients in a Legendre polynomial expansion before the data were combined. The error bars were modified to account for error in the normalization.

In addition to the two measurements at a bombarding energy of 5.5 MeV, one measurement was taken at 6.0 MeV with the gamma-ray counter fixed at 55° to the beam. These data were used in determining branching ratios for some levels. The different yield at this energy helped sort out overlapping spectra. Also, the kinematic shift in charged-particle energy and removal of the degrading foil from in front of the detector for this run assisted in determining the contributions to the spectra from (d,α) reactions.

3.2 The 0.984 MeV Level

The χ^2 analysis of the angular correlation of the $0.984 \rightarrow 0$ MeV transition showed that only spins $J = 1/2$ and $J = 3/2$ gave solutions which fell below the 0.1% confidence limit. The $J = 1/2$ solution was ten times less likely than the $J = 3/2$ solution. This is in agreement with the previous assignment for this level of $J^\pi = 3/2^+$ (En 67).

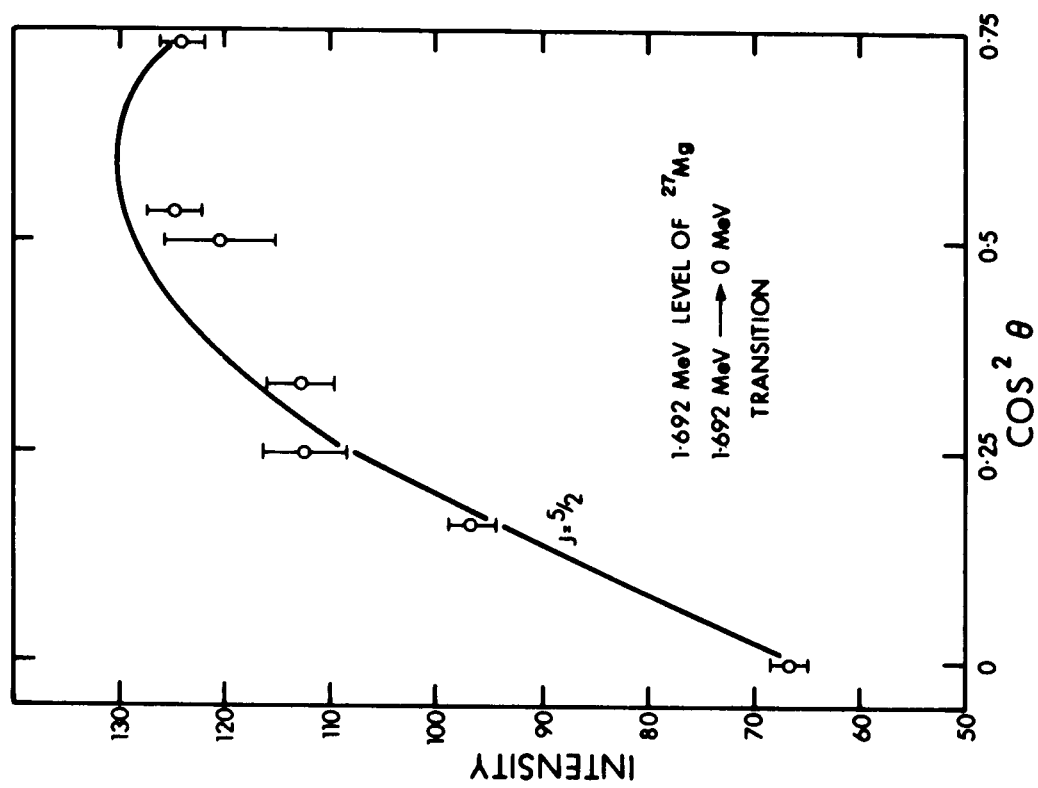
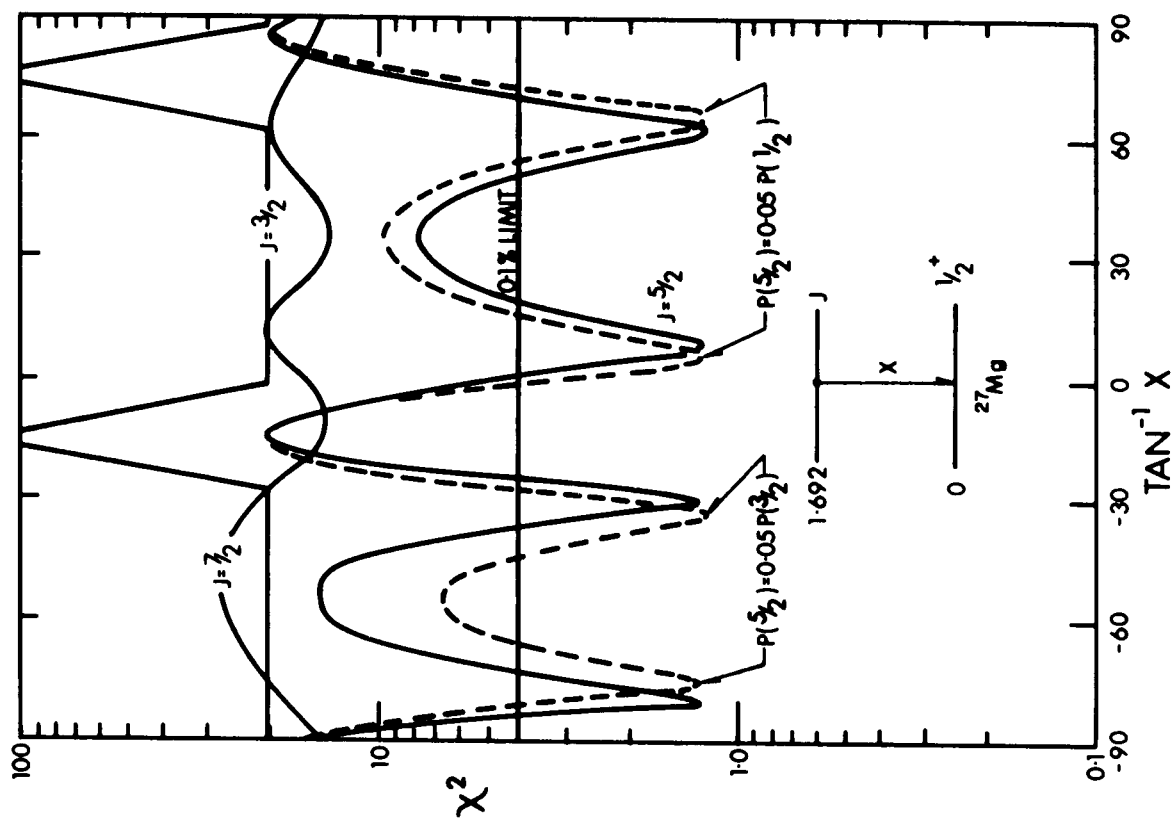
It was not possible to limit the mixing ratio solutions for this transition because acceptable fits were obtained for all mixing ratios. An attempt was made to obtain further information on this mixing ratio by simultaneously fitting the angular distribution of the two unresolved peaks from the $1.936 \rightarrow 0.984$ and $0.984 \rightarrow 0$ MeV transitions from the decay of the 1.936 MeV level. Unfortunately, this procedure also failed to limit the mixing ratio solutions for the $0.984 \rightarrow 0$ MeV transition.

3.3 The 1.692 MeV Level

The χ^2 versus $\arctan x$ plot, and angular distribution for the $1.692 \rightarrow 0$ MeV transition is shown in fig. 3.3. All spins not included on the graph had no solutions with χ^2 less than 100. The only spin value with solutions falling below the 0.1% confidence limit is $J = 5/2$. This result agrees with the previous assignment of $J^\pi = 5/2^+$ (En 67).

Four mixing ratio solutions were found. The $x = -5.7$, $x = -0.6$ and $x = 2.0$ values require greater than 800, 200 and 700 Weisskopf units (W1 60) of M3 transition strength respectively. The data on M3

Fig. 3.3 The angular distribution and χ^2 versus $\arctan x$ for the least-squares fit to the $1.692 \rightarrow 0$ MeV transition from the 1.692 MeV level in ^{27}Mg .



transition strengths for nuclei with $20 \leq A \leq 40$ is very limited (Sk 66), however, all four known M3 transition strengths are less than 10 Weisskopf units and M3 does not compete with E2 in any of these cases. Thus, these solutions can be considered unlikely.

In addition, the negative solutions can be further discriminated against by the results of a simultaneous fit to the $3.757 \rightarrow 1.692$ MeV and the $1.692 \rightarrow 0$ MeV transitions from the 3.757 MeV level. These results show that for $x(1.692 \rightarrow 0) < 0.0$ only one solution falls below the 0.1% confidence limit and this solution is ruled out to the 10% confidence limit.

The $x = 0.14$ solution requires 20 Weisskopf units of M3 transition strength. However, for the range of solutions falling below the 10% confidence limit, the M3 transition strength required ranges between 0.1 and 100 Weisskopf units.

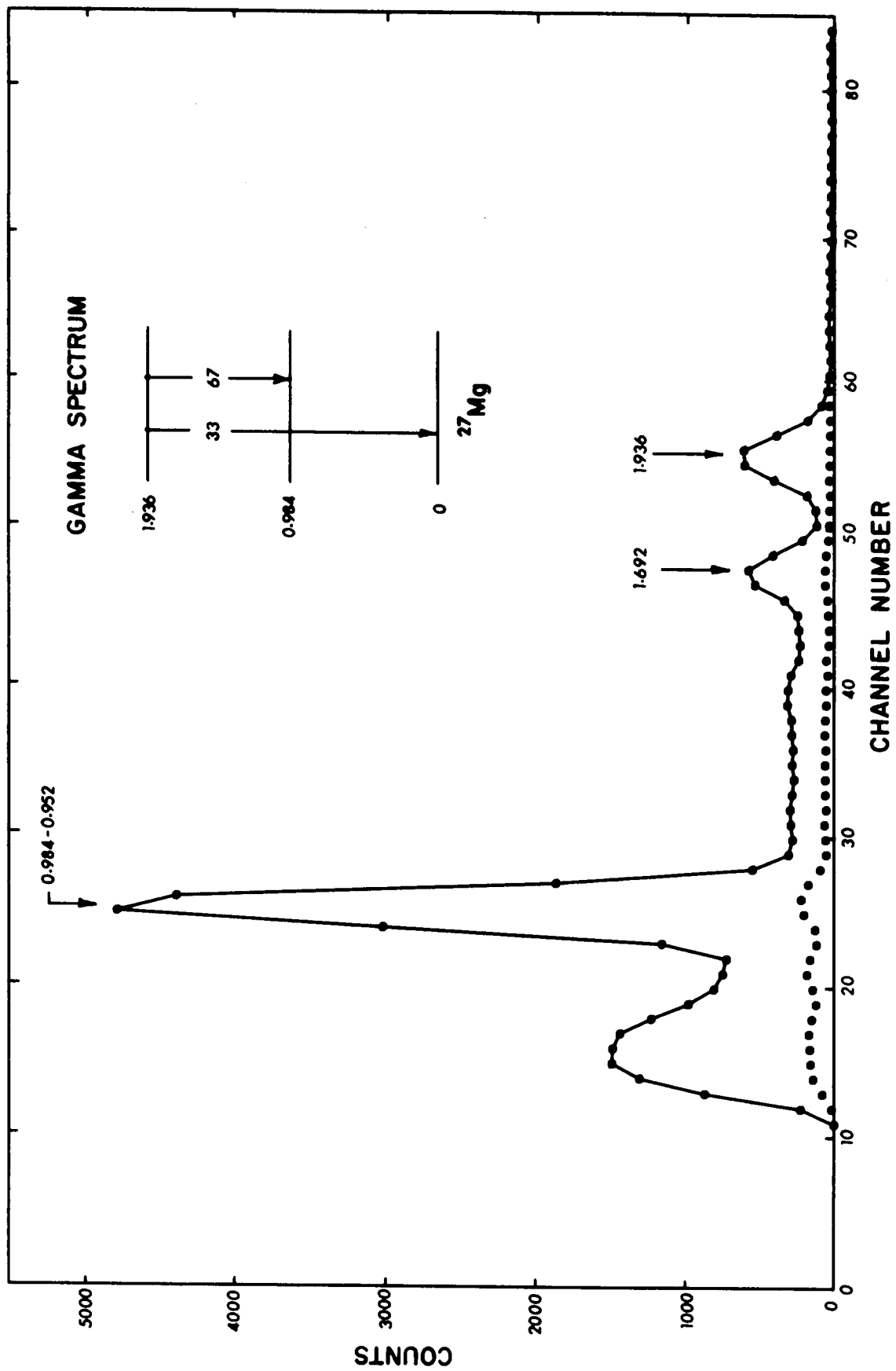
The finite size effect tends to reduce the M3 strength required for the solution near $x = 0.14$ and to increase the M3 strength required for the solution near $x = -0.6$.

Thus the 1.692 MeV level can be assigned $J^\pi = 5/2^+$ with a mixing ratio ($x = 0.14^{+0.22}_{-0.16}$) the most likely value (see table 3.1) for the $1.692 \rightarrow 0$ MeV transition.

3.4 The 1.936 MeV Level

The gamma-ray spectrum measured in coincidence with protons populating the 1.936 MeV level is shown in fig. 3.4. The decay of the

Fig. 3.4 The gamma-rays measured in coincidence with protons populating the 1.936 MeV level of ^{27}Mg . The open circles are points on the simultaneous randoms spectrum.



1.936 MeV level was found to be $(33 \pm 2)\%$ to the ground state and $(67 \pm 2)\%$ to the first excited state. This result is in agreement with previous work (Be 64) in which it was found that the decay was $(30 \pm 7)\%$ and $(70 \pm 4)\%$ to the ground and first excited states respectively.

The present data show a small gamma-ray peak with an energy of about 1.7 MeV in addition to the peaks due to transitions to the ground and first excited states. The overlap between the protons exciting the 1.692 MeV level and those exciting the 1.936 MeV level was estimated by fitting the proton peaks using Tepel's peak fitting program (Te 66). This overlap accounted for about 60% of the observed 1.7 MeV peak. If the remaining 40% of the peak is due to a transition to the 1.692 MeV level, a prominent 0.244 MeV gamma ray should have been seen when the lead was removed from the detector. That such was not the case indicates that the estimate for overlap was too small and there is probably no significant transition from the 1.936 MeV level to the 1.692 MeV level.

The strongest transition from the 1.936 MeV level gives rise to an unresolved 0.952 - 0.984 MeV doublet. The angular distribution of this doublet was fitted using all possible mixing ratio combinations for the $1.936 \rightarrow 0.984$ MeV transition and the $0.984 \rightarrow 0$ MeV transition. In addition, the doublet and the $1.936 \rightarrow 0$ MeV transition were fitted simultaneously and only the $J = 3/2$ and $J = 5/2$ solutions resulted in χ^2 values falling below the 0.1% confidence limit. This result is in agreement with the previous assignment for this level of $J^\pi = 5/2^+$ (En 67). The mixing ratio solutions which were allowed are listed in

table 3.1.

3.5 The 3.109 MeV Level

The gamma-ray spectrum measured in coincidence with protons populating the 3.109 MeV level is shown in fig. 3.5. The branching ratios determined in this work are indicated in the inset to the figure. Although the branching had not been well established for this level in previous studies the main decay was thought to be to the 1.936 MeV level. This agrees with the present results.

The gamma-ray angular distribution for the $3.109 \rightarrow 1.936$ MeV transition and the results of a least-squares fit to this distribution are shown in fig. 3.6. Only the $J = 3/2$ and $J = 7/2$ curves fall below the 0.1% confidence limit. The allowed mixing ratio solution for spin $J = 3/2$ is $(-7.1 \leq x \leq -0.38)$ and for $J = 7/2$ is $(0.09 \leq x \leq 2.6)$. No previous spin assignments or mixing ratio measurements have been made for this level.

A simultaneous fit to the angular distribution of the $3.109 \rightarrow 1.936$ MeV transition with either the $1.936 \rightarrow 0$ MeV or the $0.952 - 0.984$ MeV doublet failed to distinguish between the $J = 3/2$ and $J = 7/2$ solutions or to narrow the limits on the mixing ratios. Also, the transitions to the 0.984 MeV and 1.692 MeV levels proved to be too weak to provide further information.

Fig. 3.5 The gamma-rays in coincidence with protons populating the 3.109 MeV level of ^{27}Mg . The open circles are points on the simultaneous randoms spectrum.

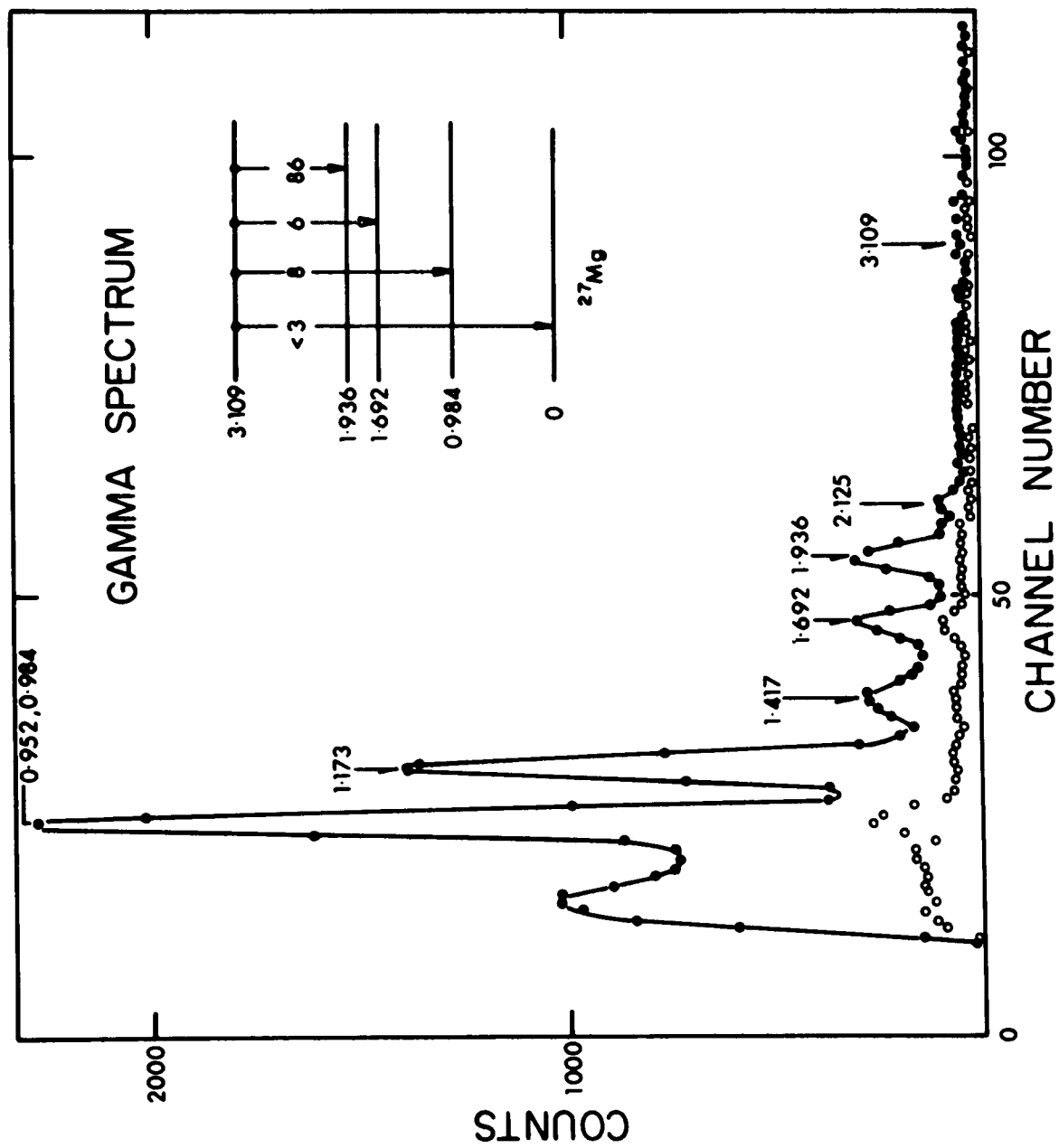
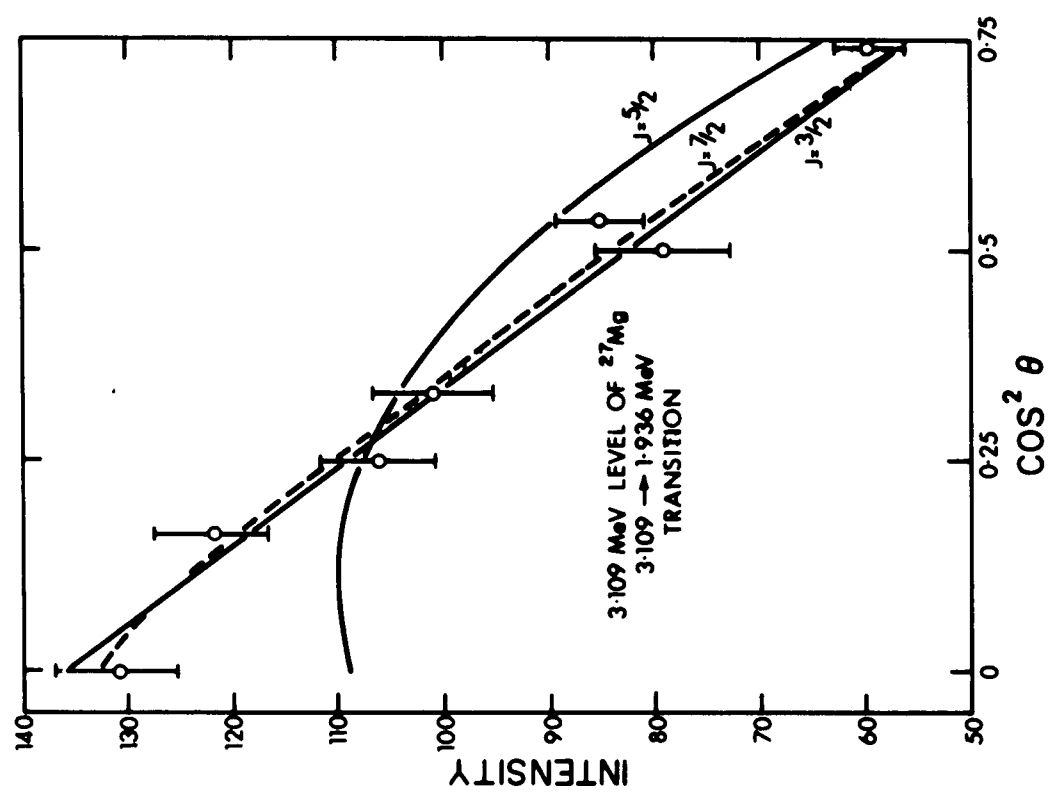
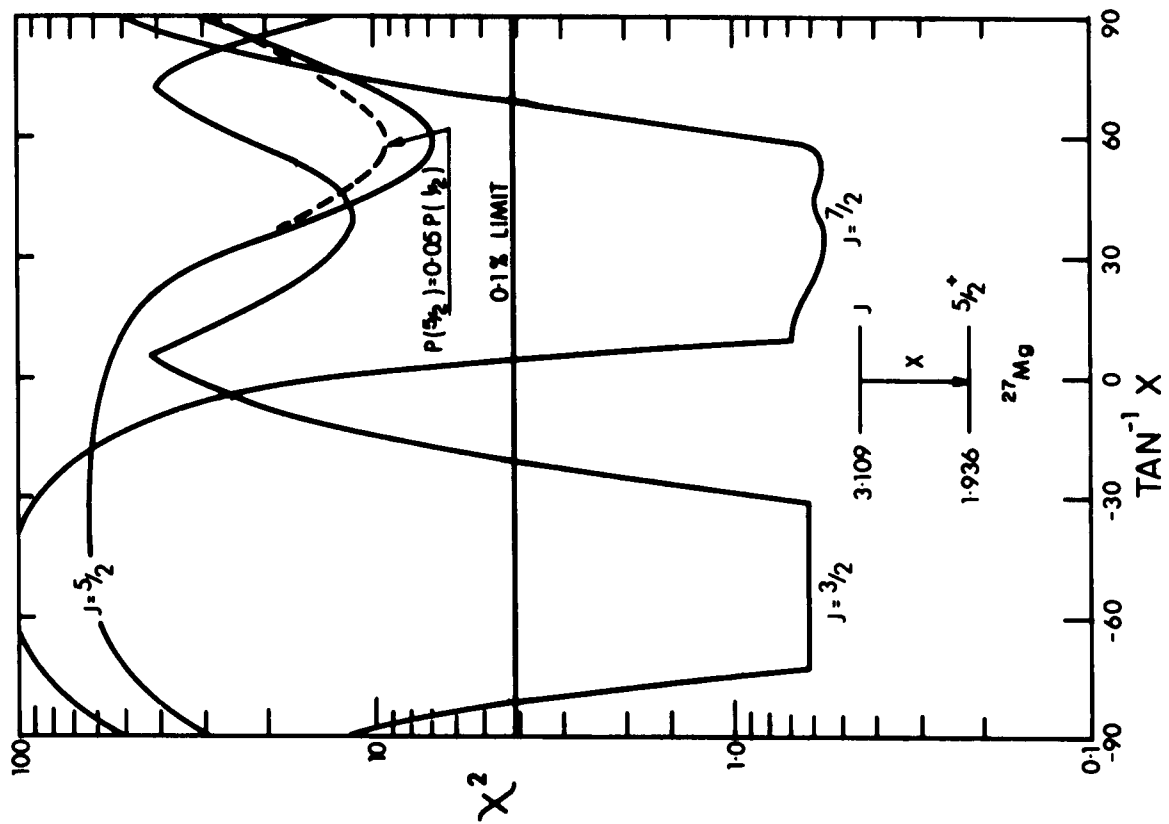


Fig. 3.6 The angular distribution and χ^2 versus $\arctan x$ for the least-squares fit to the 3.109 \rightarrow 1.936 MeV transition from the 3.109 MeV level in ^{27}Mg .



3.6 The 3.470 - 3.484 MeV Doublet

The peak corresponding to protons feeding the 3.470 - 3.484 MeV doublet was not completely separated from those feeding the 3.564 MeV level (refer to fig. 3.2). Therefore, it was necessary to correct the angular distribution for this overlap. This correction could be important since both the 3.470 - 3.484 MeV doublet and the 3.564 MeV level have similar decay schemes (refer to fig. 3.7 and fig. 3.8). The total correction for this overlap was found to be less than 10% so that the corrected gamma-ray angular distribution was not affected greatly by any inaccuracy in the overlap correction.

The corrected angular distribution for the 3.470 - 3.484 \rightarrow 0 MeV transition was fitted using the χ^2 program and only $J = 1/2$ and $J = 3/2$ were found to be acceptable solutions. This agrees with previous results which assign $J = 1/2$ for the 3.470 MeV level and $J = 3/2$ for the 3.484 MeV level (En 67).

3.7 The 3.564 MeV Level

The gamma-ray angular distributions from the 3.564 MeV level were corrected for overlap with the 3.470 - 3.484 MeV doublet. The corrected data showed that in addition to the previously reported ground state transition (Be 64) from this level there is also a $(7 \pm 2)\%$ transition to the first excited state.

The gamma-ray spectrum measured in coincidence with protons populating this level is shown in fig. 3.8.

Fig. 3.7 The gamma-rays in coincidence with protons populating the 3.470 - 3.484 MeV doublet of ^{27}Mg . The open circles are points on the simultaneous randoms spectrum.

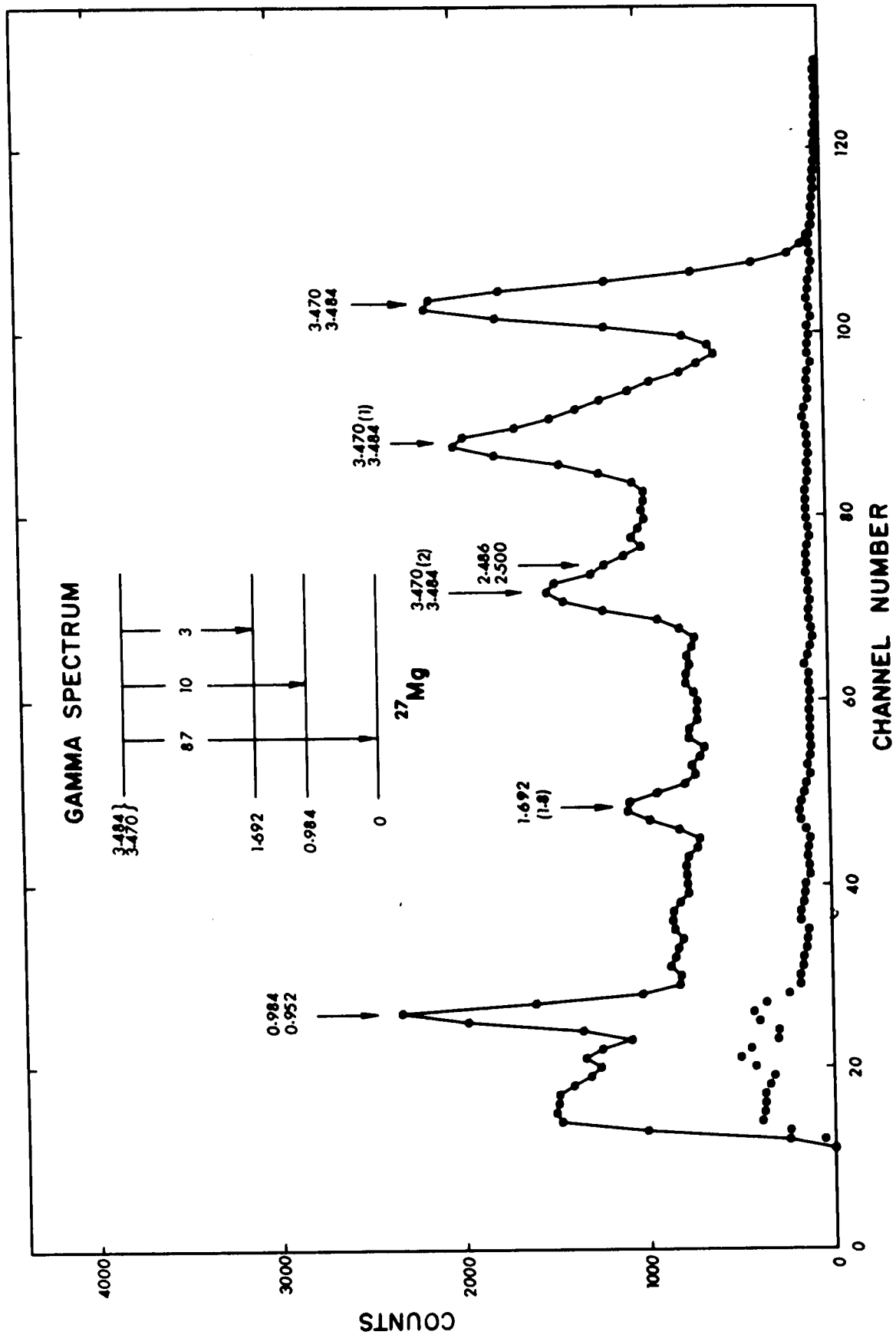
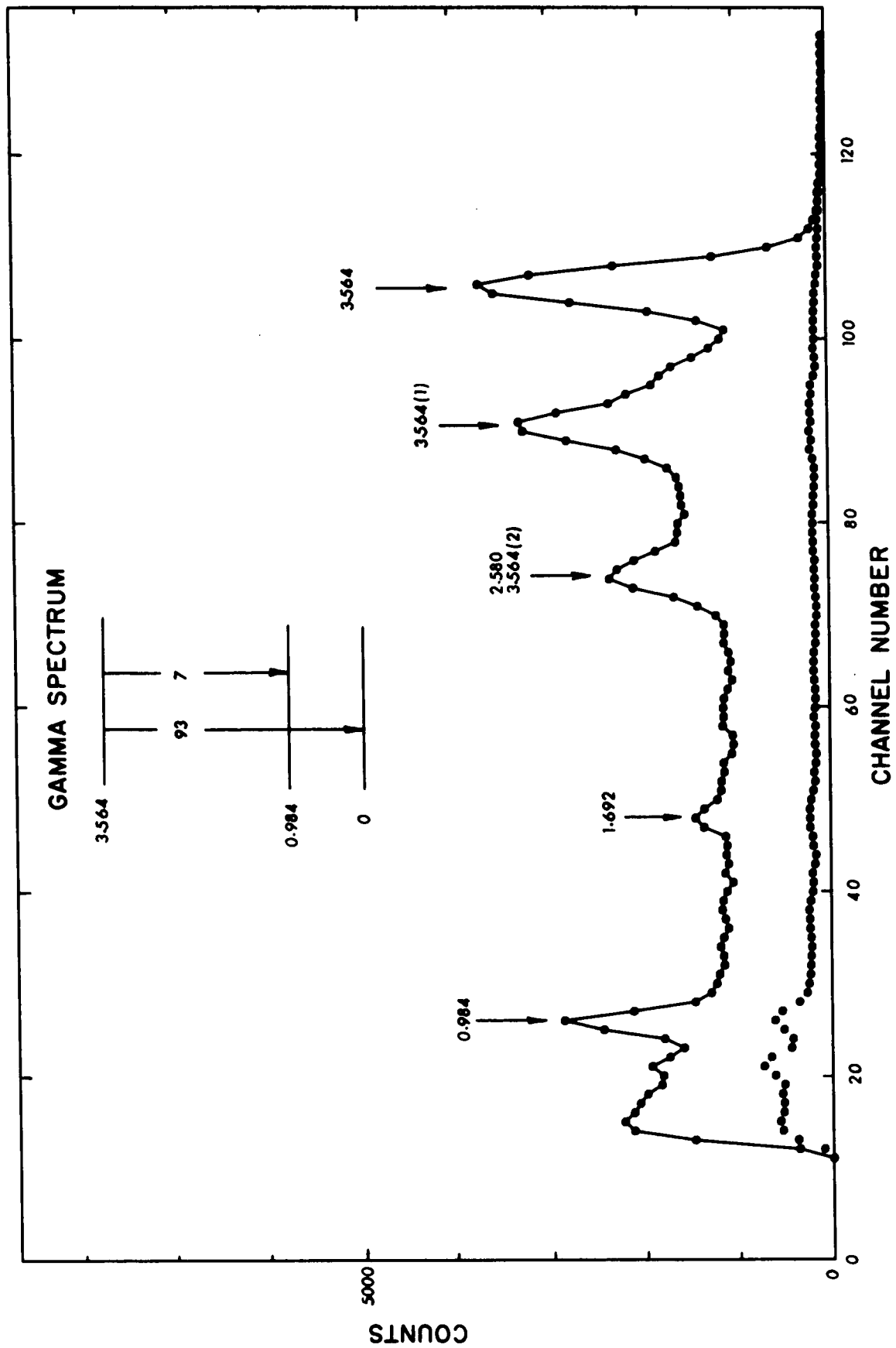


Fig. 3.8 The gamma-rays in coincidence with protons populating the 3.564 MeV level of ^{27}Mg . The open circles are points on the simultaneous randoms spectrum.



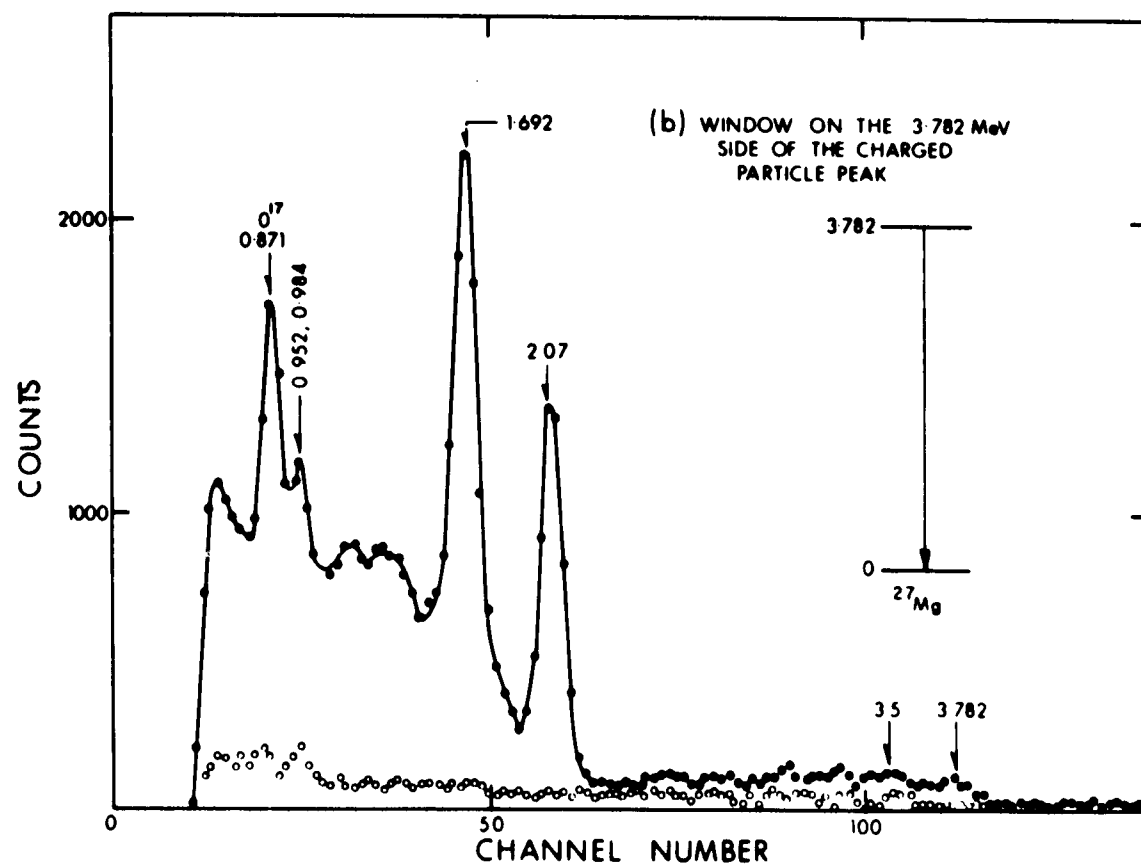
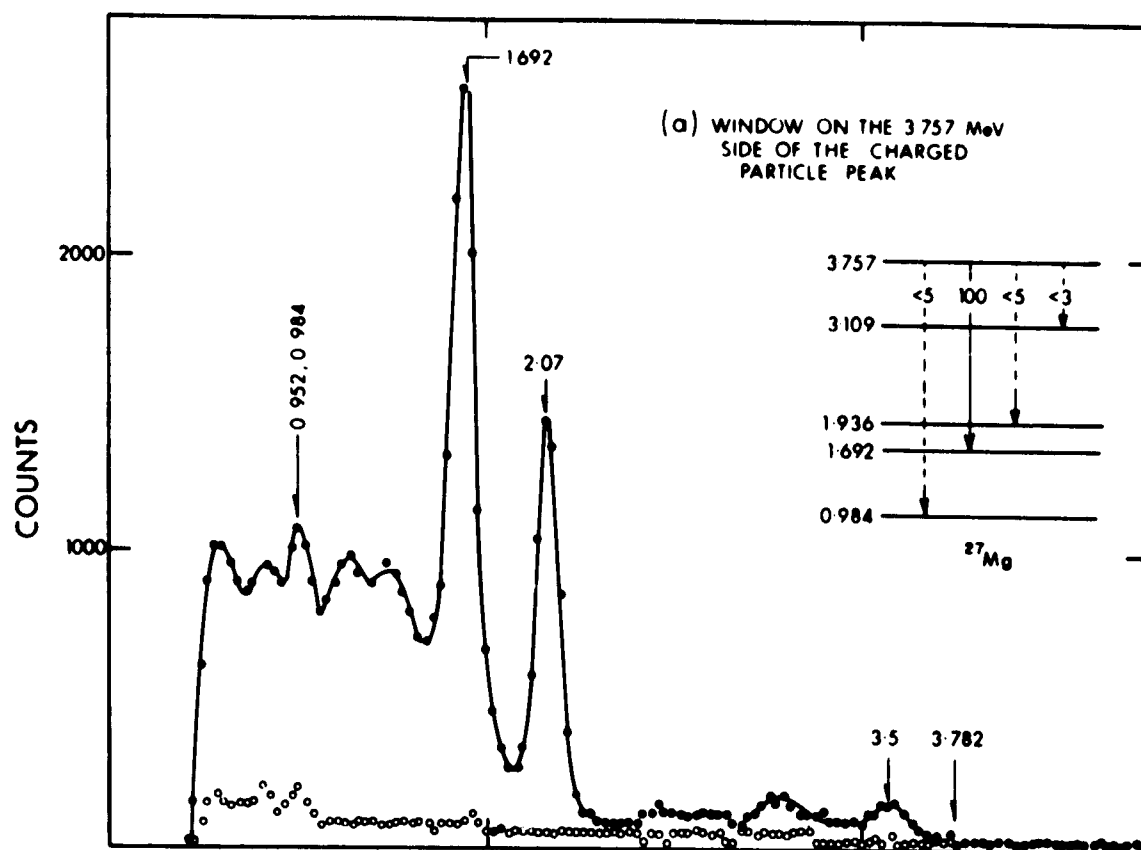
Analysis of the angular correlation of the $3.564 \rightarrow 0$ MeV transition yielded a definite $J = 3/2$ assignment with the mixing ratio solutions given in table 3.1. This result is in agreement with a previous assignment of $J^\pi = 3/2^-$ (La 67).

3.8 The 3.757 - 3.782 MeV Doublet

3.8.1 Decay modes The 3.757 - 3.782 MeV doublet could not be resolved in either the charged-particle or gamma-ray spectrum. However, information on each of the two levels was obtained by setting windows on both sides of the charged particle peak populating this doublet. The gamma-ray spectrum obtained by gating on each side of the charged particle peak is shown in fig. 3.9. The approximate window settings on the proton peaks are indicated in fig. 3.2. Clearly, both the 2.07 MeV and 1.692 MeV peaks are nearly the same size in both gamma-ray spectra. One would expect this if a single level which decays by a transition to the 1.692 MeV level was the only member of the doublet excited in the reaction. In contrast to this, the peaks near 3.8 MeV are clearly different in size for the two windows. The sum over all angles showed that only $(20 \pm 3)\%$ of this peak was in the window on the 3.757 MeV side of the peak. This indicates that the reaction populated mainly the 3.757 MeV level which decays strongly to the 1.692 MeV level, and that the reaction weakly populated the 3.782 MeV level which decays strongly to ground.

The remaining peaks in the spectrum from the doublet are not easy to classify. There are peaks near 3.5 MeV due to overlap with the 3.564

Fig. 3.9 The gamma-rays in coincidence with protons populating the 3.757 - 3.782 MeV doublet of ^{27}Mg . The spectrum obtained (a) by gating on the 3.757 MeV side of the charged-particle peak and (b) by gating on the 3.782 MeV side of the peak. The open circles are points on the simultaneous randoms spectrum.

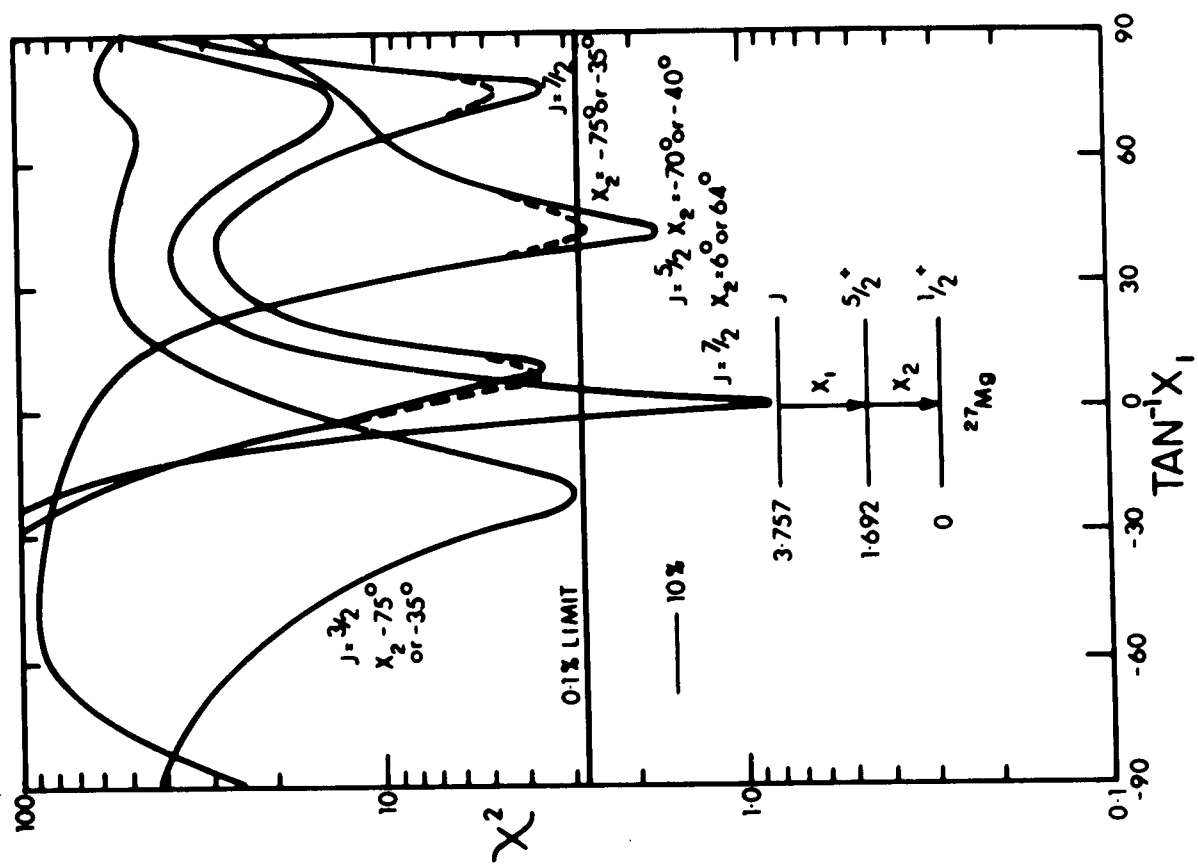
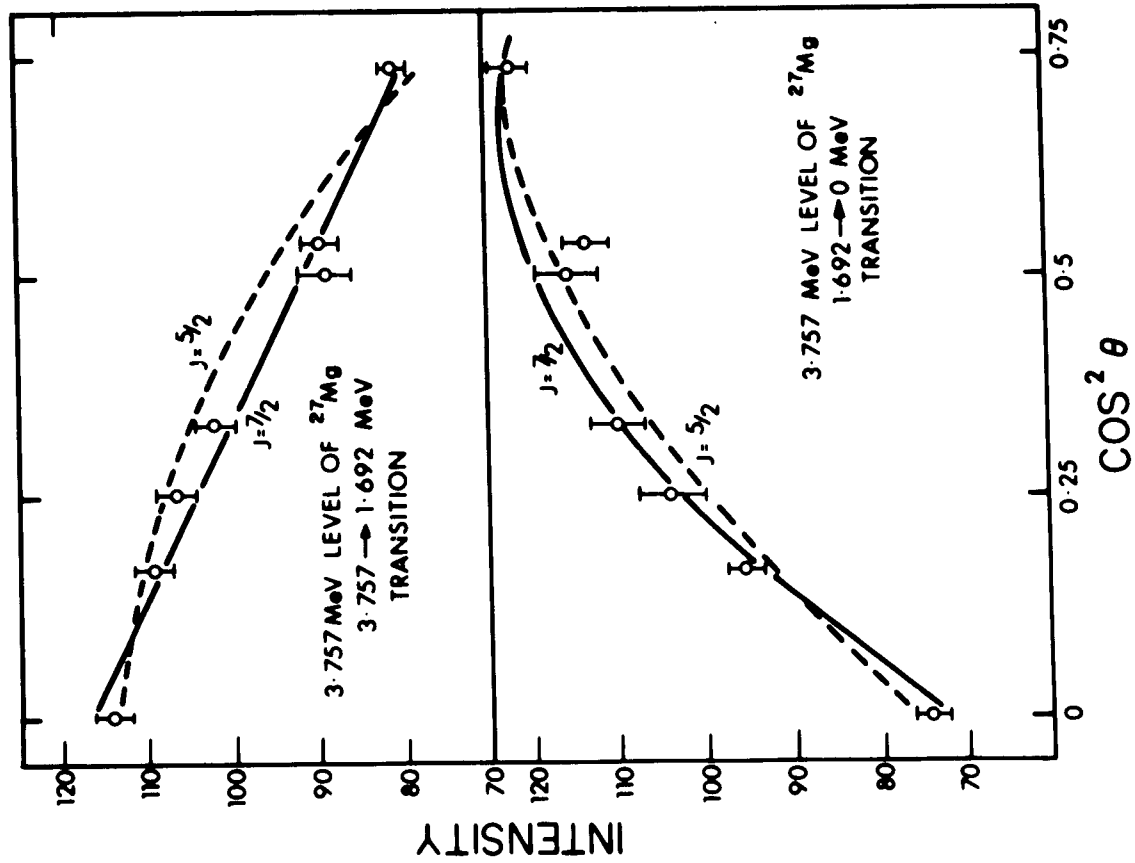


and 3.470 - 3.484 MeV levels. There is also a peak near 0.98 MeV. There was $(65 \pm 15)\%$ of the total area of this peak in the spectrum gated by the window on the 3.782 MeV side of the charged particle peak. Thus, it is possible that this level originates partly from each member of the doublet. It was not possible to determine whether this peak was due to a transition directly to the 0.984 MeV level or due to a transition through the 1.936 MeV level since the primary transitions were masked by the 3.5 MeV overlap peaks and the strong 2.065 and 1.692 MeV peaks. However, it was possible to place upper limits on these transitions.

Thus, the 3.757 MeV level decays 100% to the 1.692 MeV level with possible decays ($< 5\%$) to the 1.936 or 0.984 MeV levels. The decay of the 3.782 MeV level is uncertain because it was only weakly excited; however, this level does definitely decay to the ground state.

3.8.2 The 3.757 MeV level The angular distribution from the 3.757 \rightarrow 1.692 MeV transition was fitted using the least-squares program and acceptable solutions were obtained for spins $J = 3/2$, $J = 5/2$ and $J = 7/2$. A simultaneous fit to the 3.757 \rightarrow 1.692 MeV and 1.692 \rightarrow 0 MeV transitions was also attempted. The mixing ratios used for the 1.692 \rightarrow 0 MeV transition were those allowed by the χ^2 fit to the 1.692 MeV level as shown in fig. 3.3. The results of the simultaneous fit are given in the angular distribution and χ^2 versus $\arctan x$ curves shown in fig. 3.10. Only spins $J = 5/2$ and $J = 7/2$ fell below the 0.1% confidence limit. This is in agreement with the previous $l = 3$ assign-

Fig. 3.10 The angular distribution and χ^2 versus $\arctan x$ for the simultaneous fit to the 3.757 \rightarrow 1.692 \rightarrow 0 MeV transitions for the 3.757 MeV level of ^{27}Mg . The dotted curves in the χ^2 plot are for $P(\pm 2.5) = 0.05$ $P(\pm 0.5)$.



ment for this level (En 67) which allows $J^\pi = 5/2^-$ or $J^\pi = 7/2^-$. The present results show that the $J = 5/2$ solution is ten times less likely than the $J = 7/2$ solution. In addition, the $J = 5/2$ solution requires an unusually large M2/E1 mixing ratio for the $3.757 \rightarrow 1.692$ MeV transition and an unusually large M3/E2 mixing ratio for the $1.692 \rightarrow 0$ MeV transition. The former transition would require a M2/E1 enhancement of 10^6 Weisskopf units and the latter would require a M3 transition strength of greater than 400 Weisskopf units.

The above considerations indicate that the $J = 5/2$ solution is extremely unlikely.

The results for this level are based on the assumption that any decay to the 1.692 MeV level from the 3.782 MeV level is sufficiently weak to be neglected. With this qualification, we can say that the 3.757 MeV level is most probably $J^\pi = 7/2^-$ with a mixing ratio for the $3.757 \rightarrow 1.692$ MeV transition of (0.02 ± 0.07) .

3.8.3 The 3.782 MeV level The angular distribution from the $3.782 \rightarrow 0$ MeV transition was fitted using the χ^2 program and all spin values except $J = 1/2$ and $J = 3/2$ were rejected. The $J = 1/2$ solution was 30 times less likely than the $J = 3/2$ solution. Previous studies (En 67) have assigned an ℓ -value of $\ell = 2$ for this level which allows only $J^\pi = 3/2^+$ or $J^\pi = 5/2^+$. Therefore, one can say that the 3.782 MeV level has spin $J^\pi = 3/2^+$.

It was not possible to obtain a value for the mixing ratio of the $3.782 \rightarrow 0$ MeV transition since satisfactory solutions were obtained for

all mixing ratios.

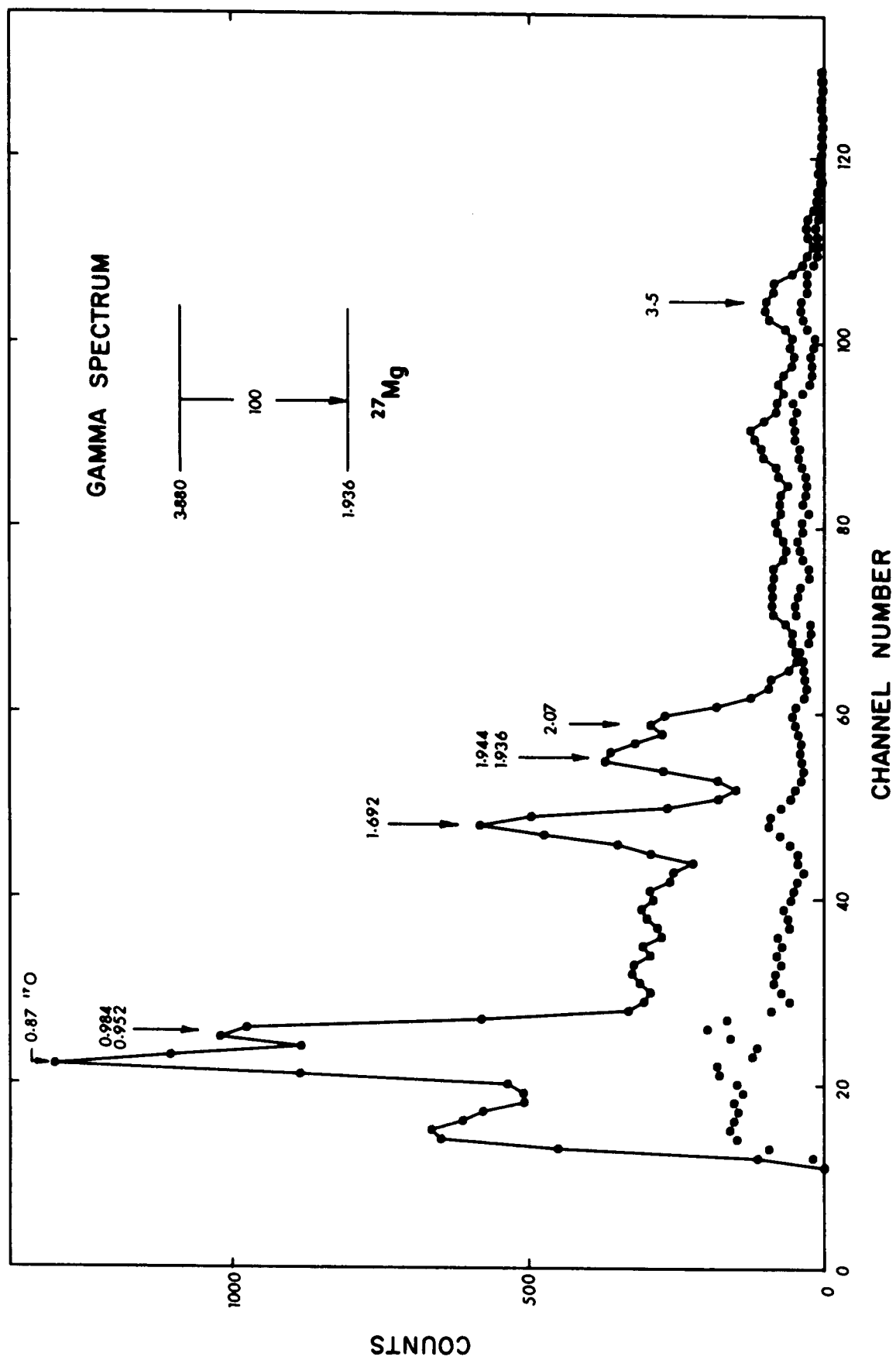
3.9 The 3.880 MeV Level

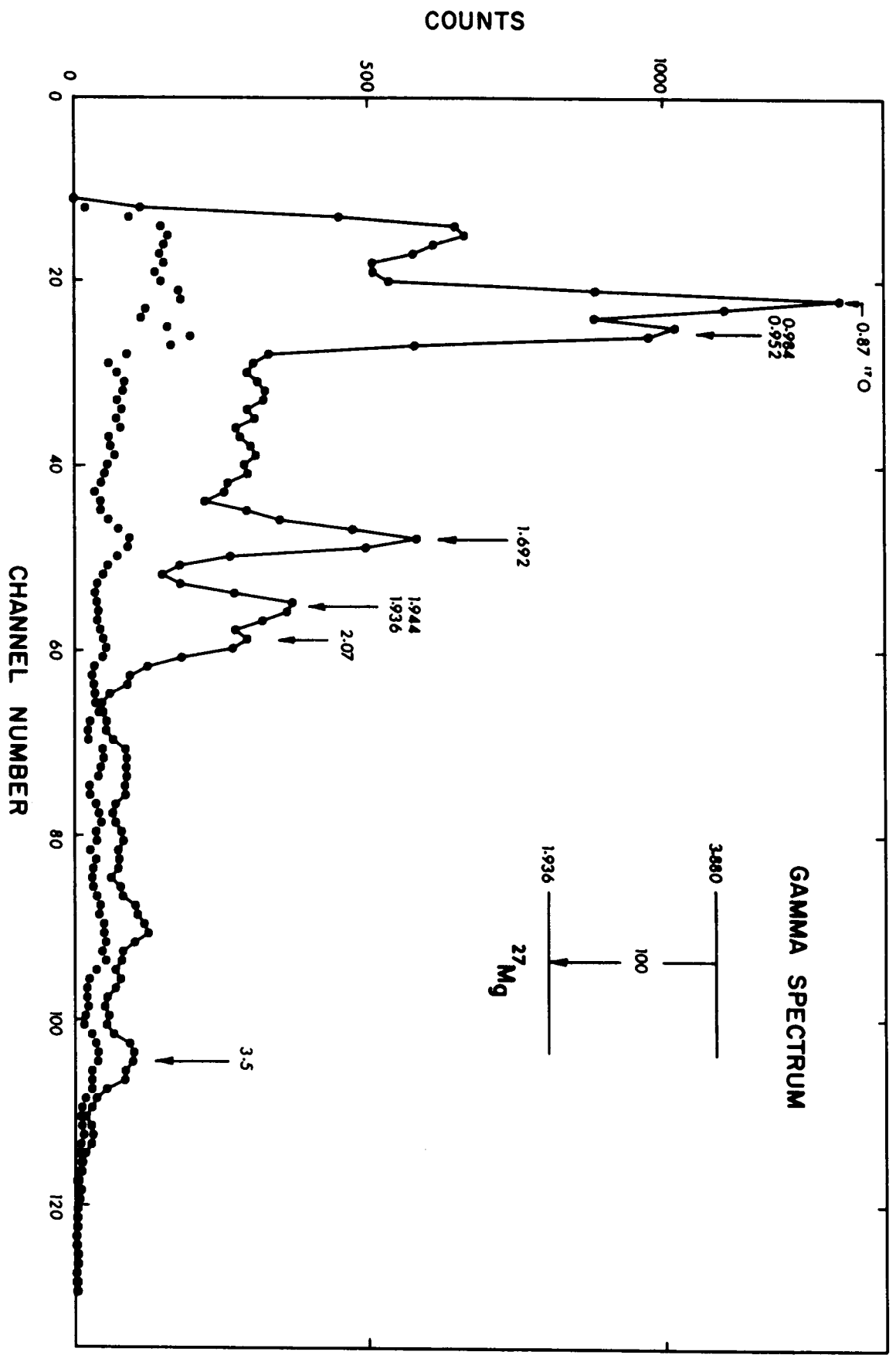
The gamma-ray spectrum in coincidence with the 3.880 MeV level is shown in fig. 3.11. There is considerable overlap with the large 3.5 MeV peaks and 3.757 MeV level giving rise to peaks near 3.5 MeV and peaks at 2.065 and 1.692 MeV. The only peaks due to the 3.880 MeV level are near 1 and 1.9 MeV. These are due to a decay to the 1.936 MeV level. The overlap with the 3.564, 3.470, 3.484, 3.757 and 3.782 MeV levels was sufficient to obscure completely any possible transitions from the 3.880 MeV level to any other states. Therefore, the $3.880 \rightarrow 1.936$ MeV decay has been tentatively assigned as 100%.

This large overlap and the presence of a 0.871 MeV contaminant peak in the gamma-ray spectrum from the $^{16}\text{O}(\text{d},\text{p})^{17}\text{O}$ reaction make it difficult to extract reliable angular distributions. The spectrum is further complicated by the presence of two unresolved doublets, the 0.984 - 0.952 MeV doublet and the 1.936 - 1.944 MeV doublet. Thus, it was not possible to obtain more information from the angular distributions except the elimination of spin 1/2 for this level.

There was no previous information on the spin or decay modes for this level.

Fig. 3.11 The gamma-rays in coincidence with protons populating the 3.880 MeV level of ^{27}Mg . The open circles are points on the simultaneous randoms spectrum.





3.10 The 4.146 MeV Level

The gamma-ray spectrum for the gamma rays in coincidence with protons feeding the 4.146 MeV level is shown in fig. 3.12. The 4.146 MeV level decays to the 0.984, 1.692 and 1.936 MeV levels with the relative strengths shown in the inset to fig. 3.12.

Satisfactory χ^2 fits to the data were obtained for $J = 1/2$ and $J = 3/2$ for a simultaneous fit to all three primary transitions. Spin values $J = 5/2$ and $J = 7/2$ also resulted in solutions with χ^2 below the 0.1% confidence limit for each of the three transitions separately. The limits obtained for the mixing ratio solutions for each of the primary transitions are given in table 3.1.

The 4.146 MeV level is known to be $\ell = 2$ which limits the spin to either $J^\pi = 3/2^+$ or $J^\pi = 5/2^+$. No previous information is available on either the branching ratios or multipole mixing ratios for this level.

3.11 The 4.394 MeV Level

The summed gamma-ray spectrum measured in coincidence with protons leading to the 4.394 MeV level is shown in fig. 3.13. The decay modes are shown in the inset to the figure. This level decays $(45 \pm 6)\%$ to the 3.109 MeV level. The spin of the 3.109 MeV level has not been completely determined but it was limited to either $J = 3/2$ or $J = 7/2$ in the present work (refer to fig. 3.6).

For the first set of χ^2 fits to the 4.394 MeV level, it was

Fig. 3.12 The gamma-rays in coincidence with protons populating the 4.146 MeV level of ^{27}Mg . The open circles are points on the simultaneous randoms spectrum.

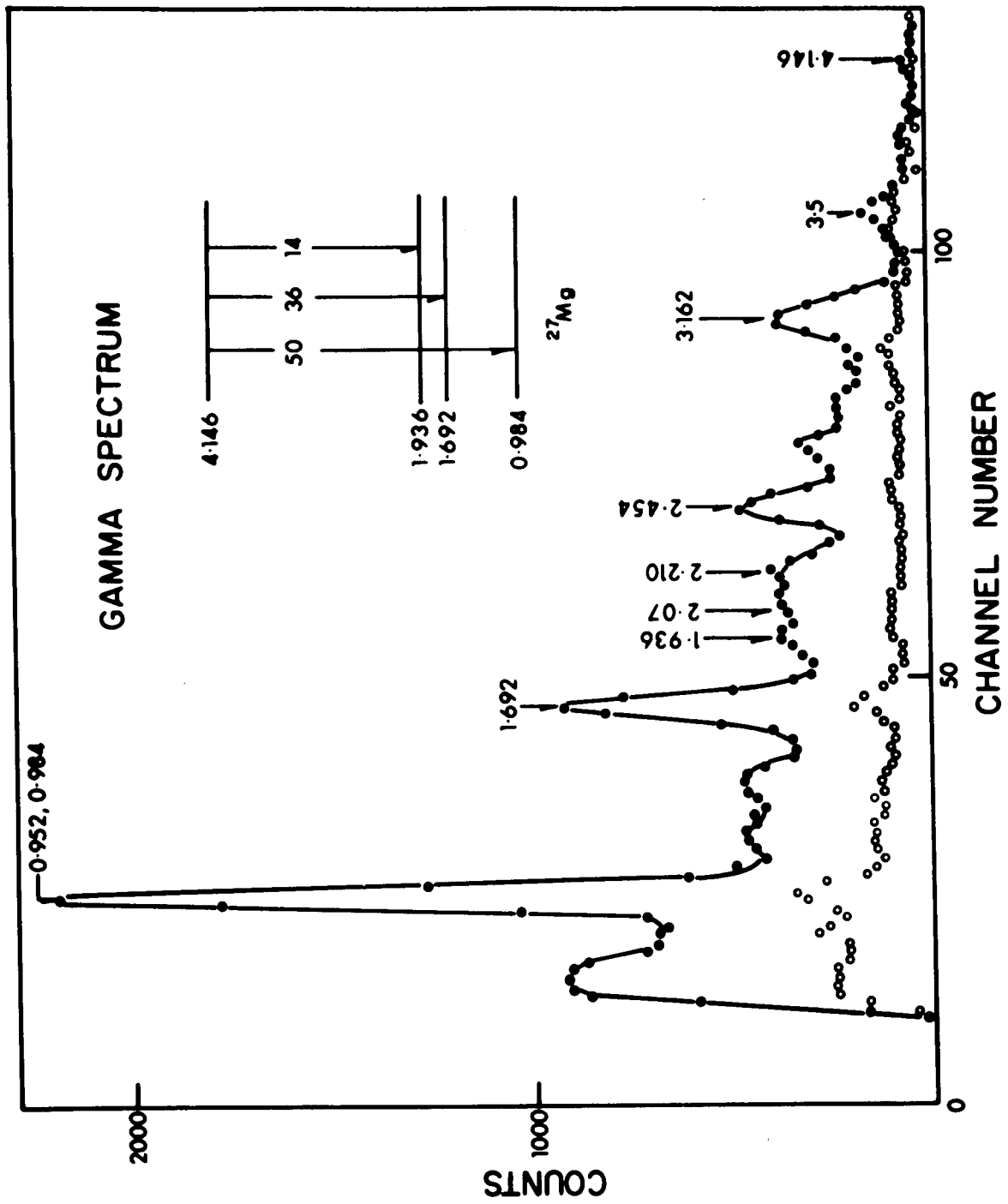
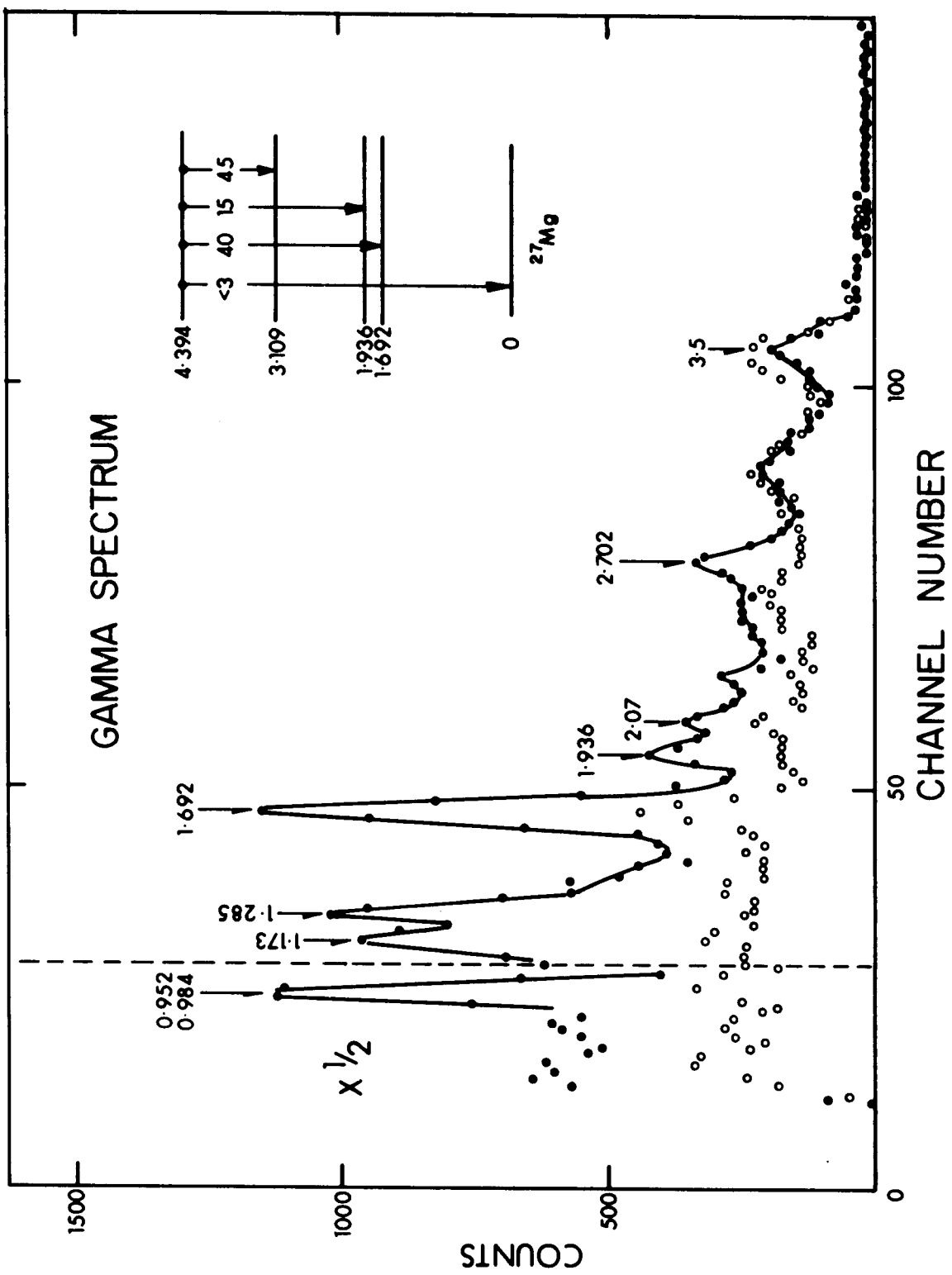


Fig. 3.13 The gamma-rays in coincidence with protons populating the 4.394 MeV level of ^{27}Mg . The open circles are points on the simultaneous randoms spectrum.



assumed that the spin of the 3.109 MeV level was $J = 3/2$. Simultaneous fits to the $4.394 \rightarrow 3.109$ MeV and $4.394 \rightarrow 1.692$ MeV transitions allowed only spin $J = 3/2$ or $J = 5/2$ for the 4.394 MeV level. The corresponding solutions for the multipole mixing ratios are summarized in table 3.1.

For the second set of χ^2 fits to this level it was assumed that the spin of the 3.109 MeV level was $J = 7/2$. All spin values were rejected to the 0.1% confidence limit except $J = 3/2$, $J = 5/2$ and $J = 9/2$. The solution for $J = 3/2$ was five times less likely than the other solutions.

Regardless of whether the spin of the 3.109 MeV level is $J = 3/2$ or $J = 7/2$, the spin of the 4.394 MeV level is limited to $J = 3/2$, $J = 5/2$ or $J = 9/2$. The mixing ratio solutions for each of these cases depends upon the spin of the 3.109 MeV level. The $J = 9/2$ solution is ruled out if the spin of the 3.109 MeV level is $J = 3/2$.

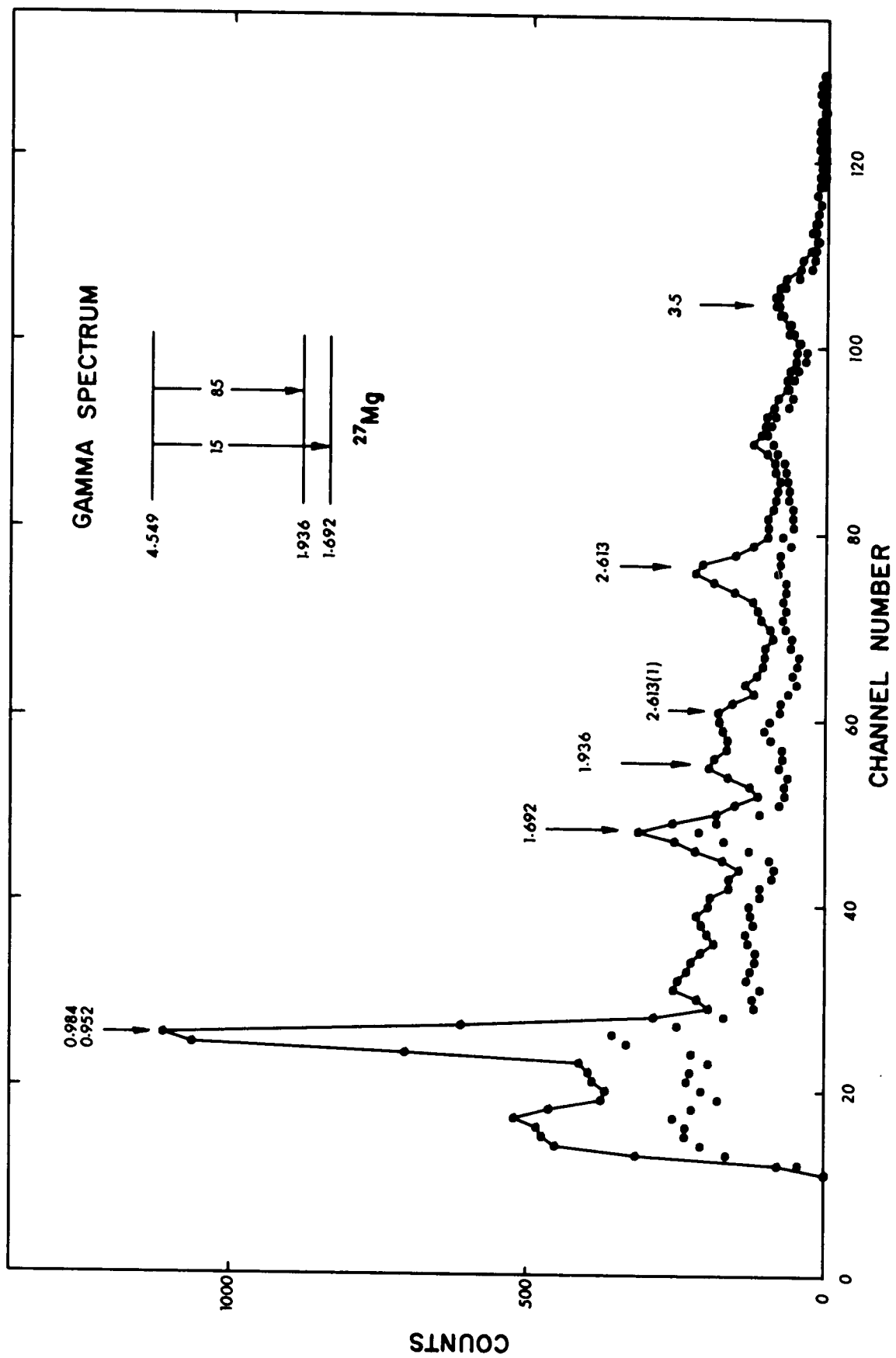
The decay to the 1.936 MeV level was also fitted using the χ^2 program but this transition proved to be too weak to provide any additional information.

There is no previous information for this level.

3.12 The 4.549 MeV Level

The gamma-ray spectrum for the gamma rays in coincidence with protons populating the 4.549 MeV level is shown in fig. 3.14. This level was found to decay $(85 \pm 13)\%$ to the 1.936 MeV level and $(15 \pm 7)\%$ to the 1.692 MeV level. In addition, there may also be a very

Fig. 3.14 The gamma-rays in coincidence with protons populating the 4.549 MeV level of ^{27}Mg . The open circles are points on the simultaneous randoms spectrum.



weak decay ($< 15\%$) to the 0.984 MeV level.

This level was only weakly excited by the reaction, consequently the gamma-ray intensities were too weak to yield reliable angular distributions. Thus, it was not possible to obtain any new information on the spin of this level.

The ℓ -value for this level is $\ell = (2)$, which limits the probable spin values to $(3/2^+)$ or $(5/2^+)$ (refer to En 67). No previous information on the gamma-ray decay modes for this level is available.

3.13 The 4.763 - 4.816 MeV Doublet

The coincidence gamma-ray spectrum measured at a bombarding energy of 5.5 MeV is shown in fig. 3.15 and that measured at a bombarding energy of 6.0 MeV is shown in fig. 3.16. There were no degrading foils in front of the detector for the measurement at 6.0 MeV and two windows (refer to fig. 3.16) were set on the doublet. The gamma rays in coincidence with protons from the 4.763 MeV side of the charged particle peak are shown in the upper half of fig. 3.16 and those in coincidence with protons from the 4.816 MeV side are shown in the lower half. The charged particle peaks (refer to the insets to fig. 3.16) were fitted with Gaussian peaks to determine the overlap. The numbers obtained in this manner were used to unfold the contributions to the two spectra to obtain branching ratios for both the 4.763 and 4.816 MeV levels. The results are shown in fig. 3.16 and tabulated in table 3.1.

All peaks in the spectrum had an isotropic angular distribution

Fig. 3.15 The gamma-rays in coincidence with the protons populating the 4.763 - 4.816 MeV doublet of ^{27}Mg measured at a bombarding energy of 5.5 MeV. The open circles are points on the simultaneous randoms spectrum.

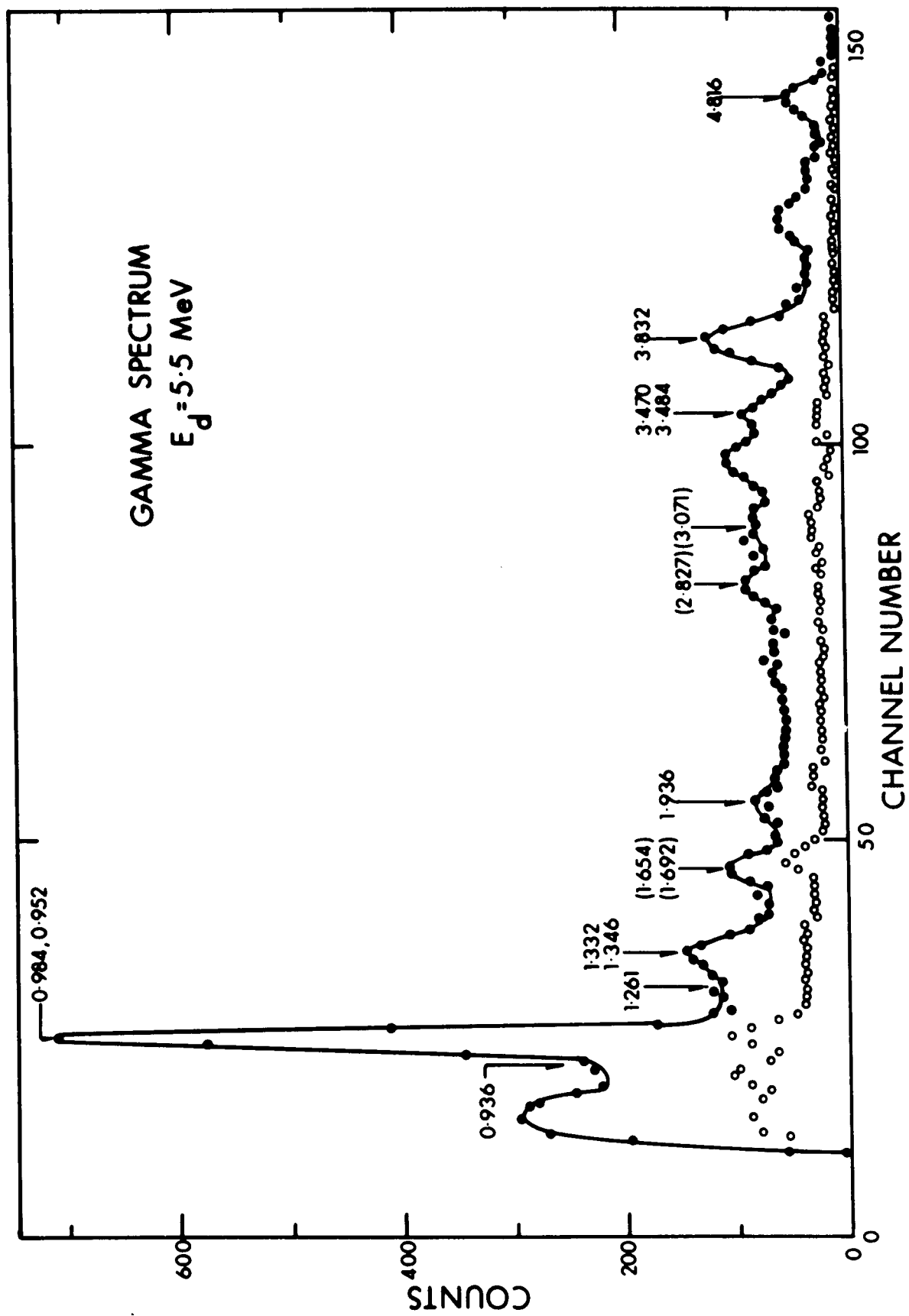
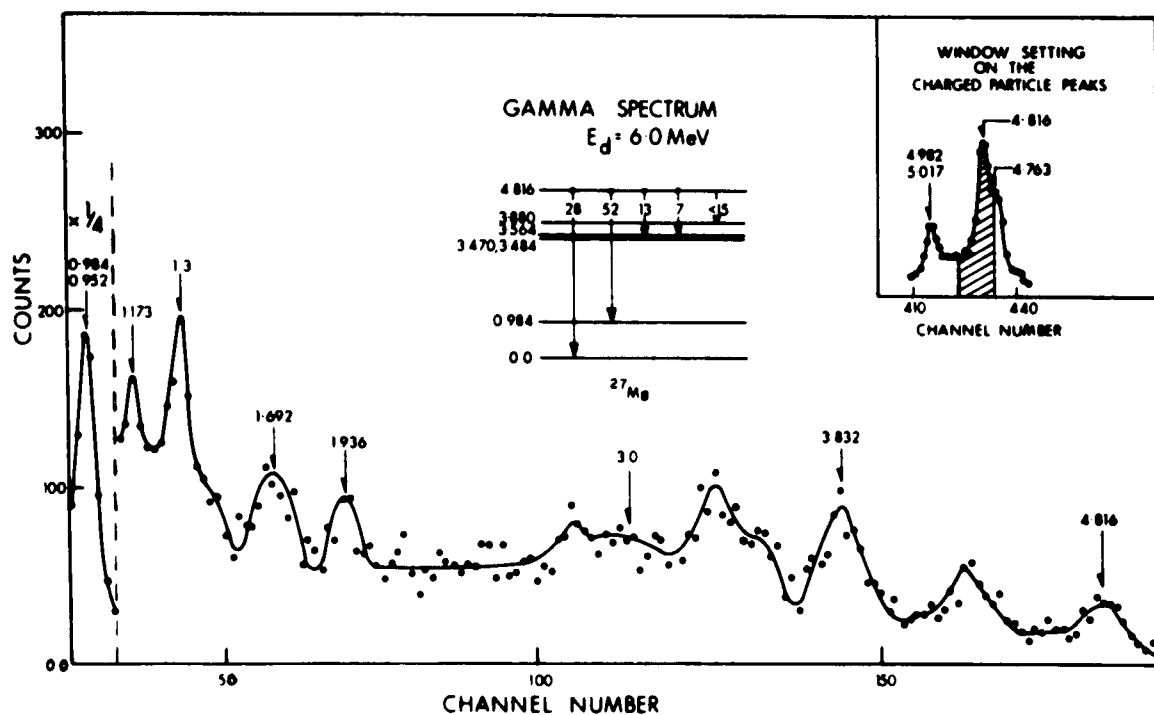
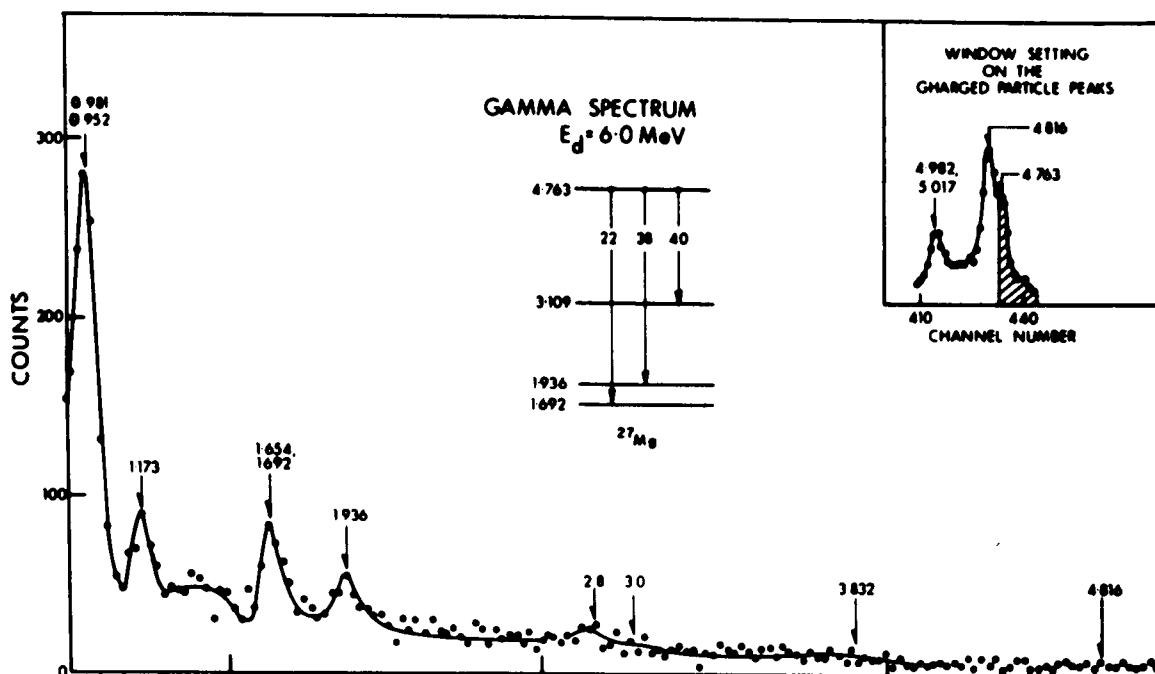


Fig. 3.16 The gamma-rays in coincidence with protons populating the 4.763 - 4.816 MeV doublet of ^{27}Mg measured at a bombarding energy of 6.0 MeV with the gamma detector at 55° . The spectrum obtained with the gate set on the 3.763 MeV peak is shown in the upper part of the figure and the spectrum obtained with the gate set on the 4.816 MeV peak is shown in the bottom part of the figure. The locations of these windows are shown in the insets. The open circles are points on the simultaneous randoms spectrum.



except the 0.984 - 0.952 MeV doublet. In particular, the $4.816 \rightarrow 0$ MeV and $4.816 \rightarrow 0.984$ MeV transitions were both isotropic. This result agrees with previous results (En 67) which give a probable assignment of $J^\pi = (1/2)^-$ for the 4.816 MeV level.

The gamma rays which could be attributed to the 4.763 MeV level were too weak to yield accurate angular distributions.

There is no previous information on the decay modes of either the 4.763 or the 4.816 MeV levels.

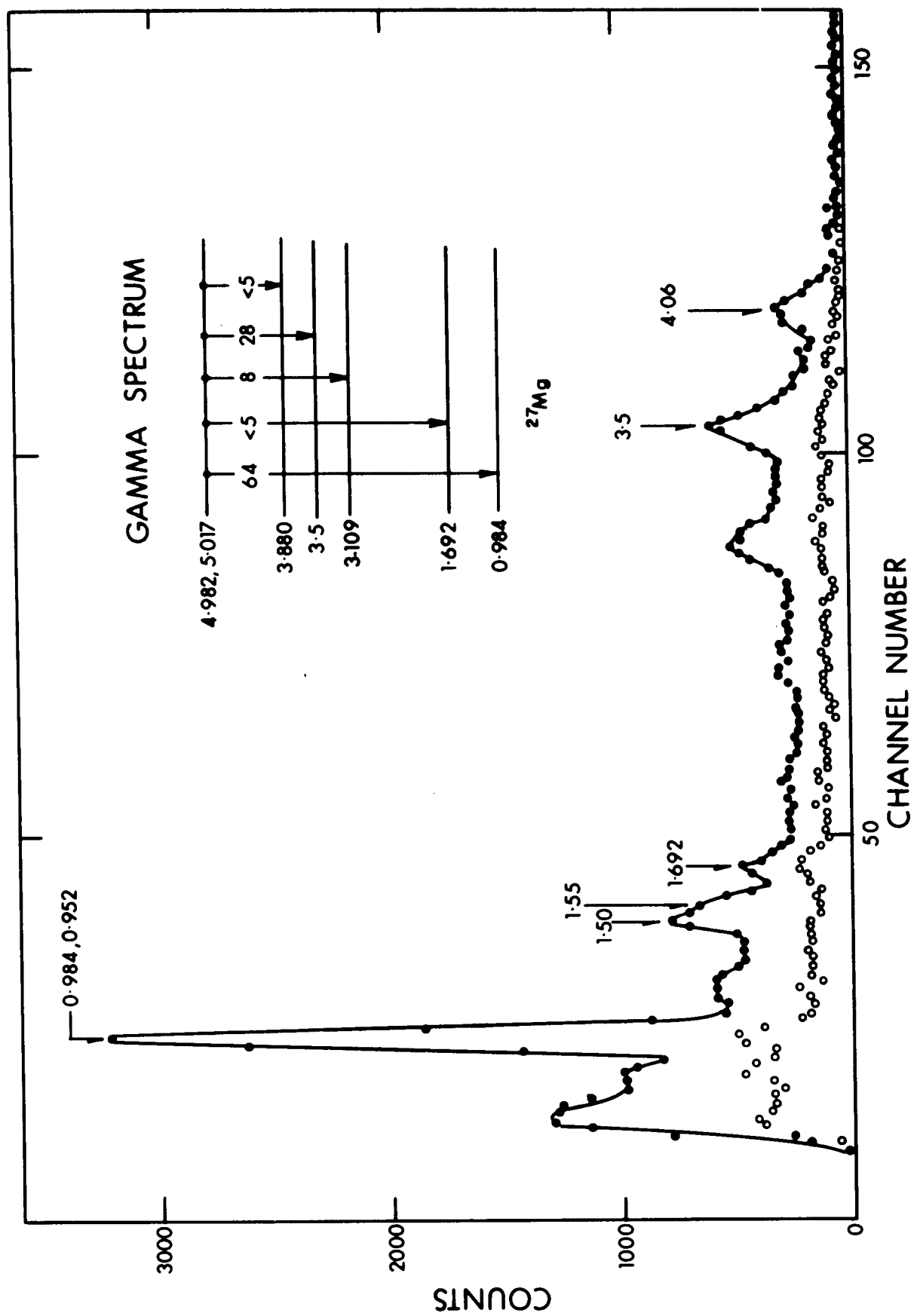
3.14 The 4.982 - 5.017 MeV Doublet

The main decay of the 4.982 - 5.017 MeV doublet is to the 0.984 MeV level (refer to fig. 3.17). There is also a decay to at least one of the levels near 3.5 MeV. Since there are a number of levels near 3.5 MeV and since the decay could be from either member of the doublet, it is difficult to determine which levels near 3.5 MeV are involved. It would appear, however, that one of the decays is to one of the members of the 3.470 - 3.484 MeV doublet.

The angular distribution of the $4.982 - 5.017 \rightarrow 0.984$ MeV transition was fitted using the χ^2 program and the allowed spins and mixing ratio combinations are summarized in table 3.1.

No previous information is available on the spins or decay modes for these levels.

Fig. 3.17 The gamma-rays in coincidence with protons populating the 4.982 - 5.017 MeV doublet of ^{27}Mg . The open circles are points on the simultaneous randoms spectrum.



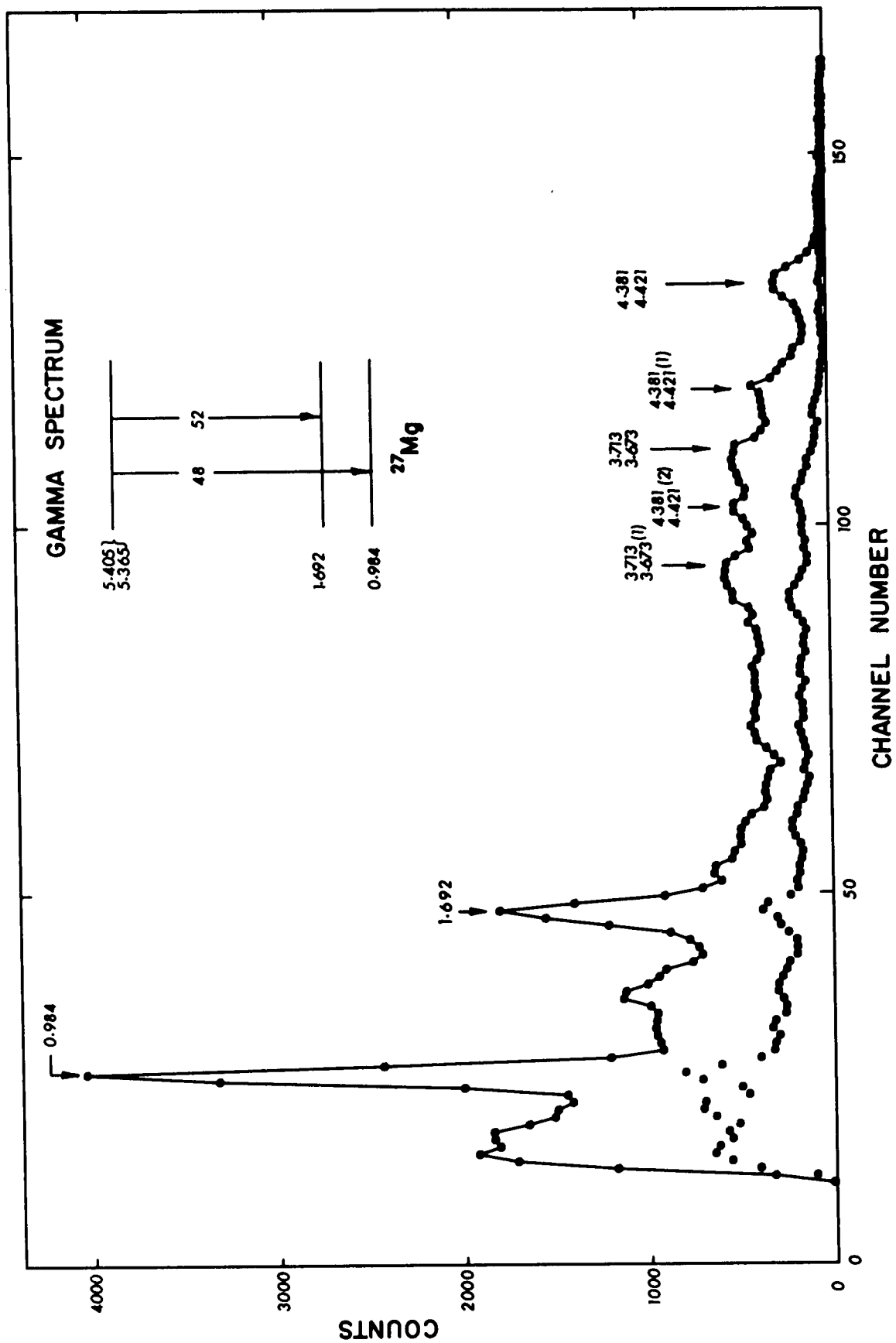
3.15 The 5.365 - 5.405 MeV Doublet

It was not possible to separate this doublet in either the charged particle or gamma-ray spectrum. The decay of the doublet is mainly to the 0.984 MeV and 1.692 MeV levels as can be seen in fig. 3.18. There was some evidence for weak decays to other levels; however, the identification of such decays was uncertain.

The angular distribution of the 5.365 - 5.405 \rightarrow 0.984 MeV transition was fitted using the χ^2 program and fits with χ^2 below the 0.1% limit were found for $J = 1/2$, $J = 3/2$, $J = 5/2$ and $J = 7/2$. The $J = 1/2$ and $J = 7/2$ solutions were 50 times less likely than the $J = 3/2$ and $J = 5/2$ solutions.

No previous information was available concerning either of these levels.

Fig. 3.18 The gamma-rays in coincidence with protons populating the 5.365 - 5.405 MeV doublet of ^{27}Mg . The open circles are points on the simultaneous randoms spectrum.



CHAPTER IV

NUCLEAR MODEL CALCULATIONS

In this chapter, the experimental data for ^{27}Mg is compared with the predictions of two nuclear models, the Nilsson model (Ni 55) and the shell model (Wo 68).

4.1 The Nilsson Model

4.1.1 Theory The Nilsson model has been described in detail elsewhere (Ni 55, Da 65) and no attempt will be made to derive the results here. The reader is referred to the review article by Davidson (Da 65) for a general view of the model and to the article by Nilsson (Ni 55) for a detailed description of the solution of the single-particle problem.

The most simple model for odd-A nuclei is the extreme single-particle shell model. This model ascribes all of the properties of the nucleus to a single nucleon moving in the average field produced by all the other nucleons (the "core"). This average field is assumed to be spherically symmetric for simplicity.

The Nilsson model is an extension of the extreme single-particle model to cases where the core assumes a permanently deformed shape and the extra core particle moves in a field which is not spherically symmetric. In this case the Hamiltonian for the system contains two

terms, H_p , the Hamiltonian of the particle and the kinetic energy of rotation of the deformed core. That is

$$H = \hbar^2 \sum_{k=1}^3 \frac{\vec{R}_k^2}{2I_k} + H_p = \hbar^2 \sum_{k=1}^3 \frac{(\vec{J}_k - \vec{j}_k)^2}{2I_k} + H_p, \quad (4.1)$$

where \vec{J} is the total angular momentum of the nucleus, \vec{R} is the core angular momentum, \vec{j} is the angular momentum of the particle, and I is the moment of inertia of the core. The coordinate systems used are the x, y, z system fixed in space and the $1, 2, 3$ system fixed with respect to the rotating core. The projections of the angular momenta in each of these coordinate systems are; M , the projection of \vec{J} on the z -axis, K the projection of \vec{J} on the 3-axis, and Ω , the projection of \vec{j} on the 3-axis.

If one assumes that the deformed core has an axis of symmetry such that $I_1 = I_2 = I_0$, equation 4.1 can be written as (Da 65)

$$H = H_R + H_p' + H_C, \quad (4.2)$$

where

$$H_R = \frac{\hbar^2}{2I_0} [J(J+1) - 2K^2], \quad (4.3)$$

$$H_p' = H_p + \frac{\hbar^2}{2I_0} j^2, \quad (4.4)$$

and

$$H_C = \frac{-\hbar^2}{2I_0} [I_{+j-} + I_{-j+}], \quad (4.5)$$

where, $I_{\pm} = I_1 \pm I_2$ and $j_{\pm} = j_1 \pm j_2$.

The last term, H_C , which has been called the "rotational particle coupling" (RPC) term (Ke 56), will have a very small effect for low-lying states of an axially symmetric system and can be treated as a perturbation. The effects of this term are considered later and only the first two terms in equation 4.2 are considered now.

If the rotation and vibration of the core are slow with respect to the single particle motion, the wave function can be written as a product of a rotational wave function, a vibrational wave function and a single particle wave function. The single-particle Hamiltonian, H_p' , chosen by Nilsson (Ni 55) can be written in the form

$$H_p' = H_0^0 - \kappa \hbar \omega_0^0 \left[\frac{4}{3} \sqrt{\frac{\pi}{5}} \eta r^2 Y_{20} + 2 \vec{l} \cdot \vec{s} + \mu \vec{l}^2 \right], \quad (4.6)$$

where H_0^0 is the Hamiltonian for a spherically symmetric harmonic oscillator, $\hbar \omega_0^0$ is approximately $41A^{-\frac{1}{3}}$ MeV (Ni 55), \vec{l} and \vec{s} are the orbital angular momentum and spin of the odd particle, Y_{20} is a spherical harmonic and η , κ and μ are parameters of the Hamiltonian. The parameter, η , is the κ -dependent deformation parameter and κ and μ are coefficients chosen such that, at zero deformation ($\eta=0$), the shell model sequence of levels is obtained. The same values of κ and μ are normally used for all nuclei in the same oscillator shell but different values are needed for each oscillator shell.

An operator which commutes with H_p' is j_3 with quantum number Ω and in the axially symmetric case we have $K = \Omega$ for the low-lying states (Pr 62, pages 240 and 256). Thus, the single particle wave functions, χ_Ω , are eigenvectors of H_p' with eigenvalues, ϵ_Ω .

One can choose a representation with H_0^0 diagonal together with \vec{l}^2 , l_3 and s_3 which all commute with H_0^0 and have quantum numbers l , Λ and Σ respectively. These quantum numbers are all single particle quantities related by $\Omega = \Lambda + \Sigma$.

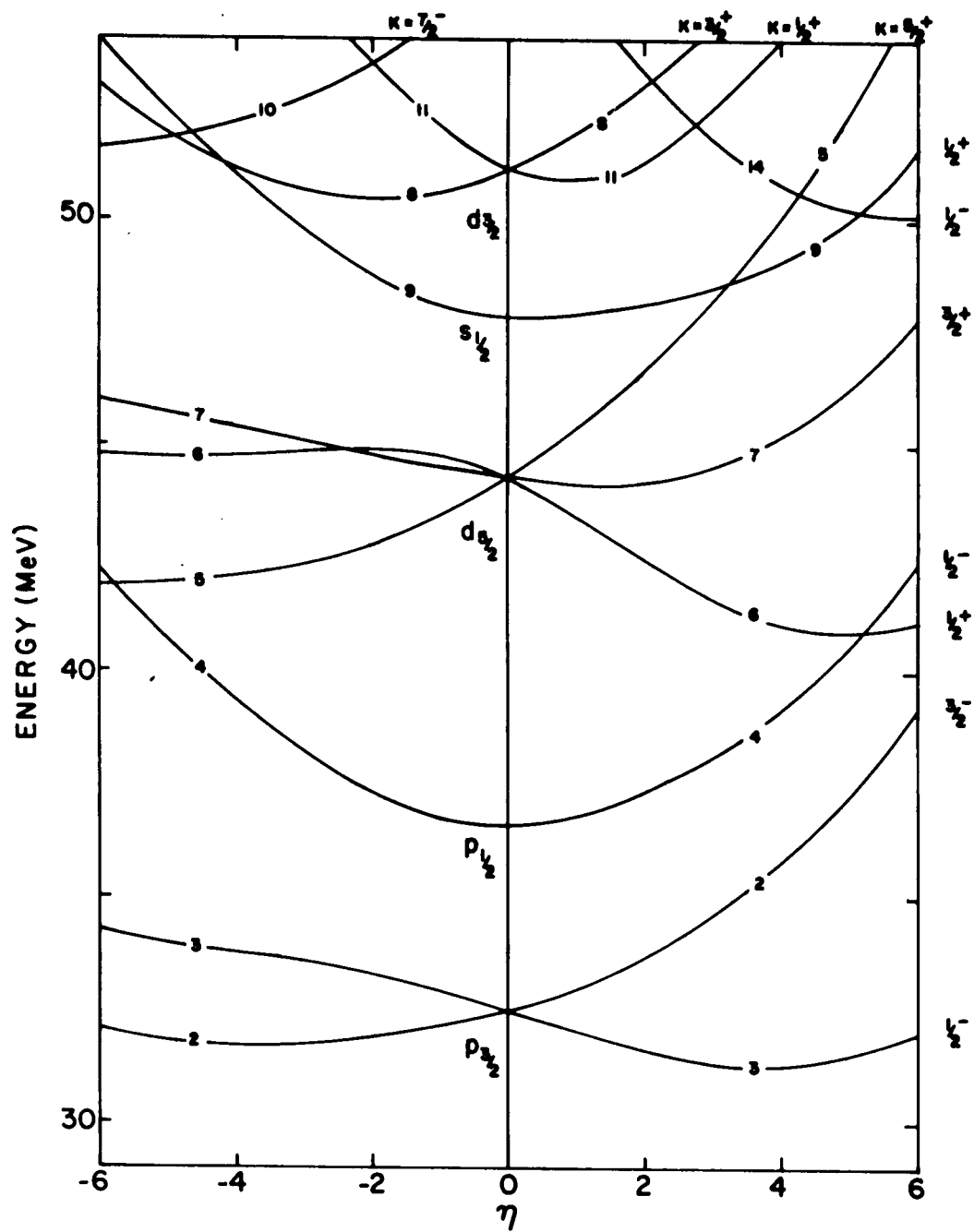
In this representation χ_Ω can be written as

$$\chi_\Omega = \sum_{\Lambda \Sigma} a_{\Lambda \Sigma} \chi_{\Lambda \Sigma} \quad (4.7)$$

The coefficients in the expansion can be obtained by diagonalizing H_p' in this representation for a given oscillator number, N, the principal quantum number. All non-zero matrix elements of H_p' are given by Nilsson (Ni 55). The eigenvalues, ϵ_Ω , give the energies of single particle excitation in a deformed field.

The single particle energies for parameters $\kappa = 0.1$ and $\mu = 0.1$ are plotted as a function of the deformation in fig. 4.1. The shell model single particle states at zero deformation are split into states of different Ω for non-zero deformation. Each of these Nilsson orbits is degenerate in $\pm \Omega$ and, therefore, particles will fill the Nilsson orbitals in pairs of opposite K so that the only contribution to K is due to the last unpaired particle. This particle may be placed in different single-particle orbitals and a rotational band with $J = K, K + 1, K + 2, \dots$ for $K \geq 3/2$ is built upon each orbital. The parity, the projection K, and the single-particle wave functions of all states in a band are the same. The energy of each state is given by ϵ_K plus H_R (refer to equation 4.3).

Fig. 4.1 Nilsson model orbits as a function of the deformation parameter, η , for $\mu = 0.1$ and $\kappa = 0.1$. The value of K and the parity for each orbit are marked on the right side of the figure. The orbit numbers are those given by Nilsson (Ni 55). The energy scale was obtained with $\hbar\omega_0^0 = 41(27)^{-\frac{1}{3}}$.



It is also possible to expand the single-particle states, χ_Ω , in terms of states of a given j , $\chi_{j\Omega}$, which are eigenfunctions of a spherically symmetric potential. The expansion of χ_Ω in terms of these states is

$$\chi_\Omega = \sum_j C_{j\Omega} \chi_{j\Omega} \quad , \quad (4.8)$$

where the $C_{j\Omega}$ coefficients are related to the $a_{\ell\Lambda\Sigma}$ coefficients by

$$C_{j\Omega} = \sum_{\ell\Lambda} \left(\ell \frac{1}{2} \Lambda \Sigma | j \Omega \right) a_{\ell\Lambda\Sigma} \quad , \quad (4.9)$$

where $(jj' mm' | JM)$ is a Clebsch-Gordan coefficient.

After the single-particle problem is solved, the effect of the RPC terms on the results can be determined. The matrix elements for H_C are given by Davidson (Da 65) in terms of the $C_{j\Omega}$ coefficients obtained from the single-particle Hamiltonian. These matrix elements connect states which differ by one unit in K . When the single-particle energy spacing are much greater than the rotational energy spacing, these terms are negligible except for the special case of $K = 1/2$. In this case, there are terms diagonal in χ_Ω which should not be neglected. With only these diagonal RPC terms included in the Hamiltonian, K is still a good quantum number and the energy of a single-particle state is given by

$$E_{JK} = \epsilon_K + \frac{\hbar^2}{2I_0} [J(J+1) - 2K^2 + \delta_{K, \frac{1}{2}} a(-1)^{J+\frac{1}{2}} (J+\frac{1}{2})] \quad , \quad (4.10)$$

where the "decoupling parameter" a is defined as

$$a = - \sum_j (-1)^{j+\frac{1}{2}} (j+\frac{1}{2}) |C_{j-\frac{1}{2}}|^2, \quad (4.11)$$

and $\delta_{i,j}$ is a Kronecker delta.

The vibration-rotation interaction complicates these results. The effect of this interaction can be taken into account by adding a term to equation 4.10 which has the form (Go 60)

$$+B [J(J+1) + \delta_{K,\frac{1}{2}} a (-1)^{J+\frac{1}{2}} (J+\frac{1}{2})]^2, \quad (4.12)$$

where B is generally treated as a parameter but an approximate expression for B is given by Gove (Go 60).

The situation is even more complex if off-diagonal RPC terms are included in the Hamiltonian. Since states with different K are connected by this interaction, the projection, K , is no longer a good quantum number. When the total Hamiltonian including all RPC terms is diagonalized, the eigenstates obtained will be a mixture of different K bands. These band-mixed states are given by

$$\chi_{Jv} = \sum_K C_v(J,K) \chi_K, \quad (4.13)$$

where the $C_v(J,K)$ are band-mixing coefficients and v is simply a label for different states of a given J .

Once the wave functions have been determined, the transition

rates between different states can be calculated using the $a_{\lambda\Lambda\Sigma}$, $C_{j\Omega}$ and $C_v(J,K)$ coefficients. These transition rates may be obtained from reduced transition rates $B(M1)$ and $B(E2)$ (refer to Pr 62, p. 299) for Nilsson states (including band mixing due to the off-diagonal RPC terms) using the equations of Brockmeir (Br 65). The reduced transition probability $B(E2)$ is of particular interest and is given by (Br 65)

$$B(E2 J_v \rightarrow J'_v) = \frac{5}{16\pi} e^2 \left| \sum_{KK'} C_v(J,K) C_{v'}(J',K') Q^{KK'} [(J2K, K' - K | J'K')] \right. \\ \left. + (-1)^{J'+K'} (J2K, -K' - K | J', -K') b_{E2}(\delta_K, \frac{1}{2}\delta_{K', \frac{3}{2}} + \delta_{K, \frac{3}{2}}\delta_{K', \frac{1}{2}}) \right|^2, \quad (4.14)$$

where the matrix elements $Q^{KK'}$ and $b_{E2}Q^{KK'}$ can be calculated from the single-particle wave functions (Br 65). The $Q^{KK'}$ is the matrix element of the quadrupole operator and is composed to two terms, Q_0 , the intrinsic quadrupole moment and a single particle term. For nuclei with a large permanent deformation, the intrinsic quadrupole moment is much larger than that due to a single particle, hence, $Q^{KK'} \approx Q_0$. The size of Q_0 is related to the deformation by (Ni 55)

$$Q_0 = 0.8 Z r_0^2 \delta (1 + \frac{2}{3} \delta) A^{-\frac{2}{3}} \quad (4.15)$$

where Z is the atomic number, r_0 is taken to be 1.25×10^{-13} cm., and the deformation parameter δ is related to η through the relation

$$\eta = \frac{\delta}{\kappa} \left[1 - \frac{4}{3} \delta^2 - \frac{16}{27} \delta^3 \right]^{-\frac{1}{6}}. \quad (4.16)$$

The large values for Q_0 in rotational bands mean that E2 transitions within the band are greatly enhanced so that E2 transitions are able to compete strongly with M1 transitions. This enhancement of E2 transitions is characteristic of rotational nuclei and can be useful in determining the band structure of a nucleus.

4.1.2 Application to ^{27}Mg The Nilsson model single-particle levels are shown in fig. 4.1. In the case of ^{27}Mg , assuming a small deformation, 14 neutrons will fill orbits 1 to 7 and the 15th neutron will go into the $K = 1/2^+$ orbit 9 to form the ground state. Other single-particle states may be obtained by exciting the odd neutron to orbit 8 or orbit 11 and hole states may be formed by exciting a particle from one of the lower orbits up to orbit 9.

It is possible to have the odd particle in an orbit with odd- N giving rise to negative parity bands. However, since the information on these levels is very limited for ^{27}Mg , the following discussion will be concerned with positive parity bands only.

The parameters involved in the Nilsson and rotational parts of the Hamiltonian are, ν , κ , η and I_0 . These parameters are not well known for ^{27}Mg so before proceeding further it is useful to obtain some estimates of their values.

A value for the moment of inertia parameter, I_0 , may be estimated by examining the core which is a ^{26}Mg nucleus. If it is assumed that the first excited state of ^{26}Mg at 1.809 MeV is the second member of a

rotational band (refer to H1 65) one obtains $\frac{\hbar^2}{2I_0} = 0.30$ MeV. It has been observed that $\frac{\hbar^2}{2I_0}$ for an odd mass nucleus is smaller than that for the neighboring even mass nucleus (Al 56, Ba 62). Therefore, one would expect $\frac{\hbar^2}{2I_0} \leq 0.30$ MeV for ^{27}Mg .

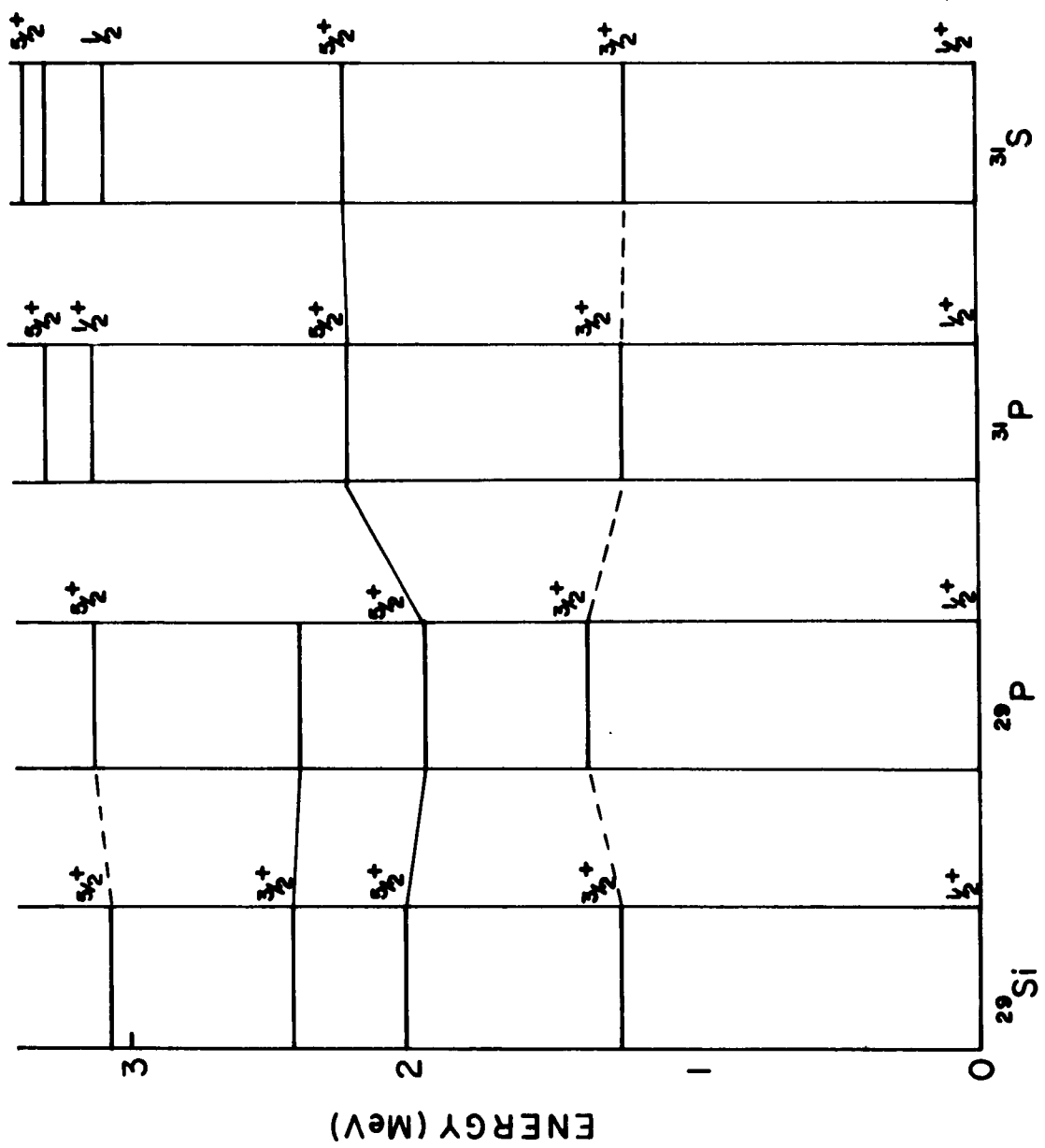
The value for κ which was suggested for s-d shell nuclei by Nilsson (Ni 55) was 0.05, however, it has been recently found that a value as large as $\kappa = 0.125$ was necessary to fit the spectrum of ^{27}Al (Lo 64).

The value for μ which was suggested for the s-d shell by Nilsson (Ni 55) was zero, however, Bishop (Bi 59) found that larger values were necessary. The value of μ which was found for ^{27}Al was 0.33 (Lo 64).

The estimates which have been made for the distortion parameter, η , for ^{27}Mg have ranged from -2 to +3.2 (Gl 65, La 67, Bi 59). Since it is not certain whether ^{27}Mg has a positive or negative distortion, it is necessary to examine both possibilities with a view to limiting this parameter.

First, the possibility that ^{27}Mg has a negative distortion is examined. This viewpoint is supported by the fact that other nuclei which have the 15th neutron as the odd particle such as ^{29}Si , ^{29}P , ^{31}P and ^{31}S have negative distortion (Go 60). The Nilsson model level scheme assigned by Gove (Go 60) for these four nuclei is shown in fig. 4.2. The first excited state in all of these nuclei is the band head of the $K = 3/2^+$ band built on orbit 8. If ^{27}Mg has a negative distortion, it would be expected to have a similar structure, particularly in view of the fact that the 0.984 MeV level has a large

Fig. 4.2 The energy level spectra of four nuclei with the 15th particle as the odd particle from Gove (Go 60). The solid lines denote levels built on Nilsson orbit 9 and the dotted lines denote levels built on orbit 8.



spectroscopic factor (Si 64, Cu 64 and Gl 65). In this configuration, the ground state band would have to have a level ordering of $1/2^+$, $5/2^+$ and $3/2^+$. There are 2 possibilities for the $J = 5/2^+$ level, the 1.692 MeV or 1.936 MeV levels, and there are two possibilities which are considered for the $3/2^+$ level, the 3.109 MeV or 3.484 MeV levels. The values of $\frac{\hbar^2}{2I_0}$ which are necessary to fit these four configurations have been calculated by Lacambra et al. (La 67). The $\frac{\hbar^2}{2I_0}$ are all between 0.41 and 0.48 MeV while $1.7 \leq a \leq 2.0$. It has already been concluded that $\frac{\hbar^2}{2I_0}$ should be less than 0.3 MeV from an examination of the ^{26}Mg core, therefore, all four configurations are unlikely and the distortion of ^{27}Mg is probably not negative.

If one assumes that it is possible for ^{27}Mg to have one of the four ground state configurations mentioned above, the $5/2^+$ state not included in the ground state band would have to be explained as the $5/2^+$ member of the band built on orbit 8. Assuming no band mixing and $\frac{\hbar^2}{2I_0} \approx 0.4$ this state would lie at about 3 MeV, which is at least 1 MeV too high. When a calculation was done including band mixing, it was found that this effect tended to spread the two $5/2^+$ levels even farther apart resulting in worse agreement with experiment. Therefore, one can conclude that a negative deformation is not consistent with the low-lying level structure of ^{27}Mg .

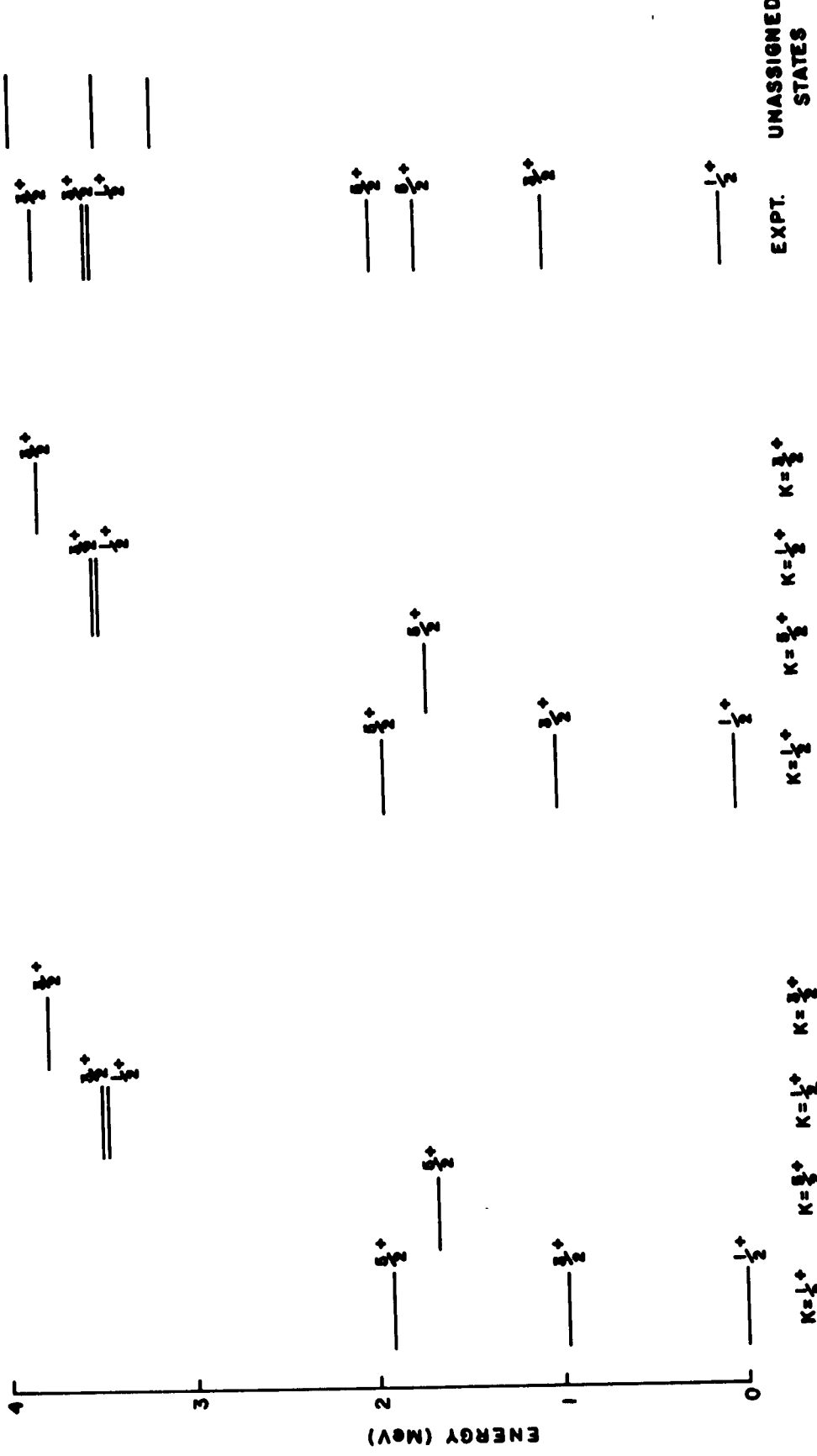
The assumption that ^{27}Mg has a positive deformation was investigated. The single-particle orbits which appear in the low-lying states are the $K = 1/2^+$ orbit 9 and the $K = 5/2^+$ orbit 5 (refer to fig. 4.1). Since ^{27}Mg has a $J = 1/2^+$ ground state, the deformation must be small

enough that orbit 9 is the ground state. In this case, there will be a low-lying $K = 5/2^+$ band based on a hole state in orbit 5. This hole state will be either the $J = 5/2^+$ 1.692 MeV level or the $J = 5/2^+$ 1.936 MeV level since the $-2K^2$ term in equation 4.10 ensures that this $K = 5/2^+$ state will have a low excitation energy. It would appear from the decay of these two levels that the $K = 5/2^+$ state is the 1.692 MeV level and that the 0.984 and 1.936 MeV levels are both members of the ground state band. This assignment is partly based on the fact that an M1 transition from the $K = 5/2^+$ band to the 0.984 MeV level is forbidden by K selection rules if the 0.984 MeV level is a member of the ground state band.

An attempt was made to find Nilsson model parameters which fit the energies of the band heads. In addition to the two band heads already mentioned, it was assumed that the 3.470 MeV level is a $K = 1/2^+$ orbit 11 band head and that the 3.782 MeV level was a $K = 3/2^+$ band head. Two assumptions were made concerning the 3.782 MeV level; in assumption 1 it was assumed that this level was due to a single particle excitation to orbit 8 and in assumption 2 it was assumed that this level was a hole state due to orbit 7. The resulting fits to the band head energies for each assumption are shown in fig. 4.3 and the corresponding Nilsson model parameters are shown in table 4.1

Also shown in fig. 4.3 is the $\frac{\pi^2}{2I_0}$ and the decoupling parameter necessary to fit the first two members of the ground state band and the decoupling parameter necessary to fit the $K = 1/2^+$ orbit 11 band

Fig. 4.3 The Nilsson model prediction of the positive parity levels of ^{27}Mg . The parameters used to fit each band are shown directly below the band. For assumption 1, the 3.782 MeV level is a $K = 3/2^+$ band head built on orbit 8 and for assumption 2, it is a $K = 3/2^+$ band head built on orbit 7.



$K = \frac{1}{2}^+$ $K = \frac{3}{2}^+$ $K = \frac{1}{2}^+$ $K = \frac{3}{2}^+$
 9 5 11 8
 $\frac{\hbar^2}{2I} = 289 \text{ keV}$ $\frac{\hbar^2}{2I} = 289 \text{ keV}$ $\frac{\hbar^2}{2I} = 289 \text{ keV}$ $\frac{\hbar^2}{2I} = 289 \text{ keV}$
 $Q = 0.265$ $Q = -0.988$ $Q = -0.988$ $Q = -0.988$

$K = \frac{1}{2}^+$ $K = \frac{3}{2}^+$ $K = \frac{1}{2}^+$ $K = \frac{3}{2}^+$
 9 5 11 7
 $\frac{\hbar^2}{2I} = 289 \text{ keV}$ $\frac{\hbar^2}{2I} = 289 \text{ keV}$ $\frac{\hbar^2}{2I} = 289 \text{ keV}$ $\frac{\hbar^2}{2I} = 289 \text{ keV}$
 $Q = 0.265$ $Q = -0.988$ $Q = -0.988$ $Q = -0.988$

ASSUMPTION 2

ASSUMPTION 1

TABLE 4.1

Nilsson Model Parameters which fit the
Energies of Four Assumed Band Heads

Parameter	Assumption	
	1	2
μ	0.102	0.091
κ	0.106	0.107
η	0.86	1.03
$\frac{\hbar^2}{2I_0}$	0.34 MeV	0.28 MeV

assuming it has the same moment of inertia as the ground state band.

The Nilsson model parameters listed in table 4.1 are only approximate because the energy level spacings do not provide a sensitive test of the wave functions. In addition, it was necessary to neglect factors such as the variation of $\frac{\hbar^2}{2I_0}$ with the projection, K, and band mixing because there are insufficient data to determine all of these parameters. Therefore, it may be useful to use the numbers in table 4.1 as a first approximation to the parameters and examine more closely properties which depend strongly on the wave functions. These properties need only be studied as a function of the parameters μ and η since the wave functions are not affected by changes in κ (refer to equation 4.6).

The first property which was examined was the variation of the

branching ratio of the 1.936 MeV level with μ and η and the result is shown in fig. 4.4. It is apparent that for μ and η near those given in table 4.1 there is very poor agreement with the measured value. A larger deformation of approximately $\eta = 2$ is necessary if the measured branching ratio is to be obtained.

The second property which was examined was the spectroscopic factor. The ratio of the spectroscopic factor of the 0.984 MeV level to that for the ground state is shown in fig. 4.5. The experimental results (Si 64, Cu 64, and Gl 65) which are also shown on the graph show some disagreement, however, one can say that a distortion of near $\eta = 2$ or 3 is necessary to obtain any of these values.

The variation of the decoupling parameters as a function of μ and η for both orbit 9 and orbit 11 is shown in fig. 4.6. For values of μ near 0.1 or 0.2, a distortion of $\eta \approx 2$ results in decoupling parameters near the experimental values (refer to fig. 4.3).

These results agree with Lacambra (La 67) who found that a distortion of $\eta = 2$ was necessary to explain the mixing ratio for the 0.984 MeV level.

Up to this point the fourth excited state of ^{27}Mg at 3.109 MeV has been omitted from the discussion of the positive parity states. The parity of this state has not been measured; however, the mixing ratio solutions (refer to table 3.1) obtained for both $J = 3/2$ and $J = 7/2$ suggest positive parity. If the parity was negative, it would require an M2 enhancement or E1 suppression from the Weisskopf estimate of greater than 10^5 to obtain the measured mixing ratios.

Fig. 4.4 The branching of the 1.936 MeV level as a function of the Nilsson parameters μ and η . The experimental branching ratio is from this work (refer to table 3.2).

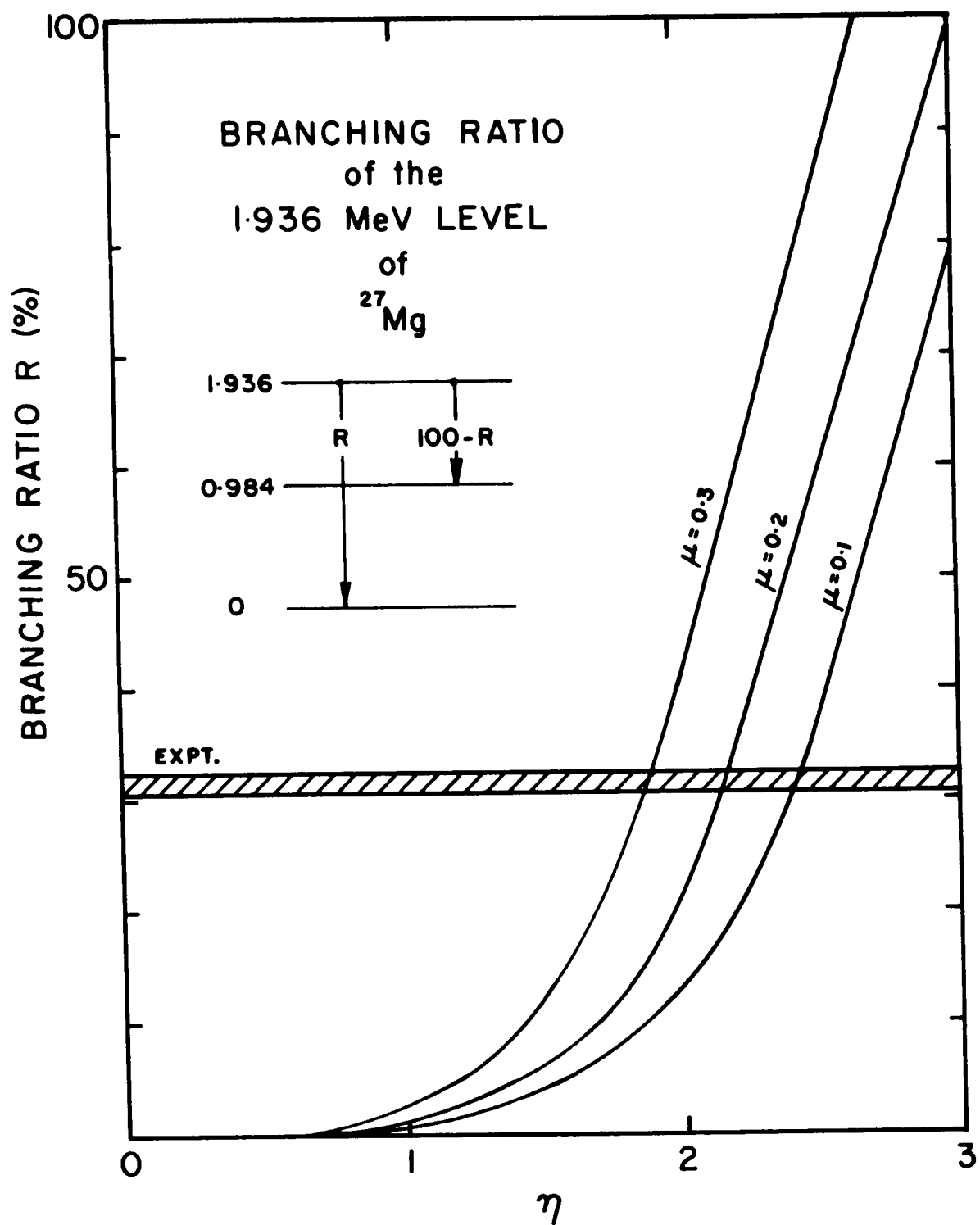


Fig. 4.5 The ratio of the spectroscopic factor of the 0.984 MeV level to that for the ground state as a function of the Nilsson parameters μ and η . The experimental ratios are from (a) Cu 64, (b) Gl 65 and (c) Si 64.

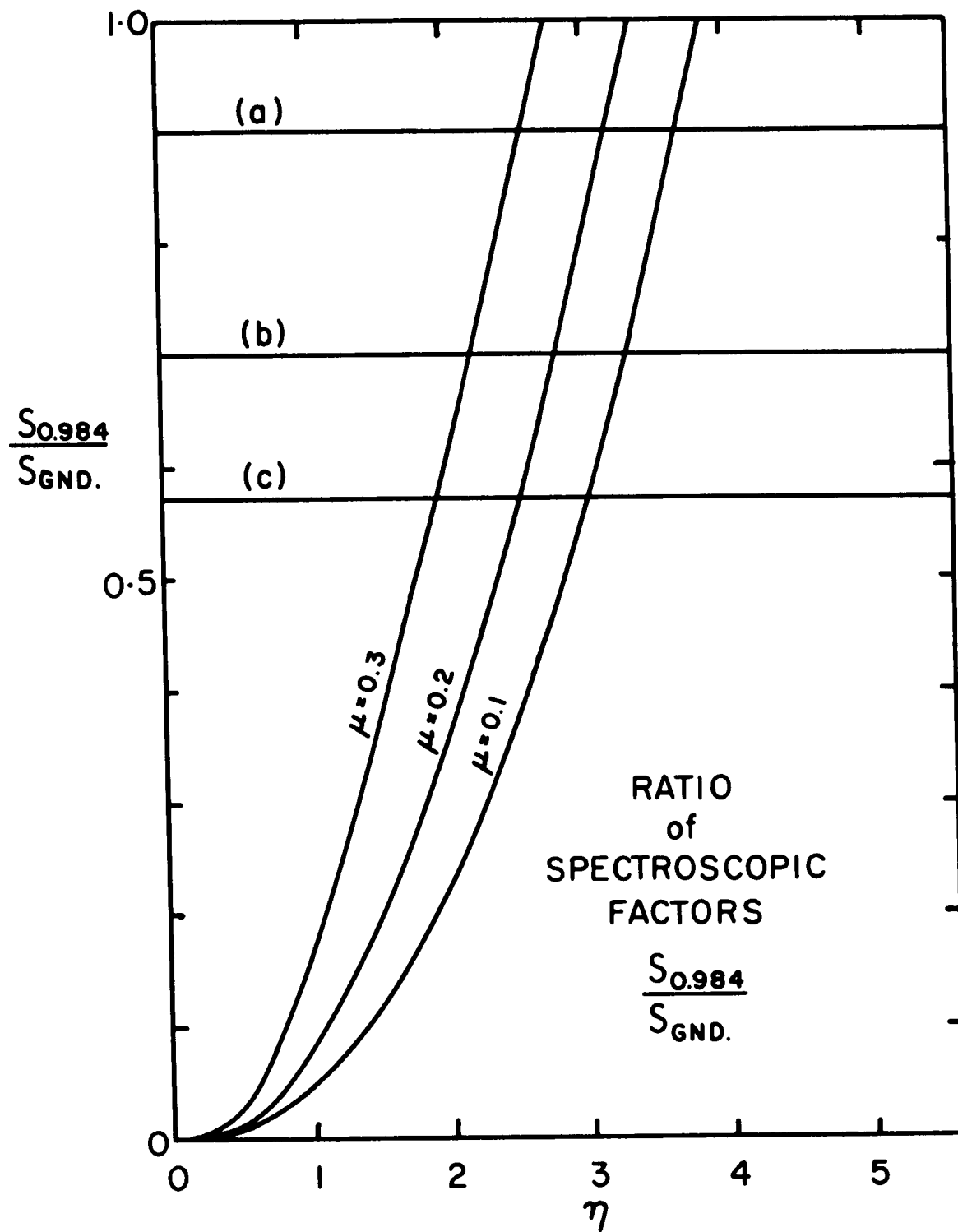
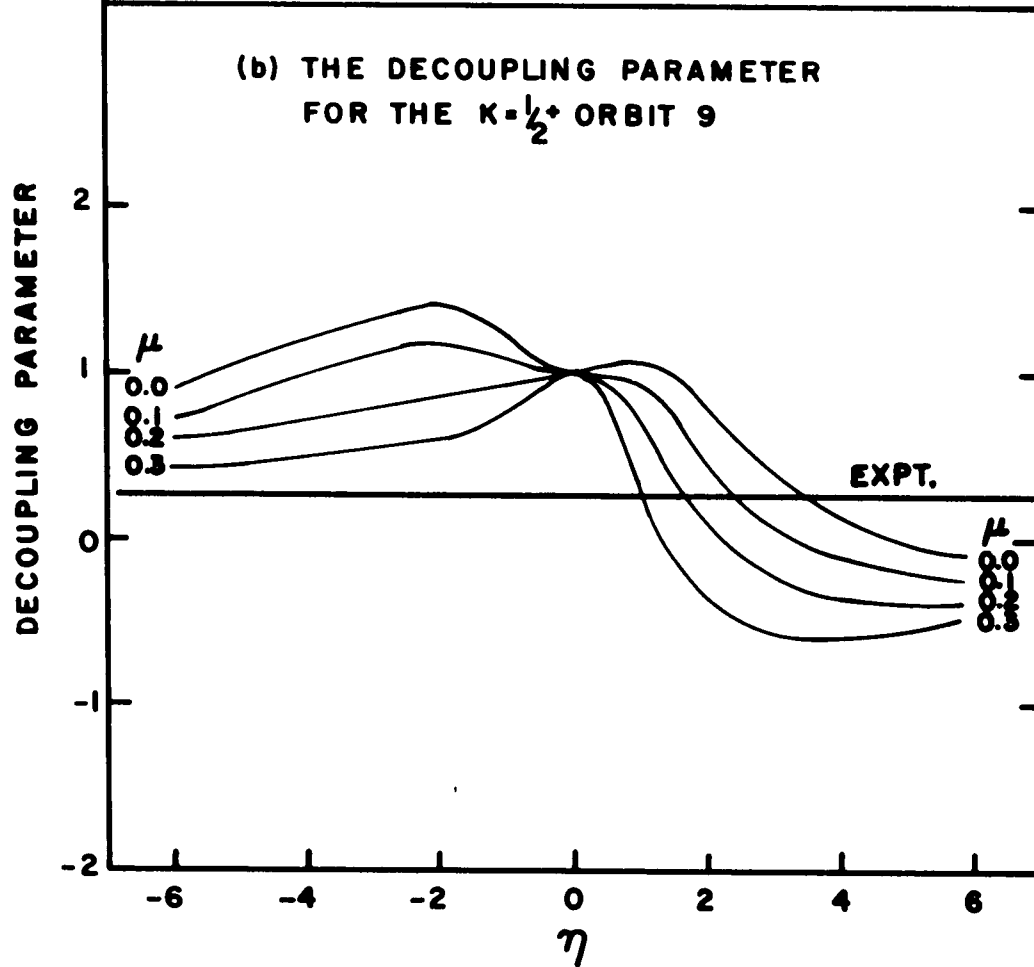
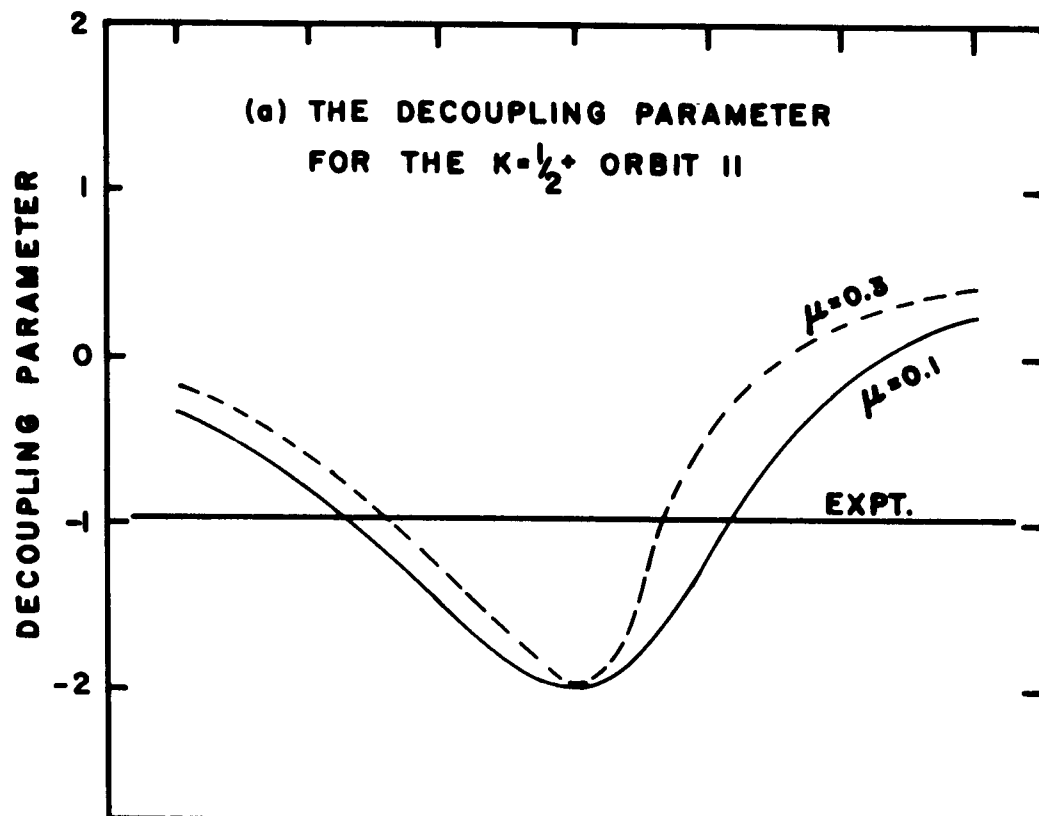


Fig. 4.6 The decoupling parameter of the $K = 1/2^+$ orbit 11 and $K = 1/2^+$ orbit 9 bands as a function of the Nilsson parameters μ and η . The experimental values are from this work (refer to fig. 4.3).



Therefore, this level very likely has a positive parity. In so far as the spin is concerned, it would be very difficult to explain the observed decay modes of this level or the mixing ratio for the 3.109 \rightarrow 1.936 MeV transition if $J = 3/2$. Therefore, the spin of the 3.109 MeV level has been assumed to be $J = 7/2$.

Assuming then that the 3.109 MeV level is the $7/2^+$ member of the ground state band, the energies of the ground, 0.984, 1.936 and 3.109 MeV levels were fitted using equations 4.10 and 4.12. The parameters which were found to give the best agreement were $\frac{\hbar^2}{2I_0} = 0.314$ MeV, $a = 0.17$ and $B = -0.0069$ MeV. The value of B calculated using the approximate formula given by Gove (Go 60) is -0.002 MeV.

The mixing ratio for the 3.109 \rightarrow 1.936 MeV transition predicted by the Nilsson model assuming both levels are members of the ground state band is $x \approx 0.1$ for values of η near two. This is within the range of the mixing ratio solutions of table 3.1. The branch to the 0.984 MeV level predicted by the Nilsson model for $\eta \approx 2$ was roughly one order of magnitude greater than the measured value.

Thus, the Nilsson model with a small distortion of $\eta \approx +1$ is able to fit the low-lying positive parity states of ^{27}Mg . However, a larger distortion of about $\eta = 2$ is needed to fit the branching ratio of the 1.936 MeV level, the spectroscopic factor of the 0.984 MeV level and the decoupling parameters of the $K = 1/2^+$ bands. More detailed information on both ^{27}Mg and the values of the Nilsson parameters applicable to this mass region are necessary if the distortion of this nucleus is to be more accurately determined.

In summary then, evidence has been found that the ground state rotational band is composed of the 0.0, 0.984, 1.936 MeV levels and possibly the 3.109 MeV level. A definite measurement of the spin and parity of the 3.109 MeV level would be useful in determining more definitely whether this level is a member of the ground state band.

4.2 The Shell Model

In this section, the shell model using a residual interaction is applied to ^{27}Mg . It is assumed that the core is ^{16}O and the remaining eleven particles are distributed among the $d_{5/2}$, $d_{3/2}$ and $s_{1/2}$ single-particle orbits. The n_i particles in the i -th orbit are allowed to couple to all possible spin values, J_i , isospin, T_i , seniority, s_i and reduced i -spin, t_i . The seniority is the number of particles remaining after all zero-coupled pairs of particles are removed and the reduced i -spin is the i -spin of the remaining particles. The possible combinations of J_i , T_i , s_i and t_i are given by Flowers (Fl 52) for a given n_i and single-particle orbit.

The Hamiltonian of the system is

$$H = \sum_i T_i + \sum_i U_i + \sum_{i<j} V_{ij} \quad ,$$

where T_i is the kinetic energy of the i -th particle, U_i is its potential energy in a central field and V_{ij} is the residual inter-

action between the i -th and j -th particles. The matrix elements of H in the many-particle system can be expressed as a linear combination of matrix elements in corresponding one-particle configurations for the one-body operators and two-particle configurations for the two body operators (de-Sh 63, page 248). Thus, in order to calculate matrix elements of H in a many-particle configuration, it is necessary to have a set of single-particle energies for calculating the one-body terms and a set of matrix elements of V_{ij} for two-particle configurations. The single-particle energies and two-body matrix elements used in this work were effective values obtained from the calculations of Kuo (Ku 67) and Wildenthal et al. (Wi 68). The matrix elements calculated by Kuo (Ku 67) were obtained using reaction matrix techniques. The matrix elements calculated by Wildenthal et al. (Wi 68) were obtained by a least-squares fitting of 80 levels in nuclei with $20 \leq A \leq 28$ to obtain values for both the two-body matrix elements and single-particle energies. Only the $d_{5/2}$ and $s_{1/2}$ orbits were allowed to be occupied in the calculations of Wildenthal.

Energy matrices were constructed using these effective interactions and diagonalized using the Oak Ridge-Rochester shell model computer program (Wo 68, Fr 68).

The number of basic states which can be formed by including all possible combinations of n_1 , n_2 and n_3 for ^{27}Mg is large and results in an energy matrix which is too large to handle. Therefore, the number of these basic states must be limited if the problem is to be solved.

The number of basic states can be greatly reduced if the procedure used by Wildenthal et al. (W1 68) is followed. Therefore, a calculation was made in which up to 4 particles could be excited from the $d_{5/2}$ to the $s_{1/2}$ orbit but no particles could be excited to the $d_{3/2}$ orbit. The matrix elements and single-particle energies of Wildenthal et al. (W1 68) were used. These single-particle energies are given in table 4.2.

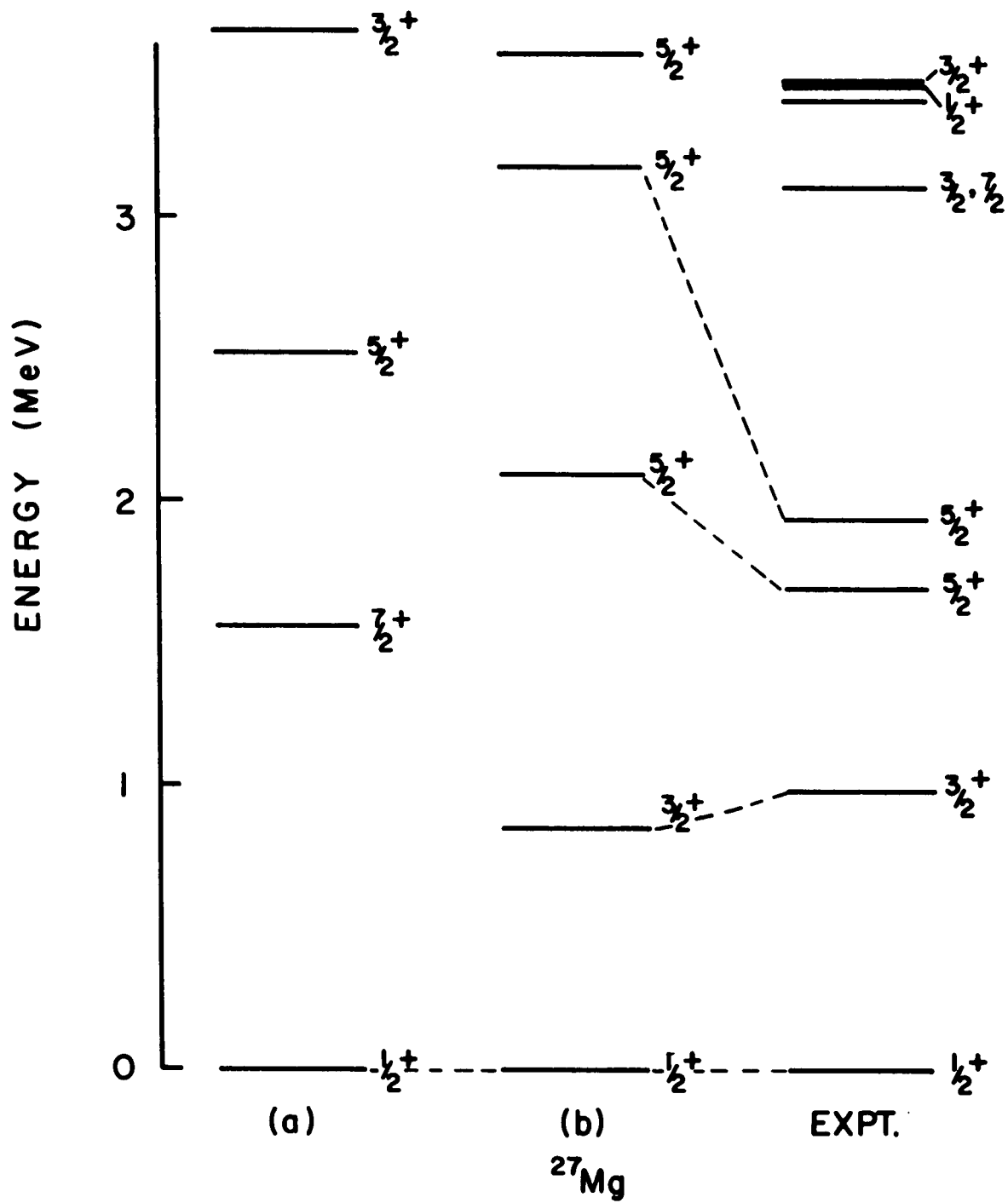
TABLE 4.2

Single-Particle Energy Spacings from
(a) Wildenthal et al. (W1 68) and (b) Kuo (Ku 67)

Orbit	E(MeV)	
	(a)	(b)
$d_{3/2}$	4.313	5.08
$s_{1/2}$	1.048	0.87
$d_{5/2}$	0	0

The results of the calculation are shown in fig. 4.7a. Except for the ground state, there is no resemblance between the predicted spectrum and the experimentally observed spectrum of ^{27}Mg . Clearly, the assumption that excitations to the $d_{3/2}$ level can be neglected is not valid for this case.

Fig. 4.7 The level spectrum for the $T = 3/2$ positive parity states of ^{27}Mg as predicted by the shell model. The spectrum (a) was obtained using two active orbits and (b) was obtained using three active orbits. The experimental spectrum is from this work (refer to fig. 3.1).



In view of these results another calculation was attempted in which a few particles were allowed to be excited into the $d_{\frac{3}{2}}$ orbit. The matrix elements and single-particle energies of Kuo (Ku 67) (refer to table 4.2) were used. The maximum number of particles which were allowed to be excited to the $d_{\frac{3}{2}}$ orbit was 3. The ways in which the eleven particles were distributed in this calculation are given in table 4.3.

TABLE 4.3

The Distribution of Particles Amongst the
 $d_{\frac{5}{2}}$, $s_{\frac{1}{2}}$ and $d_{\frac{3}{2}}$ Single-Particle Orbits

Number of Particles in Orbit		
$d_{\frac{5}{2}}$	$d_{\frac{3}{2}}$	$s_{\frac{1}{2}}$
7	0	4
8	0	3
8	1	2
8	2	1
8	3	0
9	0	2
9	1	1
9	2	0
10	0	1
10	1	0

In addition to limiting the occupation numbers of the orbits to these 10 combinations, it was found necessary to limit the ways in which particles in an orbit could couple. This was done using a seniority truncation such that the only ways of coupling allowed were those with a seniority less than or equal to 3. Even with this truncation, the matrices are 84×84 for $J = 1/2$ levels, 144×144 for $J = 3/2$ levels and 165×165 for $J = 5/2$ levels.

The results of the calculation using this truncated space is shown in fig. 4.7b. The level order of the first four states is predicted correctly and the excitation energies of the first two states are reasonably close, considering that there were no free parameters in the calculation except for the choice of truncation.

Thus, the shell model using an effective interaction appears to have some success in predicting the first two excited states of ^{27}Mg using a space which has been truncated to the particle distributions of table 4.3 and truncated to a seniority less than or equal to 3 for any given single-particle orbit.

CHAPTER V

CONCLUSIONS

The spins of the 1.692, 3.564, 3.757 and 4.816 MeV levels have been verified as $J = 5/2$, $J = 3/2$, $J = 7/2$ or $J = (5/2)$ and $J = 1/2$ or $J = 3/2$, respectively. The present results combined with previous data (En 67) lead to a unique assignment for the 3.782 MeV level of $J^\pi = 3/2^+$. In addition, the spins of the previously unstudied levels at 3.109 MeV and 4.394 MeV have been limited to $J = 3/2$ or $J = 7/2$ and $J = 3/2$, $J = 5/2$ or $J = 9/2$, respectively.

The decay modes of the previously unobserved transitions from the 3.757, 3.782, 3.880, 4.146, 4.394, 4.549, 4.763, 4.816, (4.982-5.017) and (5.365-5.405) MeV levels have been obtained and more accurate data on the decay modes of the 1.936, 3.109, (3.470-3.484) and 3.564 MeV levels have been obtained. In addition, the mixing ratios for a number of these transitions have been limited (refer to table 3.1).

A comparison of the experimental data with the predictions of the Nilsson model indicated that the low-lying positive parity spectrum of ^{27}Mg could be reproduced with $\kappa \approx 0.1$, $\mu \approx 0.1$ and a distortion of about $\eta = +1$. However, this deformation did not predict accurately the branching ratio of the 1.936 MeV level, the spectroscopic factor of the 0.984 MeV level and the decoupling parameters of the

$K = 1/2^+$ bands. These were better described with a deformation of about $\eta = 2$. More detailed information on both ^{27}Mg and the Nilsson parameters κ and μ which are applicable in this mass region are necessary if the distortion of ^{27}Mg is to be determined more accurately.

In addition, evidence was found for a ground state rotational band composed of the 0.0, 0.984 and 1.936 MeV levels. The 3.109 MeV level may also be a member of this band, however, further information on the spin and parity of this level is necessary before a definite assignment may be made.

The shell model using the effective interaction of Kuo (Ku 67) showed some success in predicting the first two excited states of ^{27}Mg using a space which was truncated in particle distribution (refer to table 4.3) and truncated to seniority less than or equal to 3 for coupling within a given single-particle orbit.

REFERENCES

- Al 56 K. Alder, A. Bohr, T. Huus, B. Mottelson, and A. Winther, Rev. Mod. Phys. 28 (1956) 432.
- Ba 62 K.H. Bhatt, Nucl. Phys. 39 (1962) 375.
- Be 64 J.A. Becker, G.E. Mitchell, and P.F. Donovan, Phys. Rev. 135 (1964) 587.
- Bi 59 G.R. Bishop, Nucl. Phys. 14 (1959) 376.
- Bo 65 M.C. Bouten-Denys, Thesis, Universite Libre de Bruxelles, 1965.
- Bo 67 M.C. Bouten, J.P. Elliot, and J.A. Pullen, Nucl. Phys. A97 (1967) 113.
- Br 65 R.T. Brockmeier, S. Wahlborn, E.J. Seppi, and F. Foehm, Nucl. Phys. 63 (1965) 102.
- Cu 64 B. Čujec, Phys. Rev. 136 (1964) B1305.
- Da 65 J.P. Davidson, Rev. Mod. Phys. 37 (1965) 105.
- de-Sh 63 A. de-Shalit and I. Talmi, Nuclear Shell Theory, Academic Press, New York and London, 1963.
- En 67 P.M. Endt and C. van der Leun, Nucl. Phys. A105 (1967) 1.
- Es 67 M.A. Eswaran, N.L. Ragoowansi, and K.K. Sekharan, Bull. Am. Phys. Soc. 12 (1967) 72.
- Es 68 M.A. Eswaran, N.L. Ragoowansi, Proc. Indian Academy of Sciences 67 (1968) 19.
- Ev 55 R.D. Evans, The Atomic Nucleus, McGraw-Hill Publishing Co., New York, 1955.
- Fe 65 A.J. Ferguson, Angular Correlation Methods in Gamma-ray Spectroscopy, North-Holland Publishing Co., Amsterdam, 1965.
- Fl 52 B.H. Flowers, Proc. Roy. Soc. (London) A212 (1952) 248.
- Fr 68 J.B. French, E.C. Halbert, J.B. McGrory, and S.S.M. Wong, to be published.

- Gl 64 R.N. Glover, ANL-6848 (p. 104-5), Atomic Weapons Research Establishment, Aldermaston, Berks, England.
- Gl 65 R.N. Glover, Phys. Letters 16 (1965) 147.
- Go 60 H.E. Gove, in Proceedings of the International Conference on Nuclear Structure, Kingston, University of Toronto Press, 1960.
- He 65 R.L. Heath, R.G. Helmer, L.A. Schmittroth, and G.A. Cazier, U.S. Atomic Energy Commission Report IDO-17017, 1965.
- Hl 61 S. Hinds, H. Marchant, and R. Middleton, Proc. Phys. Soc. (London) 78 (1961) 473.
- Hl 65 S. Hinds, H. Marchant, and R. Middleton, Nucl. Phys. 67 (1965) 257.
- Ke 56 A.K. Kerman, Kgl. Danske Vid. Selsk., Mat. Fys. Medd. 30 (1956) 15.
- Ku 67 T.T.S. Kuo, Nucl. Phys. A103 (1967) 71.
- La 67 J.M. Lacambra, D.R. Tilley, and N.R. Roberson, Nucl. Phys. 92 (1967) 30.
- Li 58 A.E. Litherland, H. McManus, E.B. Paul, D.A. Bromley, and H.E. Gove, Can. J. Phys. 36 (1958) 378.
- Li 61 A.E. Litherland and A.J. Ferguson, Can. J. Phys. 39 (1961) 788.
- Lo 64 R. Lombard, Thesis, University of Paris, 1964.
- Ni 55 S.G. Nilsson, Kgl. Danske Vid., Selsk., Mat. fys. Medd. 29 (1955) No. 16.
- Po 65 A.R. Poletti and E.K. Warburton, Phys. Rev. 137 (1965) B595.
- Pr 62 M.A. Preston, Physics of the Nucleus, Addison-Wesley Publishing Co., Reading Mass., 1962.
- Ro 57 M.E. Rose, Elementary Theory of Angular Momentum, John Wiley and Sons, Inc., New York, 1957.
- Ro 67 H.J. Rose and D.M. Brink, Rev. Mod. Phys. 39 (1967) 306.
- Ru 59 A.R. Rutledge, Atomic Energy of Canada report CRP-851, unpublished, 1959.
- Si 64 J. Silverstein, L.J. Lidofsky, G.E. Mitchell, and R.B. Weinberg, Phys. Rev. 136 (1964) B1703.

- Sk 66 S.J. Skorka, J. Hertel, and T.W. Retz-Schmidt, Nuclear Data 2 (1966) 347.
- So 67 B. Sowerby, private communication.
- Te 66 J.W. Tepel, Nucl. Instr. and Meth. 40 (1966) 100.
- Ve 68 C.W. Vermette, W.C. Olsen, D.A. Hutcheon, and D.H. Sykes, Nucl. Phys. A111 (1968) 39.
- Wa 59 A.H. Wapstra, G.J. Nijgh, and R. Van Lieshout, Nuclear Spectroscopy Tables, North-Holland Publishing Co., Amsterdam, 1959.
- Wi 60 D.H. Wilkinson in Nuclear Spectroscopy, Part B, Edited by F. Ajenberg-Selove, Academic Press, New York and London, 1960.
- Wi 68 B.H. Wildenthal, J.B. McGrory, E.C. Halbert, and P.W.M. Glaudemans, Phys. Lett. 26B (1968) 692.
- Wo 68 S.S.M. Wong, private communication.

APPENDIX A

GAMMA-RAY PEAK FITTING PROGRAM

**This appendix is a complete internal report written in
co-authorship with D.A. Hutcheon in August of 1968.**

GAMMA RAY PEAK FITTING PROGRAM

D.H. Sykes and D.A. Hutcheon

Nuclear Research Center
University of Alberta
Edmonton, Alberta, Canada

Description of Program

This program reads gamma-ray spectra from magnetic tape and does a least squares fit to the data using standard gamma-ray line shapes. Up to 4096 channels of data can be read in at one time and the data is arranged into groups or bins of 256 channels each. If the corresponding random coincidence spectra for each bin is stored in the 256 channels immediately following the true-plus-random spectra, one has the option to subtract these randoms prior to fitting the spectrum. (The "sort" routine used on the SDS 920 computer can be used to arrange the data in this manner.)

The standard gamma-ray line shapes used in fitting the spectra are formed in a semiempirical manner. The coefficients used in the shape subprogram are determined by fitting standard monoenergetic

gamma-ray peaks obtained from sources or reactions. The gamma-ray spectrum obtained from a monoenergetic source is composed of three parts corresponding to three processes of energy absorption by the crystal, the photoelectric effect, pair production and Compton scattering. Thus, the spectrum has a peak at the full energy of the gamma ray. This peak is given the shape

$$e^{-\frac{(E-E_\gamma)^2}{2\sigma}} [1 + a_1(E-E_\gamma)^{n_1} + a_2(E-E_\gamma)^{n_2}], \quad (1)$$

where

$$\sigma = b_1 + b_2 E_\gamma + b_3 E_\gamma^2. \quad (2)$$

There will be two peaks due to pair production; one at $E_\gamma - 0.511$ MeV and one at $E_\gamma - 1.022$ MeV. These peaks are also given the shape of equation 1. The ratio of the size of the first escape peak ($E_\gamma - 0.511$) to the full energy peak is given the form

$$R = C_1 + C_2 E_\gamma + C_3 E_\gamma^2. \quad (3)$$

The ratio of the second escape peak ($E_\gamma - 1.022$) to the full energy peak has the same form as equation 3.

The part of the peak shape due to Compton scattering is more difficult to treat. In this program the theoretical Compton distribution is calculated. The distribution does not allow for either detector resolution or multiple Compton scattering. To account for multiple Compton scattering accurately would be very difficult; however, a

rough correction for this effect is made as follows. First the absorption curve for gamma rays in the crystal (refer to Evans[†] P717) is used to remove from the Compton distribution all gamma rays which are re-absorbed in the crystal after being Compton scattered. The effective thickness of the crystal "THICK" is varied to give the best fit to standard spectra. Those gamma rays which are Compton scattered more than one time are accounted for approximately by folding a modified Gaussian of the form of equation 1 into the Compton distribution and increasing the effective σ to several times as large a value as was used for the peaks. This also accounts for the effect of the finite resolution of the detector on the Compton distribution.

The size of the Compton distribution relative to the full energy peak is

$$R_C = (f_a + f_b E_\gamma + f_c E_\gamma^2)/B$$

where B is the height of the Compton at its highest point near the Compton edge.

The contributions from all three processes are added together to produce the total line shapes to be used in fitting gamma-ray spectra.

The fitting procedure used in the program is a standard linear least squares fitting procedure where

$$\chi^2 = \sum_i \frac{Y_i - N_i^2}{N_i}$$

is minimized, where N_i is the number of counts in the i -th channel

[†]R.D. Evans, The Atomic Nucleus (McGraw-Hill Publ. Co., New York, 1955).

and Y_i is the predicted number of counts in the i -th channel. The areas quoted are photopeak areas corrected for photopeak efficiency. The errors in the areas are obtained by taking the square root of the appropriate matrix elements as described by Mathews and Walker[†]. In order to take account of error in the standard shapes, these error bars are multiplied by $\sqrt{\chi^2}$ for χ^2 greater than 1.0.

It is possible to fit a spectrum with up to 20 peaks in a single fit or one can strip off the highest peaks and then fit the lower energy peaks separately.

It is also possible to allow the program to search for the peak positions which give the lowest χ^2 . One can specify the maximum amount each peak can move in an iteration so that by specifying zero for some peaks it is possible to allow some peaks to vary and some to remain in a fixed position.

Explanation of Variables

All variables related to the peak shapes are determined by fitting standard spectra. The relationship between the variables used in the preceding discussion and those used in the program is given below.

[†]J. Mathews and R.L. Walker, Mathematical Methods of Physics, W.A. Benjamin Inc., New York, 1964.

Variable in Program	Variable in Report	Comments	Typical Value
SIG	σ		
EZ	E_γ (MeV)		
A1,AC1	a_1	Variables with C are Compton distribution variables (If zero set to 1.0)	0.0
A2,AC2	a_2		0.0
N1,NC1	n_1		0
N2,NC2	n_2		0
AA	b_1	Width parameters for $E_\gamma < 1$	33
BB	b_2		44
CC	b_3		-2.9
DD	b_3		-2
ESCA1,ESCA2	C_1	1 and 2 refer to first and second escape peaks respectively	-0.3,-0.26
ESCB1,ESCB2	C_2		0.21,0.11
ESCC1,ESCC2	C_3		0, 0
FA	f_a	peak/Compton parameters	0.2
FB	f_b		0
FC	f_c		0.02

A description of other variables used in the program, but not previously mentioned, is given below.

Variable	Description	Typical Value
NEFF	Number of points on the photopeak efficiency curve	20
NAPS	Number of points on the absorption curve	15
EFFIC(J)	Efficiency at energy "ENERGY(J)"	
APS1(J)	Absorption coefficient at energy EA(J)	
GAIN	$EZ = \text{BASELN} + \text{GAIN} * \text{CHAN} + \text{G2} * \text{CHAN} ** 2$	
BASELN		
G2		
CHAN	Channel number	

Variable	Description	Typical Value
THICK	Effective thickness of detector	6.0
COMWID	Factor to account for multiple Compton scattering	2.2
TAPE	IF TAPE IS REW the tape is rewound	
FAC	The random spectrum is multiplied by FAC before subtraction. IF FAC=0 it is set equal to 1.0	0
NPAR	Number of gamma ray peaks to be fitted at one time	less than 20
MAX	Maximum number of iterations to determine peak positions	20
ESTEP(J)	Size of energy step used in search	
CUT	ESTEP(J) = ESTEP(J)/CUT after every iteration If CUT = 0, it is set equal to 2.0	0
DAT1	Specifies whether the data is to be read from cards or tape	TAPE
ISUBT	If ISUBT is zero, randoms are subtracted	0
IBEGI	Begin channel of data read from cards	
IENDI	End channel of data read from cards	
DATI(1,K)	DATA points read from cards (read into bin 1)	
OTHER (K)	A title of up to 80 characters	
IRUN	Run number	
JDAY	Day	
JMONTH	Month	
JYEAR	Year	
IBEG	Begin channel of fitting region	
IEND	End channel of fitting region	
IBIN	Bin number (starting at Bin 1)	
HT SLOPE	Height and slope of background to be subtracted	

How to Operate the Program

When the program is first entered basic information common to all fits must be provided. The program asks for a number of points on a photopeak efficiency curve for the detector and a number of points on a gamma-ray absorption curve for the crystal.

After this initialization, the program uses the main line to call other routines. These routines may be called in any order simply by using different values of "ICON", the main control parameter. The value of ICON used to call each specific routine is given below:

Value of ICON	Subroutine Called
1	INPUT 1
2	INPUT 2
3	INPUT 3
4	ABIN
5	FITIT
6	EXIT

The function of each of these routines is given below.

INPUT 1	Reads parameters for the gamma-ray line shapes
INPUT 2	Reads the spectra from cards or magnetic tape
INPUT 3	Reads parameters governing the fitting
ABIN	Selects one bin of 256 channels from the spectrum read in INPUT 2. Random coincidences are subtracted.
FITIT	Calls all fitting routines for a χ^2 fit.

The formats which must be used for the input data to these routines are listed below:

Routine	Card	Variables	Format
MAIN	1	NEFF,NAPS	2X,2(2I,8X)
	2	ENERGY(J),EFFIC(J),J=1,NEFF	2X,6F10.3
	3	EA(J),APS1(J),J=1,NAPS	2X,6F10.3
	4	ICON	I1
INPUT 1	1	GAIN,BASELN,G2	2X,2F10.3,E10.3
	2	N1,N2,NC1,NC2,AL1,AL2,ALC1,ALC2	2X,4I2,2X,4E10.3
	3	FA,FB,FC	2X,7F10.3
	4	AA,BB,CC,DD,THICK	2X,7F10.3
	5	ESCA1,ESCB1,ESCC1,ESCA2,ESCB2, ESCC2,COMWID	2X,7F10.3
INPUT 2	1	DAT1,ISUBT	2X,A4,6X,I1
	<u>IF DAT1 = CARD</u>		
	2	IBEGI,IENDI	2X,2I5
	3	DAT1(1,K),K=IBEGI,IENDI	2X,7F10.3
	4	OTHER(K),K=1,20	20A4
	<u>IF DAT1 = TAPE</u>		
	2	IRUN,JDAY,JMONTH,JYEAR,TAPE,FAC	{ 2X,I4,1X,3I2, 9X,A4,6X,F10.3
INPUT 3	1	NPAR,MAX,CUT	2X,I2,8X,I2,F10.3
	IF MAX > 0 READ CARD 1a		
	1a	ESTEP(N),N=1,NPAR	2X,7F10.3
	2	IBEG,IEND	2X,2I5
	3	EZ(K),K=1,NPAR	2X,7F10.3
ABIN	1	IBIN,HT,SLOPE	2X,I1,9X,2F10.3
FITIT	No Cards		